1955

On the natural transverse modes of a submarine

Otth, Edward John

Massachusetts Institute of Technology

ON THE NATURAL TRANSVERSE MODES OF A SUBMARINE

Edward John Otth
and
Peter Wright Wood

ON THE NATURAL TRANSVERSE MODES OF A SUBMARINE

by

EDWARD JOHN OTTH, JR. Lieutenant, U.S. Navy
B. S., U.S. Naval Academy (1949)

and

PETER WRIGHT WOOD, Lieutenant (junior grade), U.S. Navy
B. S., U.S. Naval Academy (1950)

SUBMITTED IN PARTIAL FULFILLMENT OF THE
REQUIREMENTS FOR THE DEGREE OF
NAVAL ENGINEER

at the

MASSACHUSETTS INSTITUTE OF TECHNOLOGY

May, 1955

ABSTRACT

ON THE NATURAL TRANSVERSE MODES OF A SUBMARINE

by

EDWARD JOHN OTTH

and

PETER WRIGHT WOOD

SUBMITTED TO THE DEPARTMENT OF NAVAL ARCHITECTURE AND MARINE ENGINEERING ON MAY 23, 1955, IN PARTIAL FULFILLMENT OF THE REQUIREMENTS FOR THE DEGREE OF NAVAL ENGINEER.

A graphical method of determining normalized curvature patterns, deflection patterns, and frequencies for the natural modes of interest of a ship treated as a non-uniform, free-free, transversely vibrating beam is presented. Corrections for shear deflection and rotatory inertia are integrated into the method, which is based on procedures developed by Stodola and Schadlofsky. Integrations are performed mechanically by an integraph. The method is demonstrated by determining the first three horizontal modes of a three-eighths scale model of a submerged submarine.

The method is found to be convergent, yielding acceptable results, and taking account of the secondary effects considered. Three cycles of iteration for each of the first three non-trivial natural modes of the model yielded frequencies of 417, 838, and 1391 cycles per minute, respectively. Patterns obtained are tabulated in detail.

The process developed is recommended for consideration by small research facilities with limited budgets.

Thesis Supervisor: STEPHEN HARRY CRANDALL
Ph. D.
Title: Associate Professor of Mechanical Engineering

ABSTRACT

A graphical method of determining normalized curvature functions, deflection patterns, and frequencies for the natural modes of bisymmetrical beams is presented. Corrections for shear deflection and rotatory inertia are integrated into the method, which is based on procedures developed by Stodola and Kozdolsky. Integrations are performed mechanically by an integraph. The method is demonstrated by determining the first three horizontal modes of a three-eighths scale model of a submerged submarine.

The method is found to be convergent, yielding acceptable results, and taking account of the secondary effects considered. Three cycles of iteration for each of the first three non-trivial natural modes of the model yielded frequencies of 417, 839, and 1391 cycles per minute, respectively. Failures obtained are tabulated in detail.

The process developed is recommended for consideration by small research facilities with limited budgets.

Cambridge, Mass.
May 23, 1955

Secretary of the Faculty
Massachusetts Institute of Technology
Cambridge 39, Massachusetts

Dear Sir:

In accordance with the requirements for the Degree of Naval Engineer, we herewith submit a thesis entitled: "On the Natural Transverse Modes of a Submarine".

Respectfully yours,

ACKNOWLEDGMENT

This thesis was undertaken at the suggestion of Dr. A. H. Keil, Dr. H. M. Schauer, and Mr. W. W. Murray of Underwater Explosions Research Division, Norfolk Naval Shipyard, Norfolk, Virginia. The authors are grateful to Mr. Murray, who outlined the basic approach, formulated several important relationships, and guided preliminary investigations which preceded this thesis; to Lieutenant Commander R. E. Henning, U.S. Navy, officer-in-charge, Underwater Explosions Research Division, for his cooperation in making available structural data and previously calculated frequencies for the model considered; to Professor J. P. Den Hartog for his encouragement and guidance during the early stages of the thesis work; to Professor S. H. Crandall, for his patient guidance and assistance throughout the execution of this thesis; and to Miss Jill Littlefield and Miss Edith Repshis for carefully and neatly typing the manuscript and tables.

ACKNOWLEDGMENT

This thesis was undertaken at the suggestions of Dr. A. M. Hall, Dr. M. D. Tobacco, and Dr. W. Harvey at Pocahontas Mining Alone Research Division, Pocahontas Mineral Laboratory, Virginia. The authors are grateful to Dr. Harvey, who outlined the basic experiments, formulated several important relationships, and guided preliminary investigations which preceded this thesis, to Lieutenant Commander E. E. Fleming, U.S. Navy, advocate-in-charge, Underwater Explosives Research Division, for his cooperation in making available additional data and previously unpublished information for the model experiments, to Professor J. F. Dow Harvey for his encouragement and guidance during the early stages of the thesis work, to Professor D. G. Crandall, for his patient guidance and assistance throughout the execution of this thesis, and to Miss Jill Carrington and Miss Linda Hopkins for carefully and neatly typing the manuscript and tables.

NOMENCLATURE

A = total cross-section area of hull structure considered effective in bending and shear, (sq. inches)

$\bar{A}$ = axis translation of assumed or calculated deflection for orthogonality with rigid body translation

$\bar{B}$ = rotation coefficient for axis of assumed or calculated deflection for orthogonality with rigid body rotation

C_i, C_{ii}... = adjustment coefficients for correcting assumed or calculated deflections for orthogonality with previous modes

C_1 = constant of integration applied to shear (equal to zero)

C_2 = constant of integration applied to bending (equal to zero)

C_3 = constant of integration applied to slope

C_4 = constant of integration applied to deflection

E = Young's modulus, 30×10^6 psi

G = shear modulus, 11.5×10^6 psi

I, I_{zz} = moment of inertia of hull structure about vertical axis through centroid of each section.

K = ratio of average shear stress to maximum shear stress over a cross-section for horizontal transverse shear.

L = length overall of ship, ft.

M = bending moment, ft-lb.

N = an operational constant, $= \int_0^L \frac{(x - \bar{x})^2}{L} m g \frac{dx}{L}$

NOMENCLATURE

A = total cross-section area of duct structure considered effective in heating and ejector, ind. basis.

$\bar{A}$ = area transition of resolved or calculated deflection for angle-

Boundary with right hand convention

B = material constituent for each of measured or calculated quantity

for orthogonality with right hand rotation

C_D = adjustment coefficient for electrical resonance or attenuated

difference for orthogonality with right hand rotation

C_1 = constant of integration applied in short (about 0) test

C_2 = constant of integration applied in reading (about 1) to zero

C_3 = constant of integration applied to sync

C_4 = constant of integration applied in short (about 0) test

C_5 = constant of integration applied in reading (about 1) to zero

D = sheer modulus, $D = E/2(1+\nu)$ psi

D_{ij} = moment of inertia of duct structure about axis through centroid of duct section.

E = ratio of voltage about sight to maximum check output over

a cross-section for horizontal transverse shear

F = input current of duct, A

H = reading constant, Ω-ft.

I = area moment of duct, ft^4

J = torsional constant, ft^4

K = $\int_0^{\ell} \frac{E}{(\sigma - \bar{\sigma})} \, ds \, \frac{d\sigma}{ds}$

NOMENCLATURE (Continued)

P = an operational constant, = $\int_0^L \int_0^x \frac{(\xi - \bar{x})}{L} m g \, d\xi \frac{1}{L} \frac{dx}{L}$

Q = shear force, lb

T = period of vibration, milliseconds

W_1 = an operational constant = $\int_0^L y_1^2 m g \, dx/L$

W_2 = an operational constant = $\int_0^L y_2^2 m g \, dx/L$

Y_1, Y_2 = deflection patterns for a uniform prismatic bar obtained from consideration of simple bending theory only, according to Lord Rayleigh.

f = frequency of vibration, cps

g = force of gravity, 32.2 ft/sec^2

m = virtual mass per unit length, including structure, ballast, free-flooding water, etc., plus water entrained in horizontal vibration (lb sec^2/ft^2)

w = mg, virtual weight per unit length (lb/ft)

x = coordinate parallel to longitudinal axis of ship, measured from bow (ft)

$\bar{x}$ = coordinate of longitudinal centroid of virtual mass

y = coordinate parallel to beam of ship, measured from vertical plane through centroid of ship; measure of horizontal deflection

$\bar{y}$ = the deflection pattern obtained from a cycle, before orthogonalization

y^* = value of unnormalized deflection curve taken at the normalizing point

NOTATION (continued)

$\bar{y}$ = coordinate parallel to span of ship, measured from vertical plane through centroid of ship, measure of lateral deflection

$\bar{z}$ = coordinate of longitudinal centroid of virtual mass

z = coordinate parallel to longitudinal axis of ship, measured from bow (x)

m = $\rho\beta$, virtual weight per unit length (lb/ft)

m_y = virtual mass per unit length, including structure, ballast, boundary layer, etc., plus mass moment associated to horizontal vibration ($lb\ sec^2/ft^2$)

N = factor of gravity, $32.2\ ft/sec^2$

n = frequency of vibration, cps

P_1, P_2, P_3 = deflection patterns for a uniform ship normalized for convenient consideration of simple cantilever theory only, according to load variation.

M^2 = $\int_0^L x^2 m\, dx$, an operational constant

M^1 = $\int_0^L x m\, dx$, an operational constant

T = period of vibration, milliseconds

Q = shear force, lb

E = $\int_0^L \left(\frac{L}{2} - x\right) m \frac{E}{I}\, dx$, an operational constant

NOMENCLATURE Continued

z = coördinate parallel to vertical axis of ship measured from plane through centroid of ship.

Δ = virtual displacement (pounds); see

β = component of slope due to shear deflection

γ = component of slope due to bending

$\bar{\gamma}$ = component of slope due to bending before axis determination; $\bar{\gamma} + C_3 = \gamma$

η = deflection before determination of axis; $\eta + c_4 = y$

η' = slope before determination of axis; $\eta + c_3 = y'$

ξ = dummy variable, replacing x

ω = circular frequency, (radians/second)

Note: Subscript to deflection indicates mode number.
Hyphenated subscript indicates mode number and iterative cycle number.
Prime indicates differentiation with respect to x.

NOMENCLATURE (Continued)

m	=	coefficient pertaining to vertical axis of strip considered (zero at plane through centroid of strip).
n	=	normal displacement (upward) of
p	=	component of slope due to shear deflection
q	=	component of slope due to bending
r	=	component of slope due to bending unless zero deformation; $r = r_1 + r_2$
r_1	=	determine relative deformation of axis; $r_1 = \frac{M}{E} = \chi$
r_1'	=	slope relative deformation of axis; $r_1' = \frac{dr_1}{dx} = \chi'$
s	=	shearing variable, replacing $\frac{x}{a}$
t	=	tangential displacement (positive|outward)

Note: Subscript to distinguish indicates double symmetry.
Subscript comma(,) distinguish indicates double symmetry and indicates cyclic symmetry.
Prime indicates differentiation with respect to x.

ILLUSTRATIONS

TABLE OF CONTENTS

TABLE OF CONTENTS

I. INTRODUCTION

A. Historical

For the last seventy years, the subject of vibrations of ship hulls has attracted ever increasing attention from the naval architect. Early investigators, notably Otto Schlick, emphasized the empirical treatment; but so complex is the structure of a large ship, and so varied its design features, that it became clear that this approach would not fully serve the need. Ultimately then, we must look to the theoretical approach for the development of adequate formulations.

Basically, the ship is considered a slender free-free elastic beam, vibrating transversely to its long axis, for which the theory stems from Lord Rayleigh. [6]* From energy considerations he developed the basic equation based on simple bending. He then showed that for various assumed mode shapes, the one for which the energy balance gave the lowest frequency was the correct shape. He also published a modified equation, accounting for the effect of rotatory inertia, but, considering this effect negligible, did not emphasize it.

Timoshenko formulated the shear flexibility term for Rayleigh's basic equation, and this set down the well known Timoshenko mechanism, which considers the contribution of bending, shear, and rotatory inertia. While this formulation is the most complete available, it is complex and difficult to solve exactly, even for a uniform beam, and in recent years a number of papers have been devoted to this solution, generally involving Laplace transforms or series solutions. 11, 33, 34, 63, et.al.

Interest in the non-uniform beam inspired work along different lines, since a beam with a general distribution of mass, inertia, and section area is not amenable to exact solution. One approach is to attempt to formulate one or more of these distributions into expressions suitable for analytic

* Numbers in brackets refer to references listed in Appendix F.

I. INTRODUCTION

A. Historical

For the last seventy years, the subject of vibrations of ship hulls has attracted ever increasing interest from the naval architect. Early investigators, notably Otto Schlick, emphasized the propulsional treatment but as examples in the structure of a large ship, and so varied its design features, that it became clear that this approach would not fully serve the need. Ultimately then, we must look to the theoretical approach for the development of adequate formulations.

Basically, the ship is considered a slender free-free elastic beam, vibrating transversely in its long axis, for which the theory stems from Lord Rayleigh. [8]* From early investigations he developed the basic equation based on simple bending. He then showed that for various assumed mode shapes, the one for which the energy balance gave the lowest frequency was the correct shape. He also published a modified equation, accounting for the effect of rotatory inertia, but, considering this effect negligible, did not emphasize it.

Timoshenko formulated the basic differential term for Rayleigh's basic equation, and this is done (as well known Timoshenko contributor, which considers the contribution of bending shear, and rotatory inertia. While this formulation is the most complete available, it is complex and difficult to solve exactly, even for a uniform beam, and to extend [illegible] a number of plate like [illegible] to this solution. Generally involving [illegible] replace translations or motion relations. [7, 33, 34, 37, 38, et al.

Interest in the non-uniform beam problem has also [illegible] since a beam with a general distribution of mass, inertia, and section area is not amenable to exact solution. One approach is to attempt to approximate one or more of these distributions into equivalent uniform [illegible]

* Numbers in brackets refer to references listed in Appendix F.

treatment by operational calculus, e.g. [9, 10, 35, 37] . However, it is evident that a reasonably accurate method of solution which is unrestricted in its application, i.e., can treat completely general distributions of structural characteristics, has advantages over any isolated analytical solution, however rigorous. Thus we shall consider the iterative methods, both graphical and tabular.

Stodola's work on turbines [8] suggested treating non-uniform beams by integrating Rayleigh's differential equation numerically or graphically. His methods also included the use of the funicular polygon, and Rayleigh's rule of minimum frequency. In using the successive integration method, he observed that while the two-noded mode behaved well, a three-noded starting assumption diverged during iteration until it returned to the two-noded mode; he failed to recognize the mutual orthogonality of normal modes. Vianello introduced this method into general use in the field of engineering, and J. L. Taylor and Schadlofsky applied it to ships (illustrated in [68] , as is Lewis's tabular method). All worked primarily with the first, or two-noded mode, and employed the simple-bending form of the equation of Rayleigh, though Taylor recognized the importance of Timoshenko's shear term in ship vibrations. Koch [2] proved the convergence of the method, and more important, demonstrated the necessity of rigorously maintaining orthogonality with all previous modes throughout the iterative method.

Murray demonstrated the importance of transverse shear in ship vibrations [70], and introduced this effect into Schadlofsky's method, (rather than applying it as a subsequent correction to frequency as did McGoldrick [68]). This refined method, first employed by Murray and the authors in work on a submerged submarine [71], was noted also for a method of determining the slope axis by integration by parts of the

expression for orthogonality with rigid body rotation (pitch and yaw), and for calculation of higher modes than the first, facilitated by application of Koch's intermode orthogonality conditions.

Other graphical methods have been employed by Southwell, Gumbel, Morrow, and others, but were suitable generally for the first mode only.

Recently the principles employed in these iterative methods have been applied to lump parameter formulations for solution by sequence controlled digital calculators or by electrical analogy. [56, 67, 69]. In particular, Prohl and Myklestad developed finite difference equations for use in the Taylor Model Basin digital computer, taking account of simple bending, shear deflection, and rotatory inertia. Calculations made by this method for vibration in the vertical plane for the attack transport U.S.S. NIAGARA with and without the secondary effects (shear flexibility and rotatory inertia) were compared with experimental data. The increasing importance of secondary effects with increasing frequency was demonstrated, but for this vessel rotatory inertia was relatively unimportant in the vertical plane.

B. Objective

This investigation is concerned specifically with transverse vibration in the horizontal plane of a submerged submarine. Recent interest in the bodily response of a submarine to dynamic loading such as that accompanying a non-contact underwater explosion has led to the development of methods of modal analysis. These methods, and other demands of modern ship design, have underscored the inadequacy of older established methods of determining natural modes of response of a ship.

In particular, then, the object of this investigation was to establish and demonstrate a method of determining, as accurately as possible, the curvature pattern, deflection pattern, and natural frequencies of the normal

modes of interest in a transversely vibrating submarine of general mass, inertia, and section area distribution. Further, the method was to be capable of execution without resort to such expensive mechanisms as digital computers.

C. Method:

The method arrived at is basically similar to that of Schadlofsky [68], involving iterative cycles operating on an assumed deflection pattern, each cycle comprising the four successive integrations suggested by Rayleigh's equation. The Timoshenko shear deflection correction is made to the slope obtained from bending, and the rotatory inertia correction of Rayleigh is made to the derivative of the moment. Koch's orthogonality checks are made to filter out components of all lower modes, and Murray's slope axis determination is employed. Integration is performed by integraph (Plate I), and calculations by commercial desk calculator. The method is demonstrated for the first three normal modes, using structural data from an existing three-eighths scale model of a submarine, including an allowance for entrained water.

Shear lag, and the possible interaction between shear deflection and rotatory inertia are not considered.

It is noted that the problem is formulated as an eigenvalue problem, in which solutions exist only for a discrete set of squared frequencies, each of which corresponds to a particular mode pattern, except that the zero eigenvalue indicates both translational and rotational vibration of the rigid body.

c. Method:

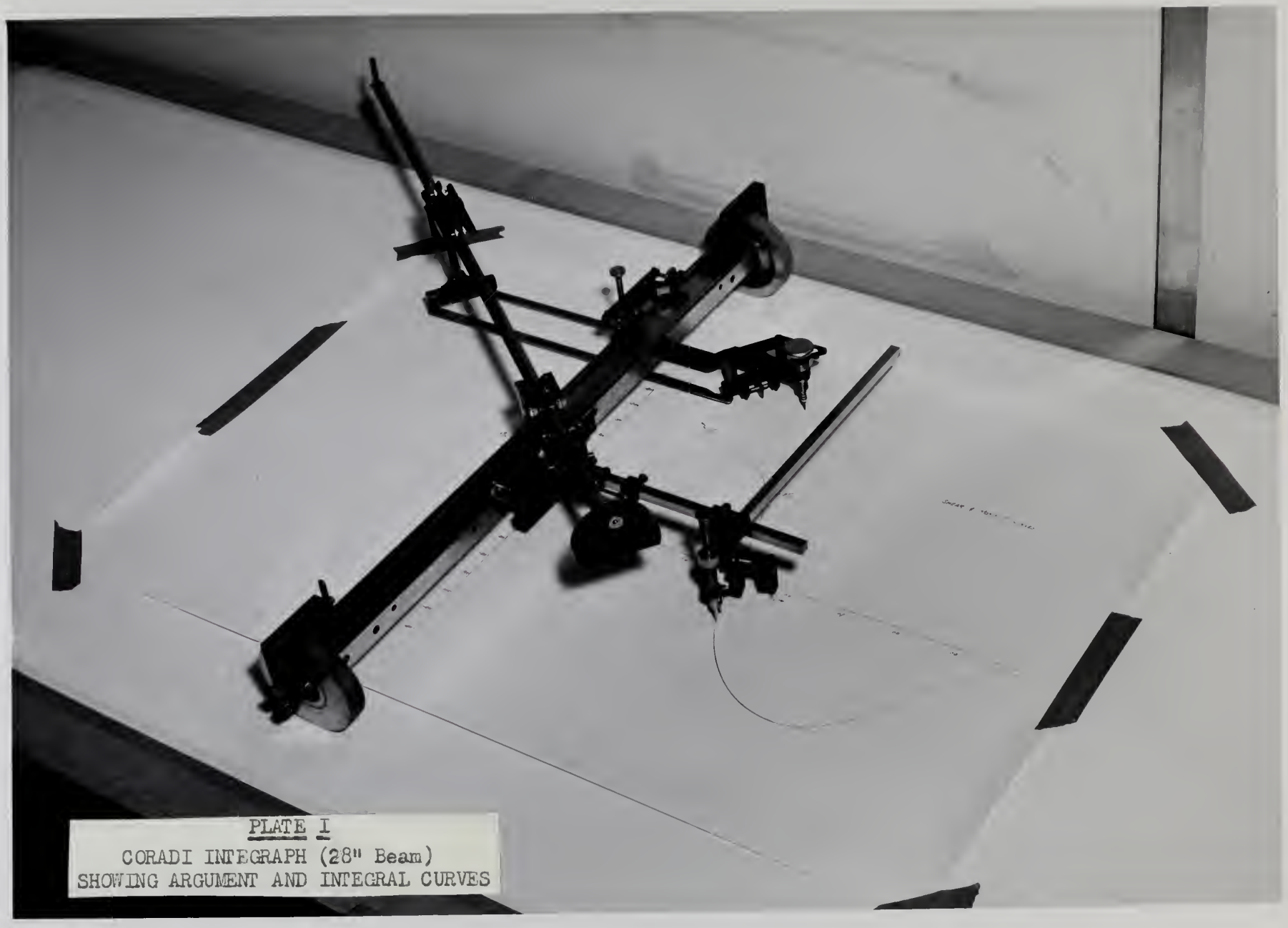

PLATE I

CORADI INTEGRAPH (28" Beam)
SHOWING ARGUMENT AND INTEGRAL CURVES

II PROCEDURE

The basic theory of vibration of a non-uniform, transversely vibrating beam as formulated by Lord Rayleigh, considering only the simple bending effect, can be expressed briefly by:

$$-\frac{\partial^2}{\partial x^2}\left(EI\frac{\partial^2 y}{\partial x^2}\right) = -my\omega^2 \qquad (1)$$

where the assumption of simple harmonic motion of circular frequency has been incorporated. Four successive integrations with respect to this equation comprise the framework upon which the iterative method of this investigation has been developed. The deflection and frequency included in the inertia loading term on the right side of (1) are assumed values, and the deflection indicated on the left, obtained by the quadruple integration, is the first estimate of the true deflection pattern. The first estimate of the square of the true circular frequency is obtained by comparison of the assumed and derived deflection antinodal amplitudes, i.e.,

$$(\omega^2)_{final} = \frac{(\omega^2 y^*)\ start}{(y^*)\ final} \qquad (2)$$

Note also that the second integral of inertia loading, which is the curve of bending moment, must be divided by the curve of local flexural rigidity before the last two integrations are performed, since EI is a variable in x.

We first modify the process by applying to the shear curve yielded by the first integration a correction for rotatory inertia, as follows:

$$\frac{dM}{dx} = Q - \frac{Im\gamma}{A} \qquad (3)$$

where γ is the bending component of slope. Since this quantity occurs later in any iterative cycle than M, we must use the γ value from the previous cycle as a best approximation. Thus this correction is not made

II PROCEDURE

The basic theory of vibration of a non-uniform, transversely vibrating beam as formulated by Lord Rayleigh, considering only the simple bending effect, can be expressed briefly by:

$$-\frac{g_{x_2}}{g_{x_1}}\left(EI\frac{g^2_{x_1}}{g^2_{x_2}}\right) = -\omega^2_{x_2} \qquad (1)$$

where the assumption of simple harmonic motion of circular frequency has been incorporated. Four successive integrations with respect to this equation compare the framework upon which the iterative method of this investigation has been developed. The deflection and frequency included in the inertia loading term on the right side of (1) are assumed values, and the deflection indicated on the left, obtained by the graphical integration, is the first estimate of the true deflection pattern. The first estimate of the square of the true circular frequency is obtained by comparison of the assumed and derived deflection ampli tudes, i.e.,

$$(\omega_2)^2_{(true)} = \frac{(y_1)_{(true)}}{(y_2)_{(true)}}(\omega_1)^2 \qquad (2)$$

Note also that the second integral of inertia loading which is the curve at bending moment, must be divided by the curve of local flexural rigidity before the last two integrations are performed, since EI is a variable in x.

We first modify the process by applying in the shear curve yielded by the first integration a correction for rotatory inertia, as follows:

$$\frac{dy}{dx} = \Omega - \frac{\int m\lambda}{g} \qquad (3)$$

where λ is the bending component of slope. Since this primarily occurs later in any iterative cycle than 1, we must use the λ value from the previous cycle as a best approximation. Thus this correction is not made

until the second cycle of each mode.

The second modification of the process is the correction of the slope curve obtained by integrating the curvature distribution. This correction introduces the effect of shear flexibility, and the total slope resulting is expressed by:

$$\eta' = \gamma + \beta \tag{4}$$

where

$$\beta = \frac{Q}{KAG} \tag{5}$$

Here the shear value Q has been obtained before the slope calculation, and the correction can be made in each cycle.

Application of boundary conditions and orthogonality conditions, including orthogonality (with respect to mass) with the zero eigenvalue motions and with all modes below the one being obtained, at the appropriate points in and after each cycle, determine the four constants of integration, and refine the pattern obtained from the iterative cycle.

In this investigation, since mass and flexural and shear rigidities have general, hence irregular distributions, analytical integration was not possible. The process was therefore carried out in each instance by means of a mechanical integraph with a 28" carriage beam (manufactured in Switzerland by G. Coradi). This instrument draws an integral curve when its stylus is made to trace the argument curve (Plate I). All calculations have been carried out and plotted at intervals of one-fortieth of ship length, as this was found to be the greatest interval which would detect important variations in the functions used.

The sequence of operations is asfollows:

(1) The structural characteristics needed are computed from available plans and tabulated (Appendix E).

analysis given and tabulated (Appendix E).

(2) A tabulation of functions of structural characteristics and of the centroid of virtual mass which will be used throughout the work is prepared. (Table IV, Appendix C). To this table are added a tabulation of a function of each modal deflection pattern obtained, for use in orthogonalizing subsequent modes.

(3) A tabulation of constants computed for repeated use is prepared (Table V, Appendix C).

(4) A tabulation of the Rayleigh mode patterns (obtained from application of his simple-bending theory for a uniform slender beam) is prepared, for all modes to be obtained. These are normalized patterns.

(5) The Rayleigh pattern for the mode being calculated is orthogonalized with translation, rotation, and all previous modes (there would be none for the two-noded mode). In practice, the Rayleigh pattern need not be used; any curve of the correct general shape is suitable for a starting guess, and the better the guess, the more rapid the conversion to an acceptable solution. Perhaps the best choice would be the pattern from a similar ship, if such is available.

The resulting orthogonalized pattern will now be used as a starting point of the iterative process.

(6) Inertia loading based on this pattern is computed and plotted as a function of X/L along the length of the ship.

(7) This is integrated to obtain shear, to which is added the rotatory inertia term, giving the derivative of bending moment. (In the first cycle of each mode shear is the differential of bending moment). M' is plotted.

(8) M' is integrated, and the integral curve is divided, at each station, by flexural rigidity to obtain curvature, which is plotted.

(9) Curvature is integrated to obtain the bending component of slope to within a constant.

(10) Shear is divided by shear rigidity, and the resulting shear slope is added to the bending component, and the total is used in an auxiliary process to determine a constant which locates the axis (the constant of the integration in (9)), which is added also, to give total slope . This is plotted.

(11) Slope is integrated to give the deflection pattern to within an additive constant, which is used in an auxiliary process to obtain the axis shift. The resultant deflection pattern is tabulated.

(12) This pattern is now submitted to the same orthogonality checks used on the starting guess. The corrected curve is normalized to give a pattern whose value is unity at the center - or center-most-after-antinode. The unnormalized value at this antinode is retained for use in the frequency calculation. The normalized pattern becomes the basis of the inertia loading for the next cycle, or is accepted as the final pattern. This decision is based on the amount of change of deflection pattern and frequency between this cycle and the previous one.

(13) Frequency is obtained by equation (2), where $(y^*)_{start} = 1$, and $(y^*)_{final}$ is the unnormalized antinode deflection retained in (12).

(14) In the final cycle of each mode, the curvature pattern is normalized by dividing throughout by $(y^*)_{final}$ and retained as the final curvature pattern.

(15) The shear slope distribution is subtracted from the corrected total slope distribution to give the corrected bending slope. This

is normalized by division by (y*) final and retained for use in the rotatory inertia correction of the subsequent cycle.

(16) The pattern obtained in (12) is now used to repeat the entire cycle, if deemed necessary.

Appendix A, Part 1 contains the derivations of the important relations used. Part 2 is a detailed outline of the procedure, containing formulations of all operations as used in the application of the method illustrated in Appendices B and C.

The method was executed using structural data for a three-eighths scale model of a submarine, and three lateral modes were computed, each having been carried through three cycles of iterations, this being sufficient to show convergence of the method and to reduce residual error, as indicated roughly by the last increment of change, to an acceptable level.

III RESULTS

By observation of the convergence of the results of iteration, patterns, normalized to give a value of unity at the center or centermost after antinode, are presented in Figure XXXIII. The corresponding curvature patterns, from which strain patterns can be obtained, were normalized in such a manner that when the factor between normalized deflection and true deflection maxima has been obtained, this same factor multiplied by the normalized curvature pattern will give the maxima of the true curvature pattern, all dimensions being consistent. These patterns are presented in Figure XXXIV.

Table I gives the final frequencies and periods of the three modes calculated for the model:

TABLE I

NATURAL TRANSVERSE FREQUENCIES AND PERIODS FOR 100.5 FOOT SUBMERGED SUBMARINE MODEL

Mode	Natural Freq. (cpm)	Ratio	Period (milliseconds)
1	417	1	143.9
2	839	2.01	71.5
3	1391 *	3.34	43.1

* See supplementary discussion, Appendix D

Table II lists the offsets of the normalized deflection and curvature patterns pictured in Figures XXXIII and XXXIV.

As to the method developed, it was found to be convergent, though it appears that the delayed introduction of rotatory inertia into the process must act to delay convergence. This is compensated for by the frequent orthogonality checks, especially their application to the starting pattern.

The results and method are discussed in the subsequent section.

III

by observation of the convergence of the results at iteration,
patterns, maintained to give a value of unity at the center. Re-
centro-symmetrical plate vibrations, four modes already published
be omitted, were encountered in which a nodeless line was the locus
between successive deflections and thus deflecting portions had zero
obtained, this zero factor multiplied by the mentioned curvature pattern
will give the position of the true curvature pattern, all dimensions
being convenient. These patterns are presented in Figure XXXIV.

Table I gives the final frequencies and periods of the three modes
calculated for the model.

Table I

RATIO: 12 INCH/SEC PRODUCTION AND PERIOD
FOR 1/8 INCH BORDER SUPPORTED MODEL

Mode	Frequency (cps)	Ratio	Period (milliseconds)
1	617	1	163.9
2	497	2.86	71.3
3	1914	3.34	43.1

* See application discussion, Appendix D

Table II lists the ratios of the mentioned deduction and curvature
patterns pictured in Figures XXXIII and XXXIV.

As to the method of solving, it was found to be convergent, though
it appears that the desired interaction of tendency towards the pre-
vious mode must act to delay convergence. This is counteracted by the
scoring pattern.

The results and method are discussed in the subsequent sections,

TABLE II

ORDINATES OF NORMALIZED DEFLECTION AND CURVATURE PATTERNS

x/l.	y_1	y''_1	y_2	y''_2	y_3	y''_3
0.000	-3.408	0	+3.041	0	+3.925	0
0.025	3.054	- 258	2.578	+ 349	3.116	+ 1916
0.050	2.695	947	2.101	2440	2.231	9581
0.075	2.347	1614	1.609	4792	1.430	14371
0.100	1.994	1840	1.161	6142	0.729	15808
0.125	1.641	2117	0.726	6515	+0.102	16968
0.150	1.299	2368	+0.336	6761	-0.417	16727
0.175	0.988	2554	-0.018	6987	0.808	15751
0.200	0.682	2811	0.307	7316	1.074	15005
0.225	0.395	3076	0.567	7506	1.178	13877
0.250	-0.125	3374	0.762	7589	1.158	11536
0.275	+0.109	3644	0.891	7527	1.071	9337
0.300	0.325	4054	0.963	7541	0.862	6815
0.325	0.511	4513	0.977	7474	0.596	3896
0.350	0.661	4921	0.940	7074	-0.295	+ 489
0.375	0.788	5093	0.845	6138	+0.036	- 2801
0.400	0.878	4468	0.706	4352	0.330	4852
0.425	0.944	3240	0.532	2295	0.602	4899
0.450	0.987	2836	0.336	1317	0.793	5445
0.475	1.000	2832	-0.133	+ 588	0.928	5977
0.500	0.989	2842	+0.085	- 154	0.996	6130
0.525	0.965	3361	0.302	1076	0.975	6860
0.550	0.912	4517	0.519	2627	0.875	8160
0.575	0.835	5131	0.693	4400	0.677	7271
0.600	0.711	5019	0.838	5625	0.417	4458
0.625	0.568	4763	0.938	6576	+0.083	- 861
0.650	0.383	4502	0.995	7397	-0.275	+ 3024
0.675	+0.169	4309	0.987	8124	0.655	6922
0.700	-0.087	4018	0.920	8658	1.002	10868
0.725	0.350	3727	0.780	8860	1.227	14653
0.750	0.654	3367	0.582	8808	1.373	17691
0.775	0.976	3045	+0.304	8570	1.389	20157
0.800	1.310	2648	-0.024	7845	1.281	21278
0.825	1.662	2365	0.411	7405	0.951	22813
0.850	2.032	2259	0.849	7406	-0.487	25419
0.875	2.389	2778	1.337	9187	+0.155	34836
0.900	2.783	3341	1.883	10760	1.044	44791
0.925	3.207	2368	2.503	7843	2.297	39530
0.950	3.624	1036	3.174	2091	3.711	21556
0.975	4.066	- 129	3.808	-5228	5.154	+ 1437
1.000	-4.502	0	-4.450	0	+6.590	0

TABLE XI

[illegible]

[illegible]	[illegible]	[illegible]	[illegible]	[illegible]	[illegible]	[illegible]
[illegible]	[illegible]	[illegible]	[illegible]	[illegible]	[illegible]	[illegible]

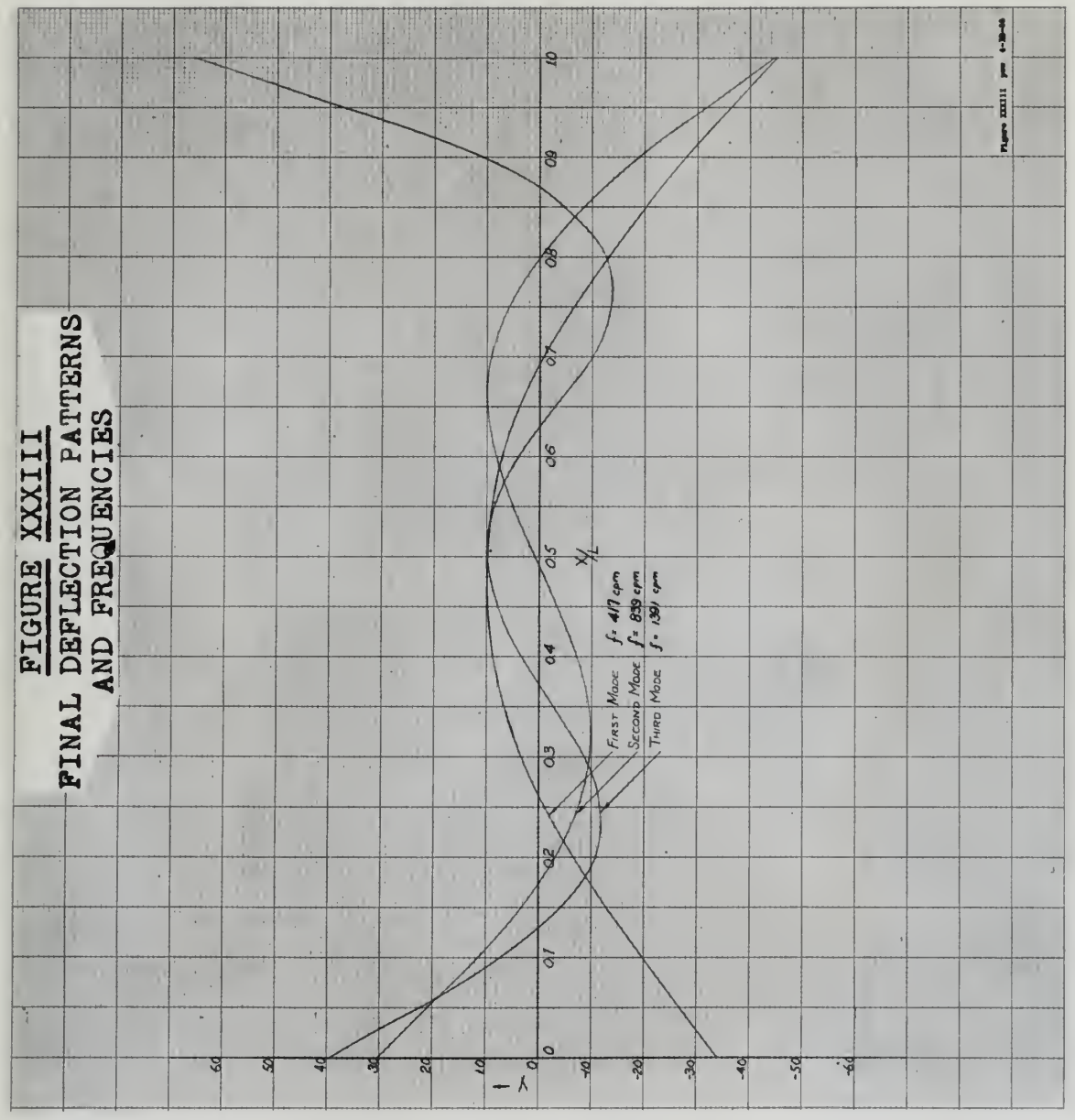
FIGURE XXXIII
FINAL DEFLECTION PATTERNS
AND FREQUENCIES
Y
X/L
FIRST MODE f= 417 cpm
SECOND MODE f= 839 cpm
THIRD MODE f= 1391 cpm

IV. DISCUSSION OF RESULTS

A. Mode Patterns:

The shape of the mode patterns (Figure XXXIII) generally met the authors' expectations. In ships and submarines, both the mass and flexural rigidity are greater at the midsection than at the ends. This has the effect of altering the mode shape so that the center deflections are smaller relative to the end deflections than in a uniform beam, and the nodal points are closer to the midship section. For example, for the first mode, the center deflection maximum of the uniform beam amounts to 60% of the end deflection, while in the case of the submarine studied, the anti-node deflection was 29.4% of the bow deflection and 22.8% of the stern deflection. The nodes for the uniform beam occur at 22% from the ends, while for the submarine investigated, they occurred at 26.2% from the bow and 30.7% from the stern respectively.

Figure I clearly demonstrates the pronounced increase in mass, sectional area, moment of inertia, and shear factor K in the vicinity of the hard tank and conning tower amidships in the case of the submarine. One can readily arrive at two consequences of this discontinuity of structural strength. The first of these has already been mentioned - that of the very high end deflections relative to those in the middle body. This behavior will obviously occur for all the modes, with the resulting trend towards patterns with many small loops in the middle with large end branches. It is easy to see how any loading, such as an explosion, occurring in the middle body of a submarine can incur very large deflections at the ends with attendant small deflection near the load. In the case of the third mode, the deflection at the stern will be six times that at the center! The reader will readily appreciate the importance of this characteristic of the mode patterns with respect to the bodily

IV. DISCUSSION OF RESULTS

A. Mode Patterns:

response of submarines. Severe whipping may be expected to occur whenever the contributions of the odd and/or even numbered mode end deflections become additive for any general vibratory motion of the submarine.

The second consequence of the irregular distribution of structural characteristics becomes manifest in the effect of rotatory inertia and shear flexibility. For a given structure mass per unit length, a submarine will be many times stiffer than a solid prismatic bar, since in the case of the former, the crossection is essentially a circular ring of material relatively distant from its centroid. This fact, coupled with that of the nature of the longitudinal distribution of flexural rigidity, explains why the magnitude of the rotatory inertia correction to the frequency of the first mode is somewhat greater for the submarine than for the uniform beam or even a surface ship. Its increased moment of inertia for a given mass/ft is compared to the uniform beam results in larger values of $\frac{Im}{A}$. Even for equal slopes, the rotatory inertia correction would be larger for the submarine. However, the increased flexibility of the end sections over their uniform beam counterparts causes the slope to increase over all the length of the submarine, the greatest increase occurring between the ends and the nodes. The steepness of all the deflection patterns near the ends results in a rather selective effect of rotatory inertia upon the patterns. In general, the effect of rotatory inertia upon the mode patterns studied was most pronounced at the ends, and resulted in an increase in the relative deflection. A comparison of experimental and theoretical mode patterns for a similar submarine where rotatory inertia was neglected in the latter calculation, shows larger experimental end deflections than the theory predicted. The authors feel that such a discrepancy may be due to the application

of an incomplete theory, particulary in the light of the results of this thesis.

Shear flexibility apparently causes little change in the shape and magnitudes of the normalized mode patterns. The shape of the KAG curve (Figure I) indicates that the location of maximum shear near the quarter points of the submarine will produce the largest value of shear slope. Actually the percent contribution to y' of shear slope was much more uniform over the full length of the submarine than was expected. This accounts for the small effect of shear deflection on the normalized patterns. As was expected, the value of β increases with increasing modes numbers, and thus the effect of shear deflection upon frequency becomes more important with increasing mode number. Frequency behavior is discussed more fully in a subsequent section. It should be mentioned, however, that with the third mode, the percentage of shear component of slope gave indications of becoming larger in the region of the middle body, where the greatest effect on ω^2 will result.

B. Curvature Patterns:

The curvature patterns, Figure XXXIV, clearly indicate possible regions of structural weakness with respect to resistance to damage from whipping. In particular, it appears that excessive strain can be expected at about X/L = 0.9 in the event of third mode whipping of significant magnitude* The magnitude of the strain wire, of course, also depends upon the radius of the submarine hull at this location.

* Note that the rudder, propellers and shafting add mass with little attendant increase in stiffness in this part of the submarine.

of an incompressible theory, particularly in the light of the results of this thesis.

Sheet flexibility apparently causes little change in the shape and magnitudes of the normalized mode parameters. The shape of the MAC curve (Figure 5) indicates that the location of maximum sheet bear the quarter points of the sweepwise will produce the largest value of sheet slope. Naturally the percent contribution to γ' of sheet slope was much more sensitive over the full length of the sweeping than was expected. This accounts for the small effect of sheet deflection on the normalized patterns. As was expected, the value of β increases with increasing modes sweep, and thus the effect of sheet deflection upon frequency becomes more important with increasing mode number. Frequency behavior is discussed more fully in a subsequent section. It should be mentioned, however, that with the third mode, the percentage of sheet contribution of slope gave indications of becoming larger in the region of the middle body, where the greatest effect on ω_r will result.

6. Curvature Patterns

The curvature patterns, Figure XXXIV, clearly indicate possible regions of structural weakness with respect to resistance to damage from whipping. In particular, it appears that excessive strain can be expected at about $X/L = 0.3$ in the event of third mode whipping of significant magnitude. The magnitude of the strain will, of course, also depends upon the radius of the sweepwise bend at this location.

* Note that the rudder, propellers and shafting add mass with little attendant increase in stiffness in this part of the sweepwise.

Except for the apparent deficiency just noted, the structural design of the submarine appears to be quite well balanced. The general shape of the curvature patterns obtained by the authors agrees quite favorably with experimentally determined curvature patterns of similar submarines.

C. Frequencies:

Frequency behavior observed in this investigation generally confirmed expectations based on theoretical consideration of the secondary elastic effects. Exact breakdown of these effects is not available in that no complete iterative calculation was conducted without these effects. Although the first cycle of each mode involved no rotatory inertia effect, it cannot be considered as yielding a useful figure for comparisons, because of the predominating effect of the starting estimate curve. However, if we accept these first cycle frequencies for a qualitative examination (Table III, Appendix B), we see the expected drop in frequency when rotatory inertia is introduced, of magnitude greater than what can be attributed to convergence alone. It further appears to be of increasing importance with higher modes.

Data showing the independent effect of shear flexibility is not available, but preliminary investigations summarized in reference [71] showed a similar depression in frequency when this effect was introduced, although the effect was separated for the first mode only. This is generally considered to be of increasing importance for higher modes.

The cumulative result of these effects is noted in the fact that experimentally determined natural frequencies correspond more nearly to the series 1, 2, 3, than to the 3^2, 5^2, 7^2, series obtained theoretically from a uniform beam without secondary effects. [69] This same tendency is observed in the frequencies obtained in this investigation, which were seen

in Table I to correspond to the series 1, 2.01, 3.34, or, for contrast, expressed in the second form; 3^2, 4.25^2, 5.2^2.

However, comparison with results of earlier computations for the same model, but without the rotatory inertia effect, cast some doubt on the accuracy of the third mode frequency of 1391 cpm, indicating it is perhaps too high. This suspicion is reinforced by the 3.34 value in the above series. The error (probably amounting to less than 4%) is considered to be due to the fact that the intermode orthogonality check as formulated is inexact for other than the trivial modes, and the error becomes of some importance for the third and higher modes. The more correct formulation is developed in Appendix D, and the third mode frequency corrected by its partial application.

D. Sources of Error:

Several sources of error arise from fields the detailed consideration of which is beyond the scope of this thesis, but are noted for completeness.

The first of these stem from the information included as Structural Data, found in Appendix D. A submarine, though more regular in design than a surface ship, is a complex structure, and the participation of its components in carrying the loading are more difficult to analyze than simple beam theory suggests. Therefore agreement is hard to find as to which members should be included in calculating moment of inertia, cross sectional area resisting shear, and the shear distribution coefficient K.

Far more controversial is the matter of entrained water; here it is especially difficult to verify a given theory because vibration theory is not sufficiently refined to permit separating out other effects which inter act with the manifestations of entrained water.

Both of the above questions have been sidestepped by utilizing data already calculated from plans, based on the assumptions outlined in

In Table I is interpreted as the series 1, 2.01, 3.34, or, for convenience, expressed in the normal form 1^2, 4.29^2, 9.3^2.

However, comparison with results of earlier computations for the same model, but without the rotatory inertia effect, case above 90 the accuracy of the third mode frequency (4.29^2 obs. indicating it is perhaps too high. This overlong is explained by the 1.34 value in the above series. The error (presently amounting to less than 4%) is considered to be due to the fact that the instantaneous eccentricity effect as for instance is (Section 3) for other than the trivial modes, and the error becomes of minor importance for the third and higher modes. The more correct identification is developed to appendix D, and the third mode frequency corrected by its partial application.

2. Sources of Error.

Several sources of error arise from fields the detailed consideration of which is beyond the scope of this thesis, but are noted for completeness. The first of these arises from the interpretation involved as structural data, found in appendix B. A secondary, though more regular in design than a surface ship, is a coming structure, and the partitioning of its components in carrying the bending and more difficult to analyze than simple beam theory suggests. The relative agreement is hard to find as to which dimensions should be included in calculating moment of inertia, cross sectional area retaining power, and the shear distribution coefficient K.

For many configurations in the region of maximum water, here it is especially difficult to verify a given theory because rotation theory is not sufficiently refined to permit explaining why other effects work together with the combinations of opposing ones.

Most of the above questions have been accounted by utilizing data already calculated from plans, based on the assumptions outlined in

Appendix E. It is not to be inferred that these matters are insignificant; they are vital to any prediction of vibration, and are the subject of considerable study.

It has been assumed that deflections are small and that the proportional limits have not been exceeded. Standard values of Young's Modulus and Poisson's Ratio have been assumed. Any departure from these assumptions in a ship tested experimentally can be expected to cause discrepancies.

The second group of errors can be traced to the procedure and to its execution.

First, failure to carry the iteration through sufficient cycles leads to an error. The residual error after a given number of cycles will be large if (a) the starting assumption of deflection was grossly in error, or (b) if orthogonality checks were not properly and regularly applied. An error was introduced also by the application of the inexact orthogonality formulation.

Next, the rotatory inertia term, being based necessarily on data from a previous cycle, is slightly in error.

Further, the failure to make this correction in the first cycle results in a discrepancy which will take several cycles to eliminate entirely.

Shear lag, and probably other lesser effects, have not been considered.

Integraph operation involves some small error. This is periodically filtered out by boundary conditions and other checks, but some residue necessarily remains. In particular, a small amount of lost motion was noted in the integraph used.

Any error in developing a given mode pattern will result in a small error in each subsequent pattern, through the intermode orthogonality checks, which necessarily employ the ordinates of previously determined modes.

Finally, the usual remarks concerning human error in computing values, and in plotting, integrating, and reading curves. It is noted, however, that the method by nature tends to reject such errors or to make them immediately obvious as the technique becomes familiar.

E. Applicability:

The method of this paper is not envisaged as replacing the rather advanced techniques of digital computers and electrical analogs. It may well complement them to some degree, but is intended primarily to serve the needs of the smaller research facility which, operating on a limited budget, is faced with the necessity of performing such determinations with simpler tools. Integraphs of the type used are found in a number of educational institutions, design offices, and shipyards, but the authors have reason to believe that more than a few of them lie neglected beneath at least a decade's accumulation of dust. The only other tool needed is an automatic or semi-automatic commercial desk calculator. It is considered that the work can be set up on appropriate forms in such a manner that a mathematics aid or junior research assistant can carry it out without special training and under only a modicum of supervision.

V. CONCLUSIONS

Convergence of the iterative method, with secondary effects, as developed in this thesis appears satisfactory, and any tendency towards instability is held in check by periodic application of orthogonality conditions. The method inherently detects and filters out errors, so that a mistake in an early cycle does not invalidate subsequent cycles of the same mode, but may delay convergence slightly.

While the procedure appears complex, it can be programmed on standard forms for application by research assistants without special knowledge of vibrations or advanced mathematics. Equipment required is standard to many installations and inexpensive relative to such special equipment as digital computers.

Results of this method appear to be acceptable; the third mode frequency is considered accurate to within 2.6% after three iterative cycles, while earlier modes, having attained better convergence in the same number of modes, are considerably more accurate.

The secondary effects are considered to have been adequately accounted for, with little added complication to the process. In particular, rotatory inertia appears to have had a somewhat greater effect than has been evidenced in studies of uniform beams; end deflections are seen to be increased relative to antinodal excursions when the effect is considered. Secondary effects thus are included not only in frequency determination, but also in deflection and curvature patterns.

A clear indication of highly loaded sections is presented by the normalized curvature distributions which result directly from the process. Structural inadequacies are thus pointed out.

It thus appears that the method developed is well suited to the purposes of small facilities conducting vibration research on limited budgets, where accurate theoretical determination of information on natural modes is needed.

V. CONCLUSIONS

VI RECOMMENDATIONS

It is recommended that the method for modal calculations which is described in this thesis be considered by small research activities for similar work. As a general rule, such activities operate under a rather limited budget with correspondingly small allocations for computing equipment of the analog or digital types. On the other hand, most of these activities will certainly own more than one desk calculator and will have the funds available for the purchase of an integraph in the event that one is not owned. At least for the modes of interest, the method used by the authors appears more than satisfactory from the standpoint of moderate equipment costs, simplicity, and availability. Digital computers are in ever increasing demand, and the delay involved in obtaining results from a central calculating contractor may be unacceptable for the small research organization. The method is clearly not competitive with that of the digital computer when the latter is readily available and a large number of mode patterns is desired.

Experimental corroboration of the authors' results would be highly desirable before the method is accepted for general application. For any given submarine design this can be accomplished by mechanical excitation of a model of the proposed vessel, provided it is of sufficiently large scale to assure structural similarity.

It is further recommended that the effect of rotatory inertia as well as shear deflection be included in the natural mode calculations regardless of the method used.

In any future application of this method, it is recommended that the more exact orthogonality conditions which arise from the inclusion of rotatory inertia effects be applied. While it is more convenient to neglect them, such practice may result in the loss of refinements, especially in the higher modes, which are of the same order of magnitude as

VI. RECOMMENDATIONS

the rotatory inertia corrections themselves.

The effect of shear lag in ship-type structures upon their vibration behavior should be investigated.

the rotatory inertia corrections themselves.

The effect of shear lag in skip-type structures upon their vibration behavior should be investigated.

VII APPENDIX

APPENDIX A

PART 1

Theoretical Basis :

The submarine is initially considered to behave as a long, thin beam with vanishing shear force and bending moment. Under this assumption, then, the classical theory of the lateral vibration of a free-free non-uniform bar applies. [6],[9] . We are concerned here with the normal modes of vibration. When a bar vibrates in one of its normal modes, the deflection at any location varies harmonically with time. If damping is neglected, the lateral displacement of the bar can be represented by :

$$y = X (A \cos \omega t + B \sin \omega t) \qquad (6)$$

where X is a function of the coordinate x, and determines the shape or pattern of the normal or natural mode of vibration which we are considering. X is known in the literature as a "normal" or "natural" function .

It is obvious that any particular normal mode of vibration is characterised solely by X_i and the frequency of that mode, ω_i . By superimposing all possible normal modes of vibration, the general expression for the free lateral vibration becomes:

$$y = \sum_{i=1}^{i=\infty} X_i (A_i \cos \omega_i t + B_i \sin \omega_i t) \qquad (7)$$

In order to calculate a normal mode pattern, one must resort to beam flexure theory. The simple (Euler) theory of bending may be assumed to hold if the vibration occurs in one of the principal planes of flexure of the bar, and if the crossectional dimensions of the bar are small compared to its length. In the actual case of a ship or submarine the first of these restrictions offers no problem, but the second can be unrealistic, particularly for a modern submarine with its "cigar"form and essentially circular sections. Strictly speaking then, the Euler bending theory is not applicable to a

APPENDIX A

Part I

Theoretical Basis

The oscillation is initially considered to behave as a long, thin beam with vertical shear force and bending moment. Under this assumption, then, the classical theory of the lateral vibrations of a free-free member may be applied. [2],[3] . We are concerned here with the normal modes of vibration. When a bar vibrates in one of its normal modes, the deflection at any location varies harmonically with time. If damping is neglected, the lateral displacement of the bar can be represented by :

$$y = X \left(A \cos \omega t + B \sin \omega t \right) \qquad (a)$$

where X is a function of the coordinate x, and determines the shape or pattern of the normal or natural mode of vibration which we are considering. X is known in the literature as a "normal" or "natural" function .

It is obvious that any particular natural mode of vibration is characterized solely by X_i and the frequency of that mode, ω_i . By superimposing all possible natural modes of vibration, the general expression for the free lateral vibration becomes:

$$y = \sum_{i=1}^{i=\infty} X_i \left(A_i \cos \omega_i t + B_i \sin \omega_i t \right) \qquad (1)$$

In order to calculate a natural mode pattern, one must resort to beam theory. The Bright (Duke) theory of vibrating may be assumed to hold if the vibration occurs in one of the principal planes of flexure of the bar, and if the cross-sectional dimensions of the bar are small compared to its length. In the natural mode of a rigid or symmetrical free-free restrictions obtain in practice, but the second has no correlation. Particularly for a modern automobile with its "super-flexible" and essentially discrete members, strictly speaking then, the Euler beam theory is not applicable to a

submarine or even a beam whose cross sectional dimensions are appreciable. For the present, however, we shall use the Euler theory as a beginning and modify it subsequently by a correction for shearing force and rotatory inertia effects.

We refer now to Figure A-1, which is a representation of a non-uniform beam and an element thereof. The symbols are in accordance with the Nomenclature, except that w here is taken as some loading in lb/ft. With the axis oriented as shown, the well known Euler differential equation for the deflection curve is:

$$EI \frac{\partial^2 y}{\partial x^2} = - M. \qquad (8)$$

FIGURE A-1

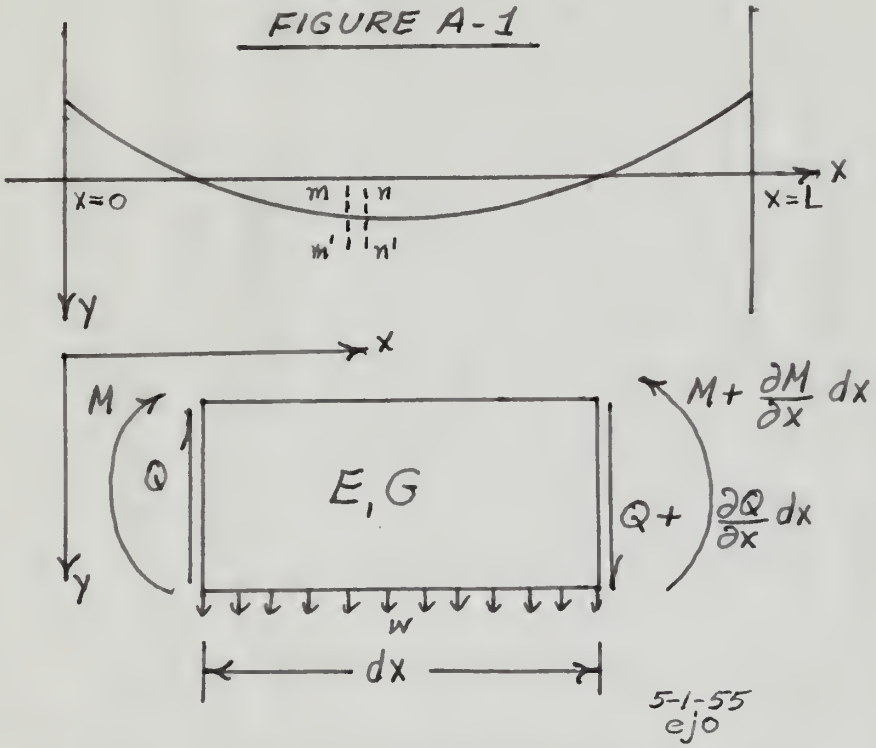

5-1-55
ejo

We differentiate (8) once to obtain the shearing force:

$$\frac{\partial}{\partial x}\left(EI \frac{\partial^2 y}{\partial x^2}\right) = - \frac{\partial M}{\partial x} = -Q. \qquad (9)$$

An additional differentiation yields the loading.

$$\frac{\partial^2}{\partial x^2}\left(EI \cdot \frac{\partial^2 y}{\partial x^2}\right) = - \frac{\partial Q}{\partial x} = w. \qquad (10)$$

FIGURE A-1

Equation (10) is the differential equation of a bar subjected to a continuous load of intensity w. In the case of free lateral vibration, one can apply D'Alembert's principle and replace w by the inertia loading

$$-\frac{m\,\partial^2 y}{\partial t^2} \tag{11}$$

Substituting (11) for w in equation (10), the general equation for the lateral vibration of the bar becomes

$$\frac{\partial^2}{\partial x^2}\left(EI\,\frac{\partial^2 y}{\partial x^2}\right) = -\,m\,\frac{\partial^2 y}{\partial t^2}\,. \tag{12}$$

Finally, since, for simple harmonic motion, $\frac{\partial^2 y}{\partial t^2} = -\,y\omega^2$ (13)

we may write equation (12) as follows:

$$\frac{\partial^2}{\partial x^2}\left(EI\,\frac{\partial^2 y}{\partial x^2}\right) = m\omega^2 y \tag{14}$$

We now return to the reality that the dimensions of the cross section are not small with respect to the length of the bar. Investigation of the effect which the cross sectional dimensions can have on the frequency are incompassed in the classical literature. [6][9][55]. Of these perhaps the most widely accepted is the treatment of the effects of rotatory inertia and shearing force by Timoshenko in reference [9][55]. There are doubtless other effects introduced by the cross sectional dimensions and configuration but for the purposes of this thesis the Timoshenko mechanism was adopted because it accounts for the two major effects mentioned above.

The effects of both rotatory inertia and shear deflection become of considerable importance in the higher modes of vibration where the bar is subdivided into shorter segments by an ever increasing number of nodes. [9][69].

a. Rotatory Inertia :

Refer again to figure A-1. One can easily see how the element dx during vibration not only performs a translatory motion, but can rotate as well. The variable angle of rotation is equal to the slope of the deflection curve, $\partial y/\partial x$, and the corresponding angular velocity and angular acceleration will be given by

$$\frac{\partial^2 y}{\partial x \partial t} \quad , \text{ and } \quad \frac{\partial^3 y}{\partial x \partial t^2} \quad .$$

The moment of the inertia forces of the element about the axis through its centroid perpendicular to the x-y plane will evidently be:

$$dM_r = - \left(I + \frac{\partial I}{\partial x} \frac{dx}{2} \right) \left(\frac{m}{A} + \frac{\partial (m/A)}{\partial x} \frac{dx}{2} \right) \left(\frac{\partial^3 y}{\partial x \partial t^2} \right) dx \qquad (15)$$

(The moment is taken positive when it is clockwise), where m/A is the mass per unit volume of the non-uniform bar.

We now expand (15), and obtain:

$$dM_r = - I \, m/A \left(\frac{\partial^3 y}{\partial x \partial t^2} \right) dx - (dx)^2 \left(\frac{\partial I}{\partial x} \frac{m}{2A} + \frac{I}{2} \frac{\partial}{\partial x} (m/A) + \frac{\partial I}{\partial x} \cdot \frac{\partial (m/A)}{\partial x} \frac{1}{(2)^2} \right) \frac{\partial^3 y}{\partial x \partial t^2} \qquad (15\,a)$$

If we neglect second order and higher infinitesimals,

$$dM_r = \left(- \frac{I \, m}{A} \frac{\partial^3 y}{\partial x \partial t^2} \right) dx \qquad (15b)$$

Remembering again that for simple harmonic motion $\frac{\partial^2 y}{\partial t^2} = - \omega^2 y$, we finally obtain:

$$dM_r = - \frac{Im}{A} \frac{\partial}{\partial x} \left(- \omega^2 y \right) dx = \frac{I \, m \, \omega^2}{A} \frac{dy}{dx} dx \qquad (16)$$

This moment should be accounted for in considering the variation of bending moment along the axis of the bar. Thus, instead of equation (4) we will have:

$$\frac{d M}{d x} = Q + \frac{I \, m \, \omega^2}{A} \times \frac{\partial y}{\partial x} \qquad (17)$$

a. Rotatory Inertia:

Refer again to Figure A-1. One can easily see how the element dz during vibration not only performs a translatory motion, but can rotate as well. The variable angle of rotation is equal to the slope of the deflection curve, $\partial y / \partial x$, and the corresponding angular velocity and angular acceleration will be given by

$$\frac{\partial \dot{y}}{\partial x} \quad \text{and} \quad \frac{\partial^2 y}{\partial x \partial t} \; .$$

The moment of the inertia forces of the element about the axis through its centroid perpendicular to the x-y plane will evidently be:

$$dM_z = -\left(I + \frac{\partial I}{\partial x}\frac{dx}{2}\right)\left(\frac{\rho}{A} + \frac{\partial}{\partial x}\left(\frac{\rho}{A}\right)\frac{dx}{2}\right)\left(\frac{\partial^2 y}{\partial x \partial t^2}\right) dx \qquad (15)$$

(The moment is taken positive when it is clockwise), where ρ/A is the mass per unit volume of the two-member bar.

We now expand (15), and obtain:

$$dM_z = -I\left(\frac{\partial^2 y}{\partial x \partial t^2}\right) dx - \left(\frac{\partial I}{\partial x}\frac{\rho}{A} + \frac{I}{2}\frac{\partial}{\partial x}\left(\frac{\rho}{A}\right)\right)\left(\frac{\partial^2 y}{\partial x \partial t^2}\right) dx \qquad (15a)$$

If we neglect second order and higher infinitesimals,

$$dM_z = -\left(I\frac{\rho}{A}\right)\left(\frac{\partial^2 y}{\partial x \partial t^2}\right) dx \qquad (15b)$$

Remembering again that for simple harmonic motion $\frac{\partial^2 y}{\partial t^2} = -\omega_s^2 y$, we finally obtain:

$$dM_z = -\frac{\rho}{A} \frac{\partial}{\partial x}\left(-\omega_s^2 \lambda\right) dx = \frac{\rho}{A}\omega_s^2 \frac{\partial \lambda}{\partial x} dx \qquad (16)$$

This moment should be accounted for in considering the variation of bending moment along the axis of the bar. Thus, instead of equation (4) we will have:

$$\frac{dV}{dx} = -\frac{\rho}{A}\omega_s^2 \lambda \qquad (17)$$

Substituting this in the equation for the deflection curve,

$$\frac{\partial^2}{\partial x^2}\left(EI\,\frac{\partial^2 y}{\partial x^2}\right) = \frac{\partial M}{\partial x} \tag{18}$$

and using expression (11) and (12), we finally obtain:

$$\frac{\partial^2}{\partial x^2}\left(EI\frac{\partial^2 y}{\partial x^2}\right) = m\omega^2 y - \omega^2 \frac{\partial}{\partial x}\left(\frac{Im}{A}\,\partial y.\partial x\right) \tag{19}$$

b. Effect of Shearing Force:

A still more accurate differential equation is obtained if not only rotatory inertia but also shear deflection is considered. The slope of the deflection curve depends not only upon the rotation of cross sections of the bar but on the deflection of the sections due to shear as well. Let γ denote the slope of the bar when shearing force is neglected and β the angle of shear at the neutral axis of the same cross section. Evidently the total slope must be the sum of γ and β, i.e.,

$$\frac{dy}{dx} = \gamma + \beta \tag{20}$$

[9]

Using the elementary bending theory, we have for bending moment and shearing force the following expressions,

$$M = -EI\,\frac{d\gamma}{dx}, \qquad Q = KAG\beta = K\left(\frac{dy}{dx} - \gamma\right)AG \tag{21 & 22}$$

K is a numerical factor which is a function of the shape of the cross sectional area, usually defined as follows:

$$K = \frac{\text{average shear stress in section}}{\text{maximum shear stress in section}} \tag{23}$$

This is the static shear stress distribution factor used by Timoshenko and discussed in standard texts.

discussed in something level.

This is the exact curve curve-tangle theory used to linearization and

(21)

curve equations where curves is section

$$\frac{dy}{dx} = \frac{1}{2}\frac{dy}{dx} \qquad \frac{dy}{dx} = \frac{1}{2}\left(\frac{dy}{dx} - y\right) dx$$

(22) & (23)

It is not clear which method is better. One edge of the curve equations here, namely defined as follows:

and showing there the intensity expression.

During the laboratory reading curve, we have for reading numbers

$$\frac{dy}{dx} = y + 5$$

(20) [2]

density the load ability curve on the axes of y and $5 + y$.

the angle of shear at the neutral axis of the beam cross section. Here

y denote the first at the new shear direction force is negative and 5

of the new red on the extension of the neutral axis is shear by wall. Let

only variable inside of stud shear-deformed is considered. The strain

of the deformation curve depends not only upon the rotation of cross sections

$$\frac{9x^2}{9-} \left(\frac{9x^2}{9x^2}\right) = \omega_2 - \omega_2 \frac{9x^2}{9}\left(\frac{1}{1-} \; 9x \; 9x^2\right) \qquad (19)$$

and using equations (11) and (12), we finally arrive:

$$\frac{9x^2}{9x^2}\left(\frac{9x^2}{9x^2}\right) + \frac{9x^2}{9x^2} \qquad (18)$$

Differentiating this to the equation for the deflection curve.

The complete mechanism of the bar including both rotatory inertia and shear deflection effects may now be formulated. Referring to Figure A-1 the differential equation of rotation of the element mnm_1n_1 will be:

$$-\frac{\partial M}{\partial x}dx + Q\,dx = \frac{Im}{A}\cdot\frac{\partial^2\gamma}{\partial t^2}dx\,. \tag{24}$$

Substituting equations (21) and (22) we obtain:

$$\frac{\partial}{\partial x}\left(EI\,\frac{\partial\gamma}{\partial x}\right) + K\left(\frac{\partial y}{\partial x}-\gamma\right)AG - \frac{Im}{A}\frac{\partial^2\gamma}{\partial t^2} = 0 \tag{25}$$

Neglecting all but first order infinitesimals, the differential equation for the translatory motion of the same element in the horizontal plane will be:

$$\frac{\partial Q}{\partial x}dx = m\frac{\partial^2 y}{\partial t^2}dx\,, \tag{26}$$

or

$$m\frac{\partial^2 y}{\partial t^2} - \frac{\partial}{\partial x}\left[KAG\left(\frac{\partial y}{\partial x}-\gamma\right)\right] = 0. \tag{27}$$

Taken together, equations (25) and (27) comprise the simultaneous differential equations which describe the more complete mechanism of lateral vibration for non-uniform bars.

$$\frac{\partial}{\partial x}\left(\frac{\partial \psi}{\partial x}\right) + \frac{\partial}{\partial z}\left(\frac{\partial \psi}{\partial z} - x\right) \mu\sigma = \frac{\mu}{\mu_1}\frac{\partial \psi_s}{\partial x} \quad (25)$$

$$\frac{\partial \Omega}{\partial x} dz = \frac{\partial \psi_s}{\partial z} dx \quad (26)$$

$$\frac{\partial}{\partial z}\left[\mu\sigma\left(\frac{\partial \psi}{\partial z} - x\right)\right] = \mu \frac{\partial \psi_s}{\partial z} \quad (27)$$

$$\frac{\partial}{\partial x}\left(EI\,\frac{\partial \gamma}{\partial x}\right) + K\left(\frac{\partial y}{\partial x} - \gamma\right)AG - \frac{Im}{A}\,\frac{\partial^2 \gamma}{\partial t^2} = 0 \qquad (25)$$

$$m\,\frac{\partial^2 y}{\partial t^2} - \frac{\partial}{\partial x}\left[\left(\frac{\partial y}{\partial x} - \gamma\right)KAG\right] = 0 \qquad (27)$$

Timoshenko's analysis of rotatory inertia and shear deflection effects for a uniform bar may be found in reference [9]. He obtains two simultaneous equations similar to (25) and (27).

$$EI\,\frac{\partial^2 \gamma}{\partial x^2} + K\left(\frac{\partial y}{\partial x} - \gamma\right)AG - \frac{Im}{A}\,\frac{\partial^2 \gamma}{\partial t^2} = 0 \qquad (28)^*$$

$$m\,\frac{\partial^2 y}{\partial t^2} - K\left(\frac{\partial^2 y}{\partial x^2} - \frac{\partial \gamma}{\partial x}\right)AG = 0 \qquad (29)^*$$

He then proceeds to eliminate from equations (28) and (29) γ, and obtains thereby the well known fourth order coupled equation:

$$EI\,\frac{\partial^4 y}{\partial x^4} + m\,\frac{\partial^2 y}{\partial t^2} - \left(\frac{mI}{A} + \frac{EI\,m}{KAG}\right)\frac{\partial^4 y}{\partial x^2 \partial t^2} +$$

$$\frac{m^2 I}{K\,A^2 G} \times \frac{\partial^4 y}{\partial t^4} = 0 \qquad (30)$$

* Timoshenko's notation has been altered to conform with the authors'.

$$\frac{\partial}{\partial x}\left(\frac{\partial f}{\partial x}\right) + \frac{\partial}{\partial y}\left(\frac{\partial f}{\partial y} - \lambda\right) dA - \frac{1}{2m}\frac{\partial^2 f}{\partial \lambda^2} = 0 \tag{32}$$

$$\frac{\partial^2 f}{\partial \lambda^2} - \frac{\partial}{\partial x}\left[\left(\frac{\partial f}{\partial y} - \lambda\right) dA\right] = 0 \tag{31}$$

Timoshenko's analysis of rotating inertia and beam deflection

The effects by a method not only to found in reference [1]

He obtains two simultaneous equations similar to (32) and (31)

$$\text{or} \quad \frac{\partial^2 f}{\partial \lambda^2} + \frac{\partial}{\partial x}\left(\frac{\partial f}{\partial y} - \lambda\right) dA - \frac{1}{2m}\frac{\partial^2 f}{\partial x^2} = 0 \tag{30}$$

$$\frac{\partial^2 f}{\partial x^2} - \frac{\partial}{\partial y}\left(\frac{\partial f}{\partial x}\right) dA = 0 \tag{29}$$

We then eliminate the eliminate from these equations (32) and (31) by

and obtain finally the next known fourth order coupled equation:

$$\frac{\partial^4 f}{\partial \lambda^4} + \frac{\partial^2 f}{\partial y^2} - \left(\frac{1}{m} + \frac{m+2}{2I - m}\right)\frac{\partial^2 f}{\partial x^2} +$$

$$\frac{2I - m}{m+1} \times \frac{\partial^4 f}{\partial \lambda^4} = 0 \tag{28}$$

* Timoshenko's notation has been altered to conform with the notation

Equations (25) and (27) appear not to be susceptible to such an operation, since I, A, m, and K are all functions of x in this case. Considerable effort was spent by the authors in an attempt to eliminate γ from equations (25) and (27), without success. If the operation is possible, and this the authors doubt, the resulting equation will at best be too complex and unwieldly for practical application.

The difficulties involved in the solution of equation (30) are well known. It is quite obvious that the irregular variation of I, m, K, and A with x in the case of a ship dictates that equations (25) and (27) must be solved in an approximate manner using the graphical, lumped parameter, or Rayleigh-Ritz procedure. The task is so formidable that the authors could find no exact solution in the literature encompassing both shear and rotatory inertia effects applied to an irregular non-uniform bar.

To recapitulate, the basic equations used by the authors are, in simplified form:

$$Q' = - m \omega^2 y \tag{31}$$

$$Q = KAG\beta = KAG (y' - \gamma) \tag{32}$$

$$M' = Q + \frac{Im \omega^2 \gamma}{A} \tag{33}$$

$$\gamma' = \frac{M}{EI} \tag{34}$$

$$y' = \gamma + \beta \tag{35}$$

The boundary conditions applicable to the quadruple integration are:

$$Q = 0 \text{ for } \quad = 0, \quad x = L \tag{36}$$

$$M = 0 \text{ for } \quad = 0, \quad x = L \tag{37}$$

Equations (31) - (37) describe an eigenvalue problem, with ω^2 being the eigenvalue. Solutions will exist only for a discrete set of ω^2. For each such value of ω^2 a unique mode pattern will correspond. An exception to this is the case when $\omega^2 = 0$, where two possible modes exist: $y = 1$ (rigid body translation), and $y = 1 - \frac{x}{x}$ (rigid body rotation). The two modes for this unique case have been orthogonalized for convenience.

Useful orthogonality relations exist between the normal mode patterns. In particular, for each

$$\int_0^L m\, y_i\, dx = 0 \tag{38}$$

$$\int_0^L x\, m\, y_i\, dx = 0 \tag{39}$$

and approximately, for the lower modes,

$$\int_0^L m\, y_i\, y_j\, dx = 0, \qquad i \neq j \tag{40}*$$

Murray [71] by application of integration by parts to equations (38) and (39) discovered another interesting orthogonality relation, which has apparently not been noted previously in the literature,

$$\int_0^L y_i'\, dx \int_0^x m\, (\xi - \bar{x})\, d\xi = 0 \tag{41}$$

Equation (41) is used by Murray and the authors to evaluate the constant of integration of $\int \gamma' dx$, and thus exactly determine the location of the true slope axis (This axis has previously been located arbitrarily at the mid-length point of the slope curve).

* The reader is referred to Appendix D for the derivation of the exact inter-mode orthogonality conditions and for a discussion as to the applicability of the approximate condition, Equation 40.

Equations (31) - (37) describe an eigenvalue problem, with ω^2 being the eigenvalue. Solutions will exist only for a discrete set of ω^2. For each such value of ω^2 a unique mode pattern will correspond. An exception to this is the case where $\omega^2 = 0$, where two possible modes exist:
$\lambda = 1$ (rigid body translation), and $\lambda = \xi - \frac{\bar{x}}{\bar{x}}$ (rigid body rotation).
The two modes for rhizomatic case have been orthogonalized for convenience.

Useful orthogonality relations exist between the normal mode patterns. In particular, for each

$$\int_0^{\bar{L}} \lambda^2 \, d\xi = 0 \tag{38}$$

$$\int_0^{\bar{L}} \xi \lambda^2 \, d\xi = 0 \tag{39}$$

and generally, for the lower modes,

$$\int_0^{\bar{L}} \lambda^i \lambda^j \, d\xi = 0, \qquad i \neq j \tag{40}$$

Murray [12] by coincidence is interpreted by parts to equations (38) and (39) discovered another interesting orthogonality relation, which has apparently not been noted previously in the literature.

$$\int_0^{\bar{L}} \lambda^i \, d\xi = \int_0^{\bar{x}} (\xi - \bar{x}) \, \lambda^i \, d\xi = 0 \tag{41}$$

Equation (41) is used by Murray and Stokes to evaluate the constant of integration of $\int \lambda^i d\xi$. and then exactly determine the location of the mid-length point of the beam curve).

* The reader is referred to Appendix D for the derivation of the exact interaction conditions and for a discussion of the equivalence of the approximate conditions.

If we take $y' = \eta' + C_3$ and substitute in equation (41), it is easily seen that C_3 may be evaluated as

$$C_3 = \frac{\int_0^L \eta' \int_0^x m\,(\xi - \bar{x})\,d\xi\,dx}{\int_0^L \int_0^x m\,(\xi - \bar{x})\,d\xi\,dx} \,. \tag{42}$$

In a like manner, use is made of equation (38) to determine C_4, where $y = \eta + C_4$.

It must be emphasized that orthogonality among all the modes must be rigorously maintained. [2][71] A starting pattern for the iterative cycle is not strictly admissable unless it has been explicitly adjusted to conform with the orthogonality conditions described in equations (38), (39), and (40). The resultant pattern is not valid until the same adjustment procedure has been rigorously executed.

Orthogonality with respect to rigid body translation is insured by use of a zero shift of the y-axis: $y_i = \bar{y}_i + \bar{A}$. It is clear from equation (38) that:

$$\bar{A} \int_0^L m\,dx = -\int_0^L \bar{y}_i\, m\, dx \,. \tag{43}$$

Orthogonality with respect to rigid body rotation is insured by use of a rotation of the y-axis: $y_i = \bar{y}_i + \bar{B}\,(x-\bar{x})$. From equations (38) and (39) we may write

$$\int_0^L m\, y_i\,(x - \bar{x})\,dx = 0, \tag{44}$$

and substitution of the above expression in equation (44) yields:

$$\bar{B} \int_0^L (x - \bar{x})^2 m\,dx = -\int_0^L m\bar{y}_i\,(x - \bar{x})\,dx \,. \tag{45}$$

It is further required that both the starting and resultant deflection patterns be orthogonal with respect to each flexural mode prior to the one of immediate interest, we formulate the expression

$$y_i = \bar{y}_i + \bar{A} + \bar{B}(x - \bar{x}) + C_1 y_1 + C_2 y_2 + \cdots C_{i-1} y_{i-1} \quad (46)$$

Constants C_1, C_2 etc are readily determined by substituting $y_1 = \bar{y}_1 + C_1 y_1$, etc. into equation (40). For example, if we are interested in adjusting the second mode so that it is truly normal to the first mode we set

$$y_2 = \bar{y}_2 + C_1 y_1$$

whence from (40)

$$C_1 \int_0^L m\, y_1^2\, dx = - \int_0^L m\, \bar{y}_2\, y_1\, dx \quad (47)$$

In general

$$C_i \int_0^L m\, y_j^2\, dx = - \int_0^L m\, \bar{y}_i\, y_j\, dx \quad (48)$$

Not until the operations indicated by equation (46) are carried out should a cycle be begun nor a resultant deflection curve be accepted. Since the frequency depends upon the value of the resultant curve at the normalizing point, y_i^*, the frequency should be calculated only after orthogonalization is completed.

Part II

Detailed Outline of Procedure :

This section supplements the general outline of the procedure of this thesis presented in Section II, and sets down the mechanics of the operations implementing the relationships derived in the theoretical section, Part I of this Appendix.

Some remarks helpful in interpreting the analytical expressions and the curves of Appendix B are in order. Roman numerals indicate figures in Appendix B.

(1) All curves plotted from data given or calculated are plotted at intervals of 0.025 L and faired through all spots. This is considered to give the least number of stations which will give a sufficiently accurate determination of true curve shape.

(2) Since the length coördinate has been nön-dimensionalized (= x/L), each integration performed with respect to it results in a factor of L in the denominator of the integral expression. These factors are removed at two points in the cycle: when determining curvature, and when normalizing deflection. However, their presence within the cycle results in appropriate modification of correction terms calculated to add to functions in the cycle.

(3) Since the virtual mass distribution of the starting data was in pound units, the m of the theoretical relationships has been replaced by mg, the g (acceleration of gravity) has been carried throughout as a constant and is removed at the normalizing stage and in the frequency determination. The g constant necessarily appears also in the various auxiliary functions involving m.

Part II

Detailed Outline of Procedure :

This section supplements the general outline of the procedure of this thesis presented in Section II, and sets down the mechanics of the operations implementing the relationships derived in the theoretical section, Part I of this Appendix.

Some remarks helpful in interpreting the analytical expressions and the curves of Appendix B are in order. Roman numerals indicate figures in Appendix C.

(1) All curves plotted from data given or calculated are plotted at intervals of 0.025 L and faired through all spots. This is considered to give the least number of stations which will give a sufficiently accurate determination of true curve shape.

(2) Since the length coordinate has been non-dimensionalized (= x/L), each integration performed with respect to it results in a factor of L in the denominator of the integral expression. These factors are removed at two points in the cycle: when determining curvature, and when normalizing deflection. However, their presence within the cycle results in appropriate modification of correction terms calculated to add to functions in the cycle.

(3) Since the virtual mass distribution of the existing data was in pound units, the m of the theoretical relationships has been replaced by m/g . The g (acceleration of gravity) has been carried throughout as a constant and is removed at the normalizing stage and in the frequency determination. The g constant necessarily appears also in the various auxiliary functions involving m .

(4) The horizontal backstepping of the various integral curves in the figures of Appendix B is inherent in the operation of the mechanical integraph used. (See Plate I) For convenience, the backstep has been set at integral numbers of inches, either two, three, or four inches, and is readily apparent from the y-axis labelled for each integral curve. Coördinates along the horizontal axis have not been renumbered for each axis shift, but should be transposed mentally in examining integral curves. Vertical shifts of integral curves are made where presentation is facilitated thereby.

(5) Also inherent in the integraph is a scale reduction of the integral curve with respect to its argument. Scale factors used in this investigation ranged from three to 7.5; while not indicated directly on the curves, they of course determine the scales marked on the integral axes. The continuous maintenance of correct scales is vital to accurate determination of frequency from the deflection normalizing factor.

(6) Figures illustrating the method have been so arranged that the four principal integrations comprising a single cycle appear in one figure (e.g. Figure VI) while the auxiliary curves pertaining to the same cycle appear on one or two separate sheets following (e.g. Figure VII). At the end of each mode is a figure (XII, XX, XXXII) illustrating the convergence of the normalized deflection patterns from the orthogonalized uniform beam pattern ultimately deemed acceptable as the normal mode pattern.

Sequence of Operations:

When the tables and smooth curves (I) of structural information have been prepared, it is necessary to obtain the coördinate of the longitudinal centroid of the appropriate virtual mass. This may be done by

any standard technique, but figure II illustrates a simple and unique method. The tangent to the end of the second integral of the mass distribution is extended to the base line, and the resulting intersection, relative to the origin of the second integral curve, is the abscissa of the longitudinal centroid of the mass. The proof of this is given in [7].

Sufficient information is now on hand to prepare the tables of working functions, including

$$mg \ , \ mg\, I/L^2A, \quad 10^6 L^2/EI, \quad KAG/10^6, \quad (\xi - \bar{x})/L,$$

$$mg\,(\xi - \bar{x})/L, \text{ and } \quad g\int_0^x m\,(\xi - \bar{x})\,d\xi\,/L^2$$

As they become known, there will be added to the working functions table the following tabulated functions:

$$y_1, \ y_1 m \ , \ y_2, \ y_2 m \ , \text{ etc.}$$

This table is prepared for intervals of 0.025 L.

Certain definite integrals and other constants useful throughout the application of the method are also calculated and listed at this point:

$$\Delta/L = \int_0^L mg\,dx/L \tag{49}$$

$$N = \int_0^L (x - \bar{x})^2\, mg\,dx/L^3 \tag{50}$$

$$P = \int_0^L\int_0^x (\xi - \bar{x})\, mg\,d\xi\,dx/L^4 \tag{51}$$

Subsequently, when data is available, the following are added:

$$W_1 = \int_0^L y_1^2\, mg\,dx/L \tag{52}$$

$$W_2 = \int_0^L y_2^2\, mg\,dx/L, \text{ etc.} \tag{53}$$

It is now possible to commence the process. While any approximation to the mode shape can be used as the starting curve, it is found that the most accurate approximation to the final mode shape available will lead to accelerated convergence, hence fewer cycles of

any standard technique, but figure 11 illustrates a simple and unique method. The tangent to the end of the second integral of the mass distribution is extended to the base line, and the resulting intersection, relative to the origin of the second integral curve, is the abscissa of the longitudinal centroid of the mass. The proof of this is given in [4].

Sufficient information is now on hand to prepare the tables of working functions, including

$$m\beta \ , \quad m\beta\,\Gamma\backslash\Gamma_2{}^4, \quad 10^6\Gamma_2{}^3\backslash EI, \quad EA\backslash 10^6, \quad (\bar{z}-z)\backslash\Gamma,$$

$$m\beta\,(\bar{z}-z)\backslash\Gamma, \quad \text{and} \quad \beta\int_0^x m\,(\bar{z}-\bar{z})\,d\,\bar{z}\backslash\Gamma_2$$

as they become known. There will be added to the working functions table the following calculated functions:

$$\Gamma^4\ \gamma^1{}_m \ , \quad \gamma^2, \ \gamma^2{}_m \ , \quad \text{etc.}$$

This table is prepared for intervals of 0.025 L.

Certain definite integrals and other constants useful throughout the application of the method are also calculated and listed at this point:

$$\Delta\backslash\Gamma = \int_0^1 \beta\,dz\backslash\Gamma \tag{29}$$

$$M = \int_0^1 (\bar{z}-z)\,m\beta\,dz\backslash\Gamma^2 \tag{30}$$

$$P = \int_0^1 \int_0^x (\bar{z}-z)\,m\beta\,d\bar{z}\,dz\backslash\Gamma^4 \tag{31}$$

Subsequently, when data is available, the following are added:

$$M^2 = \int_0^1 \gamma^2{}_m\,\beta\,dz\backslash\Gamma, \quad \text{etc.} \tag{32}$$

$$M^1 = \int_0^1 \gamma^1{}_m\,\beta\,dz\backslash\Gamma \tag{33}$$

It is now possible to commence the process. While any approximation to the mode shape can be used as the starting curve, it is found that the most accurate approximation to the final mode shape

iteration for the desired accuracy.

The proposal here is to take a known pattern, as from a similar ship or a uniform beam, and force it to comply with conditions of orthogonality applicable to the ultimate normal pattern. Thus in the investigation conducted for this thesis, the normalized ordinates of the patterns found by Lord Rayleigh are taken arbitrarily as a starting point.

The following description traces the development of a third, or four-noded mode, to demonstrate the typical case of a higher mode.

From the working function table and the values of Y_3, tabulations are obtained and plotted of mgY_3, $mg(x - \bar{x})\, Y_3/L$, $mgy_1 Y_3$, and $mgy_2 Y_3$. The four resulting curves are integrated (XXII), and the values obtained are divided by the operational constants indicated to obtain

$$\bar{A} = - \frac{\int_0^L mg\, Y_3\, dx/L}{\Delta/L} \tag{54}$$

$$\bar{B} = - \frac{\int_0^L mg\, (x - \bar{x})\, Y_3/L}{N} \tag{55}$$

$$C_i = \frac{-\int_0^L mgy_1 Y_3\, dx/L}{W_1} \tag{56}$$

$$C_{ii} = \frac{-\int_0^L mgy_2 Y_3\, dx/L}{W_2} \tag{57}$$

Now the values of $(x - \bar{x})/L$ are multiplied by $\bar{B}$; the values of y_1 are multiplied by C_i; and the values of y_2 are multiplied by C_{ii}. Then we obtain

$$\bar{y} = \bar{A} + \bar{B}\, (x - \bar{x})/L + C_i y_1 + C_{ii} y_2 \tag{58}$$

All values of $\bar{y}$ are divided by y^*, its value at its normalizing point (the center-or centermost-after antinode as obtained by a plot of that region)

iteration for the desired accuracy.

The proposed issue is to take a known pattern, as from a slotted cavity or a uniform array, and derive it to comply with conditions of arbitrary practicality applicable to the ultimate desired pattern. Then to the investigation conducted for this thesis, the normalized eigenmodes of the radiating loaded by some topology are taken arbitrarily as a starting point.

The following manipulations lead to the development of a mixed, or love-ended mode, or demonstrate the typical case of a higher mode.

From the working Equation below and the values of λ^3, tabulations are obtained for the operational constants indicated to obtain $\beta_3 \lambda^3$. The four resulting curves are interpolated (SCALED) and the values $\beta_3 \lambda^3$, $\beta_4 \lambda^3$, $\beta_5 \lambda^3$, $\beta_6 \lambda^3$, $\beta_7 \lambda^3$, $\beta_8 \lambda^3$, $\beta_9 \lambda^3$, $\beta_{10} \lambda^3$, and $\beta_{11} \lambda^3$. The four resulting curves are interpolated (SCALED) and the values

$$\bar{I} = \bar{I} + \bar{E} \cdot [\bar{E} - \bar{E}] \cdot \Gamma + C^{1\lambda} + C^{11} \lambda^3 \tag{31}$$

We obtain

$$C^{11} = \frac{\int_0^{\beta_3} \beta_3 \lambda^3 \, d\beta_3 \, \Gamma}{\beta^3} \tag{32}$$

$$\frac{\int_0^{\beta_3} \beta_3 \, (\beta - \bar{E}) \, \lambda^3 \, \Gamma}{\lambda} \tag{33}$$

$$\bar{I} = \frac{\int_0^{\beta_3} \beta_3 \lambda^3 \, d\beta_3 \, \Gamma}{\Delta^3} \tag{34}$$

to obtain a tabulation of y, the orthogonalized, normalized starting curve for the first cycle of iteration. (But see discussion of orthogonality in Appendix D).

The cycle itself (XXIII) commences with the curve of inertia loading = $-ymg$, which is calculated, plotted, and integrated, to give a function of shear,

$$gQ/L = -ymg \qquad (59)$$

where the constant of integration is zero, since the integral curve starts at the origin, and the boundary condition of zero end shear dictates that the true shear curve should also pass through the origin. However, the right end of the integral curve may differ from zero by a small amount (usually less than 5% of the maximum ordinate of the curve). When this occurs, a linear correction is applied to the curve to again conform to the above boundary condition. This is done by drawing a new axis joining the ends of the shear curve, measuring its ordinates from this curve but normal to the old axis, then replotting on the old axis. This correction is illustrated in Figure VI, where the reader should compare the curves marked gQ/L and gQ/L (corrected), but has been omitted from the presentation elsewhere to avoid congesting the plots unnecessarily. In the first cycle, the corrected curve gives $gM'/L = gQ/L$.

(At this point in all but the first cycle, each value of shear receives an additive correction to account for rotatory inertia, the correction being a function of the bending slope γ obtained from the previous cycle in a manner to be described. This slope, in the form $L\gamma$, is multiplied by the working function mgI/L^2A and the product added to the shear term to give a curve of

$$gM'/L = gQ/L + \gamma g\, m\, I/LA \qquad (60)$$

This is the only procedural respect in which subsequent cycles differ from the first).

The curve of $g\,M'/L$ is integrated, and the boundary condition of zero end moment is applied in exactly the manner described above for the shear correction. In both cases the correction can be considered to filter out accumulated errors resulting from small inaccuracies of integraph operation and calculation. The values of $g\,M, L^2$, a direct function of moment in the hull girder, are tabulated from the corrected curve, and each is multiplied by the corresponding value of $10^6 L^2/EI$, to give a function of curvature, $g\gamma' \times 10^6$, which is plotted.

Curvature is integrated to give bending slope to within an additive constant. To this component is added the shear component of slope,

$$g\beta \times 10^6/L = (g\,Q/L) \div (KAG/10^6) \qquad (61)$$

based on the shear values obtained after correction of the first integral in the cycle.

The addition gives a function of total slope, still without the constant of integration:

$$g\eta' \times 10^6/L = g\bar{\gamma} \times 10^6/L + g\beta \times 10^6/L \qquad (62)$$

To determine the constant, or axis shift, use is made of Murray's formulation (see Part I of this appendix) on an auxiliary plot (XXIV). The values of $g\eta' \times 10^6/L$ from the above addition are multiplied by the working function

$$\int_0^x m\,g\,(\xi - \bar{x})\,d\xi \;/L^2$$

and the product plotted and integrated on the auxiliary plot. The value of the definite integral obtained,

$$10^6 g\,C_3/L = -\frac{\int_0^L g\eta \times 10^6/L \int_0^x mg\,(\xi - \bar{x})\,d\xi\,dx/L^3}{P} \qquad (63)$$

This is the only procedure (aspect) in which consequent cycles differ (save the first).

The curve of $\delta\ln I_n$ is integrated, and the boundary condition of zero end moment is applied in exactly the manner described above for the shelf correction. In both cases the correction can be considered to filter out accumulated errors resulting from small inaccuracies of integraph operation and calculation. The values of $\delta\ln I_n$, a direct function of moment in the end girder, are isolated from the corrected curve, and each is multiplied by the corresponding value of $10^6 \cdot E_1$, to give a function of curvature, $\delta\chi \times 10^6$, which is plotted.

Curvature is integrated to give bending slope to within an additive constant. To this component is added the slope component of

$$\delta\theta \times 10^6 = (\delta \text{ Curv.}) \div (\text{MAG}) 10^6 \qquad (41)$$

based on the shear values existed after correction of the first integral in the cycle.

The addition gives a function of that slope, still without the constant of integration:

$$\delta\theta_1 \times 10^6 = \delta\theta_2 \times 10^6 + \delta\theta \times 10^6 \qquad (42)$$

To determine the constant, an axis shift, use is made of Mohr's formulation (see Part 1 of this appendix) on an auxiliary plot (XXIV). The values of $\delta\theta_1 \times 10^6$ from the above additions are multiplied by the weighing function

$$\int_0^x \delta\theta \,(\xi - \bar{x})\, d\xi$$

and the product plotted and integrated on the auxiliary plot. The value of the definite integral obtained,

$$10^6 \delta\theta' = \frac{\int_0^x \delta\theta \times 10^6 (\xi - \bar{x})\, d\xi}{I_c} \qquad (43)$$

is added to the uncorrected total slope to give the function of true slope:

$$g\eta' \times 10^6/L = g\eta' \times 10^6/L + 10^6 g\, C_3/L \qquad (64)$$

This is plotted on the cycle plot and integrated, yielding, to within an additive constant of integration, a function of deflection, $g\eta \times 10^6/L^2$. To obtain the constant, this is multiplied by mg and the product plotted on the auxiliary plot (XXIV) and integrated. The value of the definite integral is divided by a function of displacement to give the constant

$$10^6 g\, C_4/L^2 = - \frac{\int_0^L (g\eta \times 10^6/L^2)\, mg\, dx/L}{\Delta/L} \qquad (65)$$

This is added to the values of $g\eta \times 10^6/L^2$ to give the deflection pattern

$$gy \times 10^6/L^2 = g\eta \times 10^6/L^2 + g C_4 \times 10^6/L^2 \qquad (66)$$

This pattern is orthogonalized in the same manner as was described for the Rayleigh pattern, to give $g\bar{y} \times 10^6/L^2$. The value at the normalizing point, $gy^* \times 10^6/L^2$, is recorded, and divided into all ordinate values, to yield the normalized deflection pattern, y_{3-1}, of the first cycle. It is this pattern which is used to compute the inertia loading for the next cycle of the iteration.

The value of $gy^* \times 10^6/L^2$ is multiplied by L^2, and the product resulting is divided into the values of $g\sigma' \times 10^6$ from the last cycle of the iteration for each mode to yield the normalized curvature for the mode, which now will have the correct relationship to the normalized deflection pattern.

The value of ω^2 corresponding to the cycle just completed is

$$\omega^2 = \frac{1}{gy^* \times 10/L^2} \qquad (67)$$

$$\omega_c = \frac{84}{84 - 10^4 \lambda_c} \qquad (47)$$

The value of ω_c corresponding to the cycle just completed is

for the mode, which now will have the correct relationship to the normalized deflection ratios.

cycle of the iteration for each mode to yield the normalized curvature product resulting is divided into the values of 8.4×10^4 from the last

The value of $84 \times 10^4 \lambda_c$ is multiplied by ξ_c^2, and the

leading for the next cycle of the iteration.

of the first cycle. It is this pattern which is used to compute the inertia

ordinate values, to yield the normalized deflection pattern, λ-1.

normalizing point. $84 \times 10^4 \lambda_c$, is recorded, and divided into all

ended for the multiply pattern, to give $84 \times 10^4 \lambda_c$. The value at the

This pattern is orthogonalized in the same manner as was dis-

$$84 \times 10^4 \lambda_c = 84 \times 10^4 \xi_c + 8 C_c^4 \times 10^4 \lambda_c \qquad (46)$$

deflection pattern

This is added to the values of $84 \times 10^4 \lambda_c$ to give the

$$10^4 C_c^4 = \frac{\sum (84 \times 10^4 \lambda_c) m \, dx}{\sum m \, dx} \qquad (45)$$

ment to give the inertia.

The value of the modulo integral is divided by a function of displace-

and the product plotted on the auxiliary plot (XXIV) and integrated.

$84 \times 10^4 \xi_c$. To obtain the inertia, this is multiplied by m

within an additive constant of integration, a function of deflection,

This is plotted on the cycle plot and integrated, yielding, to

$$84 \times 10^4 \lambda = 84 \times 10^4 \xi_c + 10^4 C_c^4 \qquad (44)$$

is added to the uncorrected total slope to give the function of true slope,

The value of ω^2 computed from the last cycle performed is accepted as the natural frequency corresponding to the mode being considered.

In preparation for the rotatory inertia correction, the shear curvature is subtracted from the total curvature to give the corrected bending curvature

$$\delta\gamma \times 10^6/L = \delta\gamma' \times 10^6/L - \delta\beta \times 10^6/L \qquad (68)$$

which is normalized by dividing by $\delta y^* \times 10^6/L^2$ to yield the required value of γL.

The value of ω_g assumed from the last cycle performed is accepted as the natural frequency corresponding to the mode being considered.

In preparation for the rotatory inertia correction, the shear curvature is subtracted from the total curvatures to give the unreduced bending curvature

$$89\times10^{6}\,\Gamma_{\cdot} = 31_{\cdot} \times 10^{6}\,\Gamma_{\cdot} - 8\%_{6} \times 10^{6}\,\Gamma_{\cdot} \qquad (84)$$

which is normalized by dividing by $87 \times 10^{6}\,\Gamma_{\cdot}$ to yield the required value of $\beta\,\Gamma_{\cdot}$.

APPENDIX B - SUMMARY OF DATA AND CALCULATIONS

Figures I through XXXIV in this section depict the application of the method developed in this thesis to the model for which characteristics are tabulated in Appendix B. The calculation of argument curves plotted from data is illustrated in the sample calculations of Appendix C.

Table III summarizes the effect of each iterative cycle, and its associated orthogonalization check, on the natural frequency of the mode considered. The corresponding effect on deflection patterns is presented in Figures XII, XX, and XXXII, for the first, second, and third modes respectively.

APPENDIX E - SUMMARY OF DATA AND CALCULATIONS

Figures LXXIV through XXXIV in this section depict the application of the method developed in this thesis to the model for which characteristics are tabulated in Appendix E. The calculation of argument curves plotted from data is illustrated in the sample calculations of Appendix C.

Table III summarizes the effect of each iterative cycle, and its associated crossover-location check, as the natural frequency of the model converged. The corresponding effect on deflection patterns is presented in Figures XXX, XL, and XXXII, for the first, second, and third modes respectively.

TABLE III

BEHAVIOR OF FREQUENCY FROM CYCLE TO CYCLE

MODE	CYCLE	FREQUENCY, cps.
1	1	449.8*
	2	423.5
	3	417
2	1	865*
	2	840
	3	838.8
3	1	1507*
	2	1377
	3	1391

* The first cycle of each mode necessarily does not include a consideration of rotatory inertia.

TABLE III

[illegible]

[illegible]

[illegible]	[illegible]	[illegible]
1	1	[illegible]
	2	[illegible]
	3	[illegible]
2	1	[illegible]
	2	[illegible]
	3	[illegible]
3	1	[illegible]
	2	[illegible]
	3	[illegible]

* The first words of each note [illegible] does not [illegible] a [illegible] of [illegible].

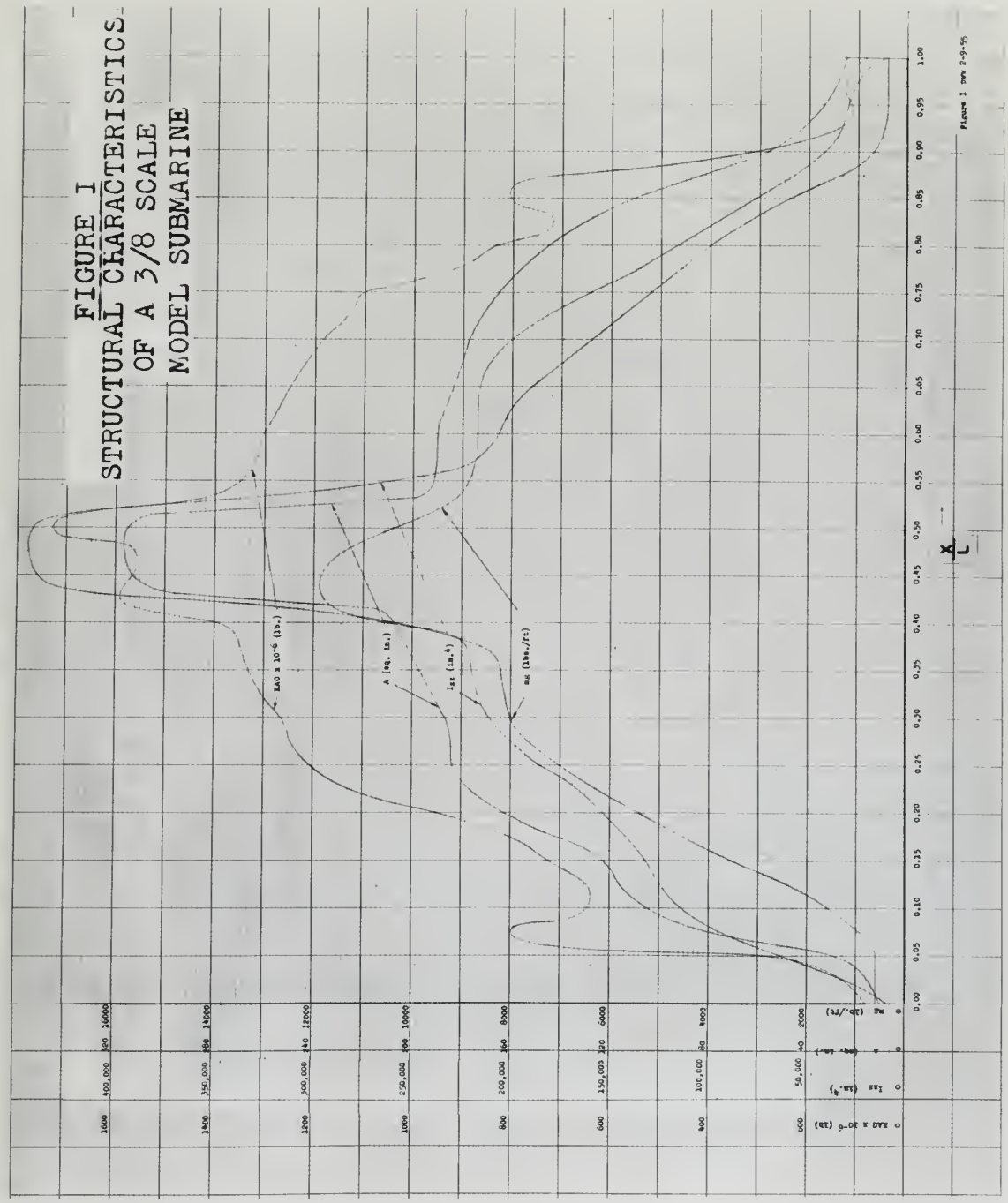
FIGURE I
STRUCTURAL CHARACTERISTICS
OF A 3/8 SCALE
MODEL SUBMARINE
EAO x 10⁻⁶ (lb.)
A (sq. in.)
Izz (in.⁴)
wg (lbs./ft)
x/L
Figure 1 DWW 2-9-55

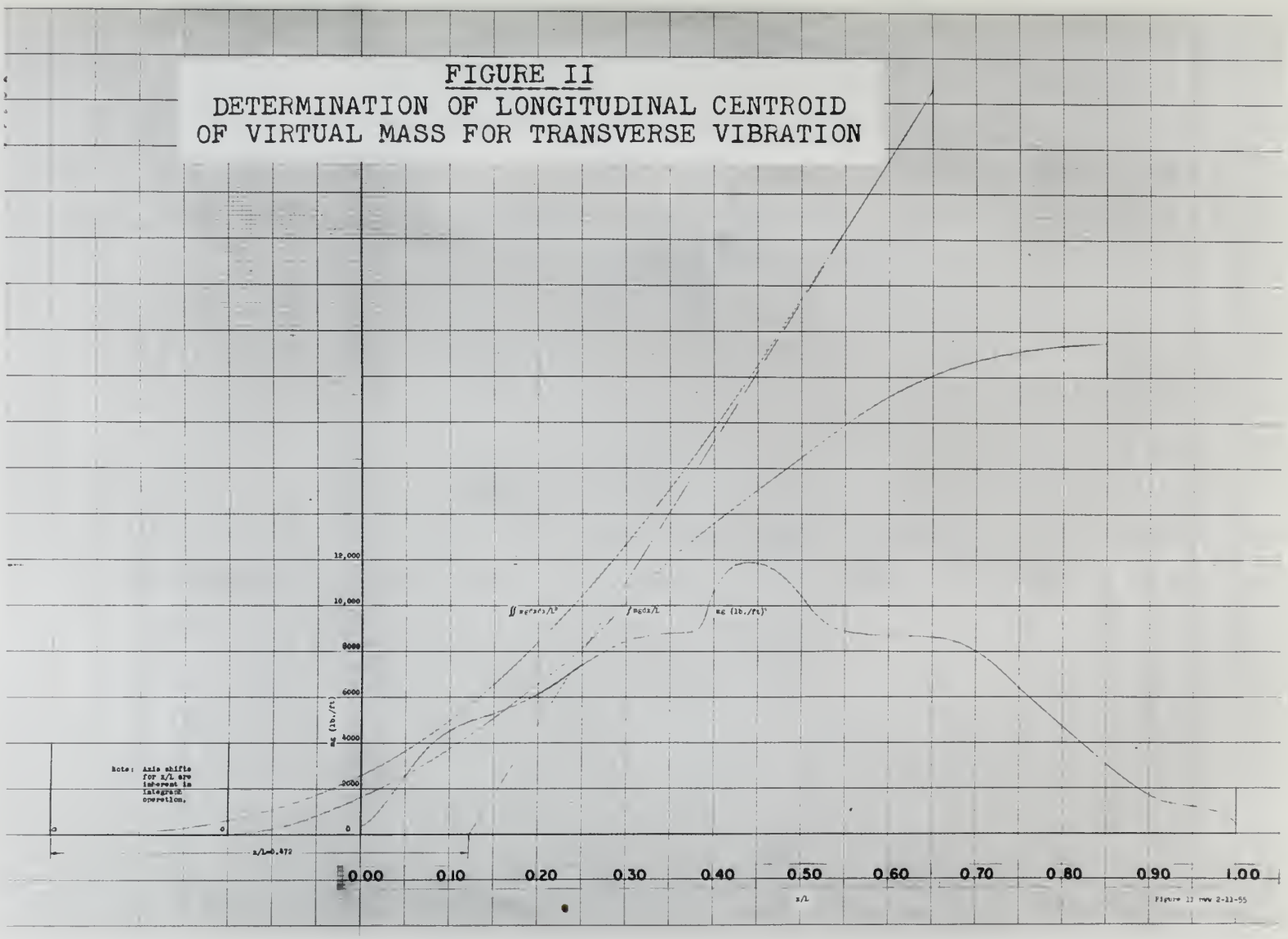
FIGURE II
DETERMINATION OF LONGITUDINAL CENTROID
OF VIRTUAL MASS FOR TRANSVERSE VIBRATION
12,000
10,000
8000
6000
4000
2000
0
mg (lb./ft)
Note: Axis shifts for x/L are inverse in integrate operation.
x/L=0.472
0.00
0.10
0.20
0.30
0.40
0.50
0.60
0.70
0.80
0.90
1.00
x/L

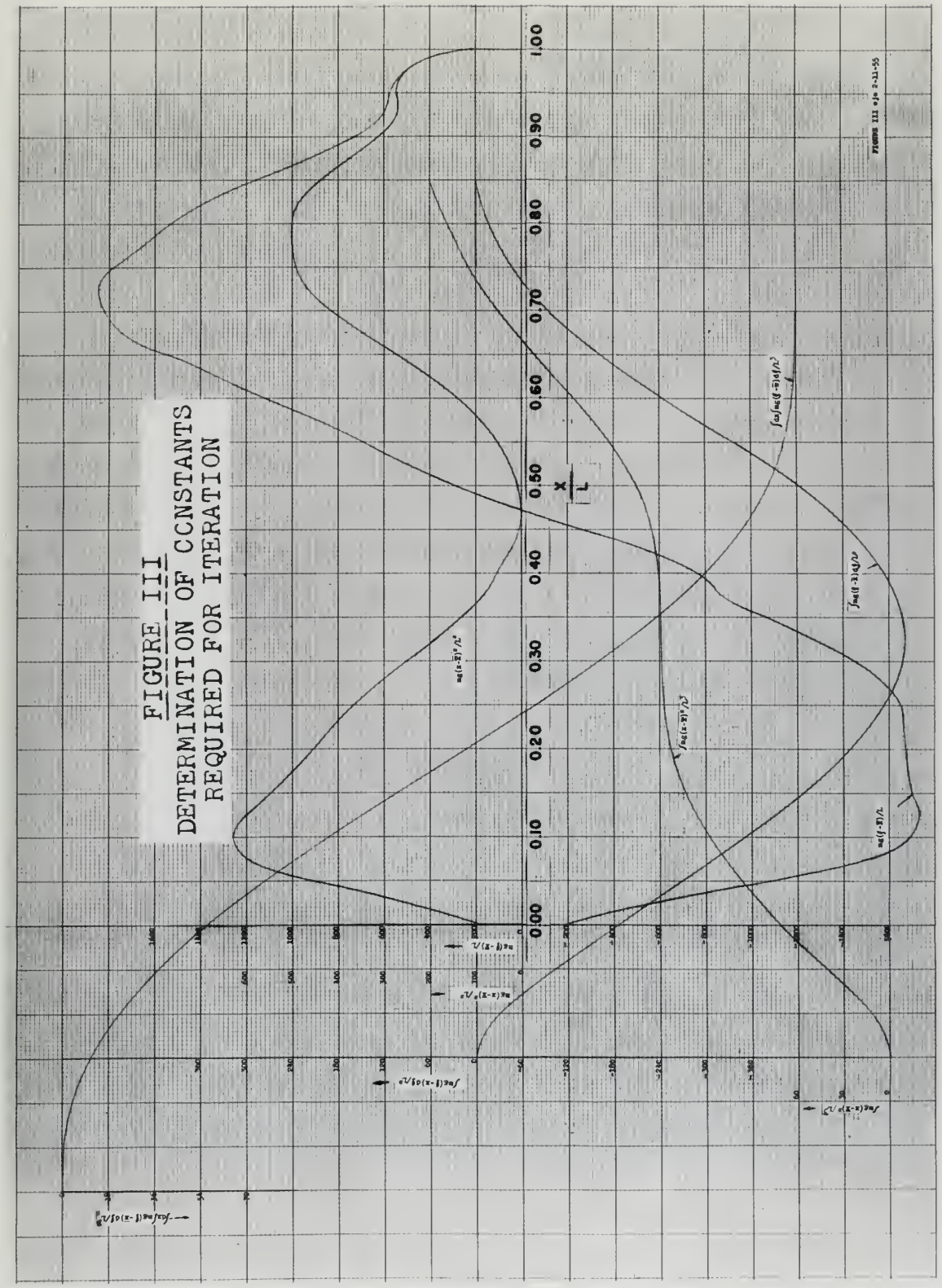

FIGURE III
DETERMINATION OF CONSTANTS
REQUIRED FOR ITERATION

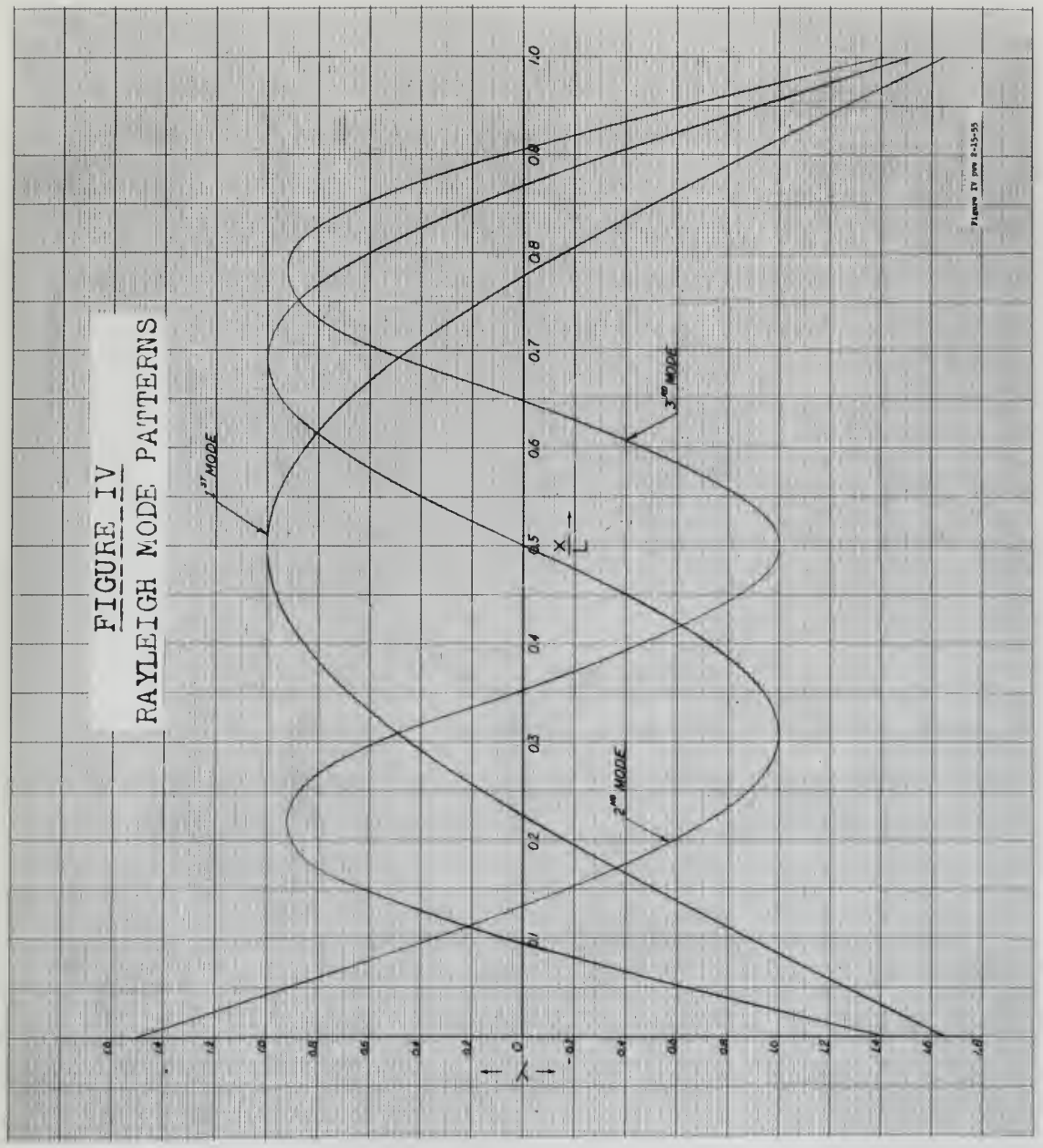

FIGURE IV
RAYLEIGH MODE PATTERNS

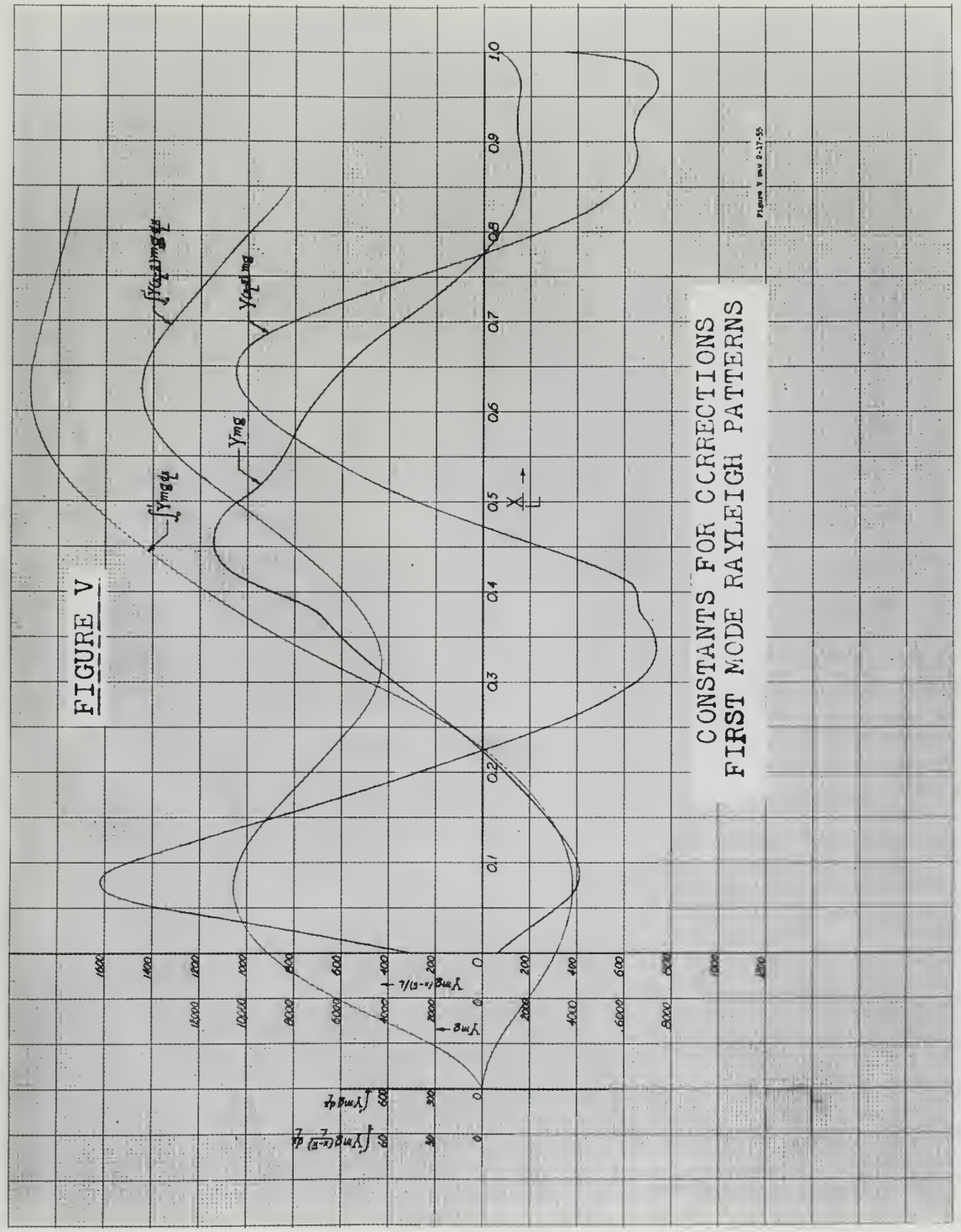
FIGURE V
CONSTANTS FOR CORRECTIONS
FIRST MODE RAYLEIGH PATTERNS
Ymg
Ymg1
Ymg2
Ymg3
Ymg4
Ymg5
Ymg6
Ymg7
Ymg8
Ymg9
Ymg10
Ymg11
Ymg12
Ymg13
Ymg14
Ymg15
Ymg16
Ymg17
Ymg18
Ymg19
Ymg20
Ymg21
Ymg22
Ymg23
Ymg24
Ymg25
Ymg26
Ymg27
Ymg28
Ymg29
Ymg30
Ymg31
Ymg32
Ymg33
Ymg34
Ymg35
Ymg36
Ymg37
Ymg38
Ymg39
Ymg40
Ymg41
Ymg42
Ymg43
Ymg44
Ymg45
Ymg46
Ymg47
Ymg48
Ymg49
Ymg50
Ymg51
Ymg52
Ymg53
Ymg54
Ymg55
Ymg56
Ymg57
Ymg58
Ymg59
Ymg60
Ymg61
Ymg62
Ymg63
Ymg64
Ymg65
Ymg66
Ymg67
Ymg68
Ymg69
Ymg70
Ymg71
Ymg72
Ymg73
Ymg74
Ymg75
Ymg76
Ymg77
Ymg78
Ymg79
Ymg80
Ymg81
Ymg82
Ymg83
Ymg84
Ymg85
Ymg86
Ymg87
Ymg88
Ymg89
Ymg90
Ymg91
Ymg92
Ymg93
Ymg94
Ymg95
Ymg96
Ymg97
Ymg98
Ymg99
Ymg100

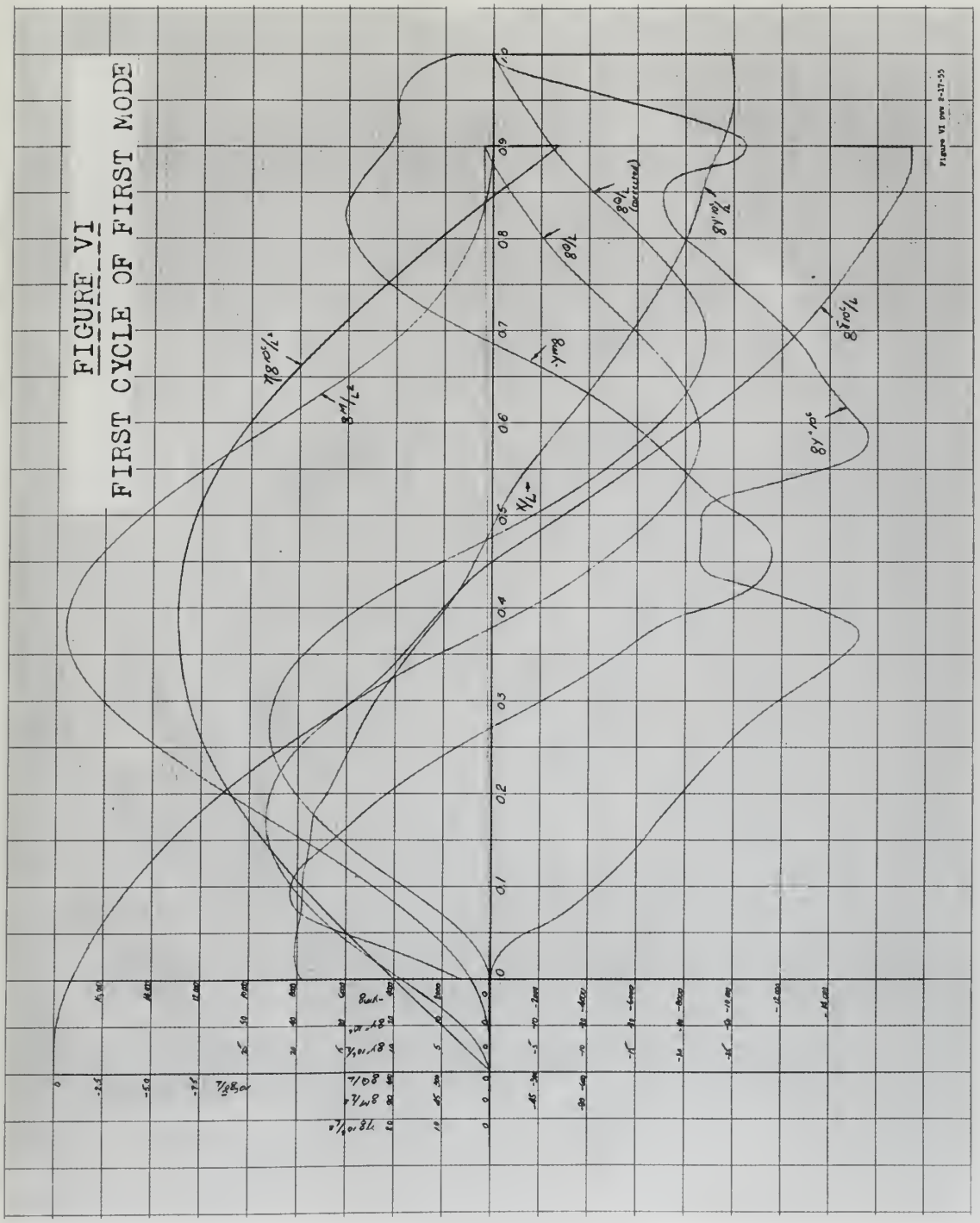
FIGURE VI
FIRST CYCLE OF FIRST MODE

FIGURE VII
ADJUSTMENT CONSTANTS
FIRST CYCLE, FIRST MODE

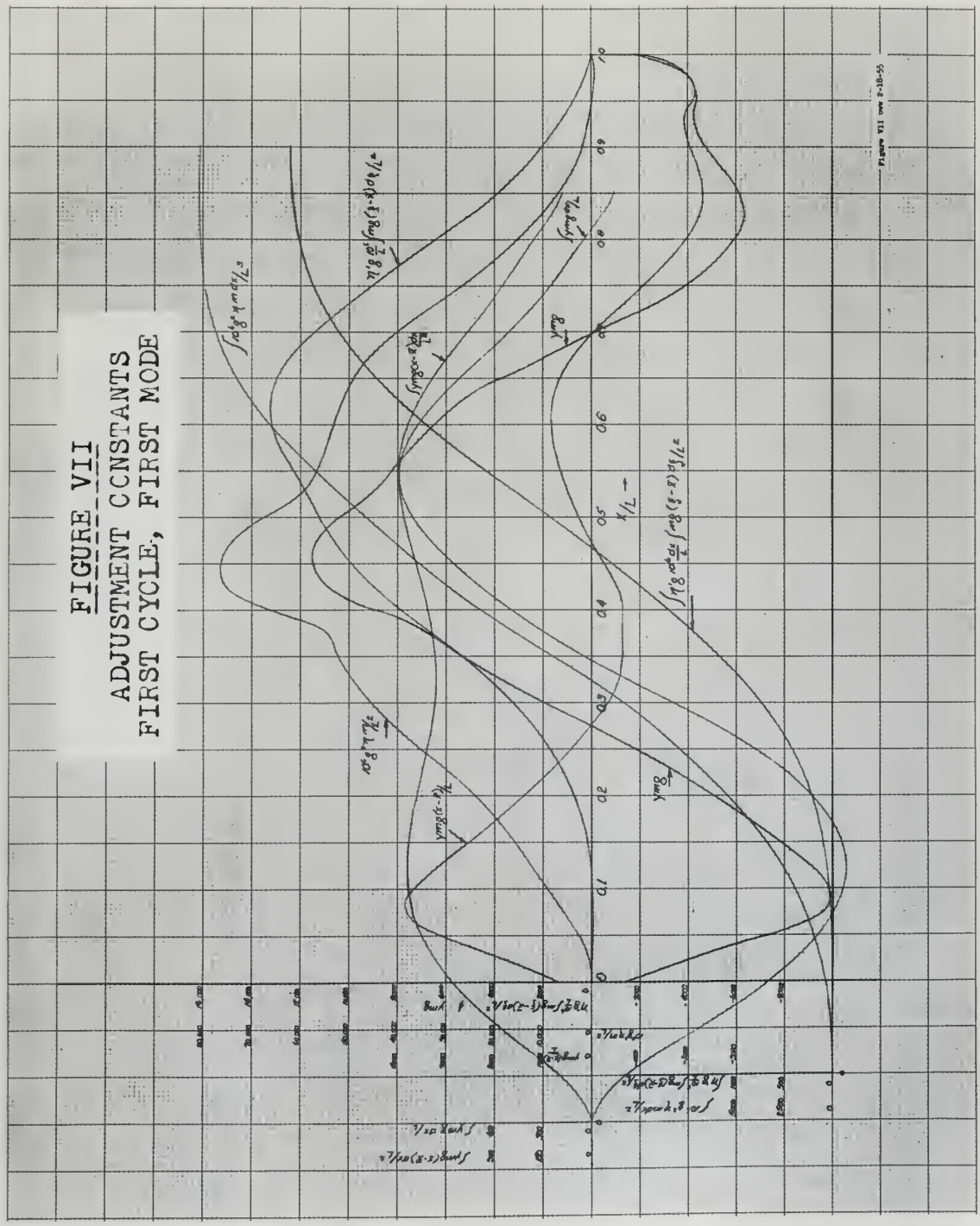

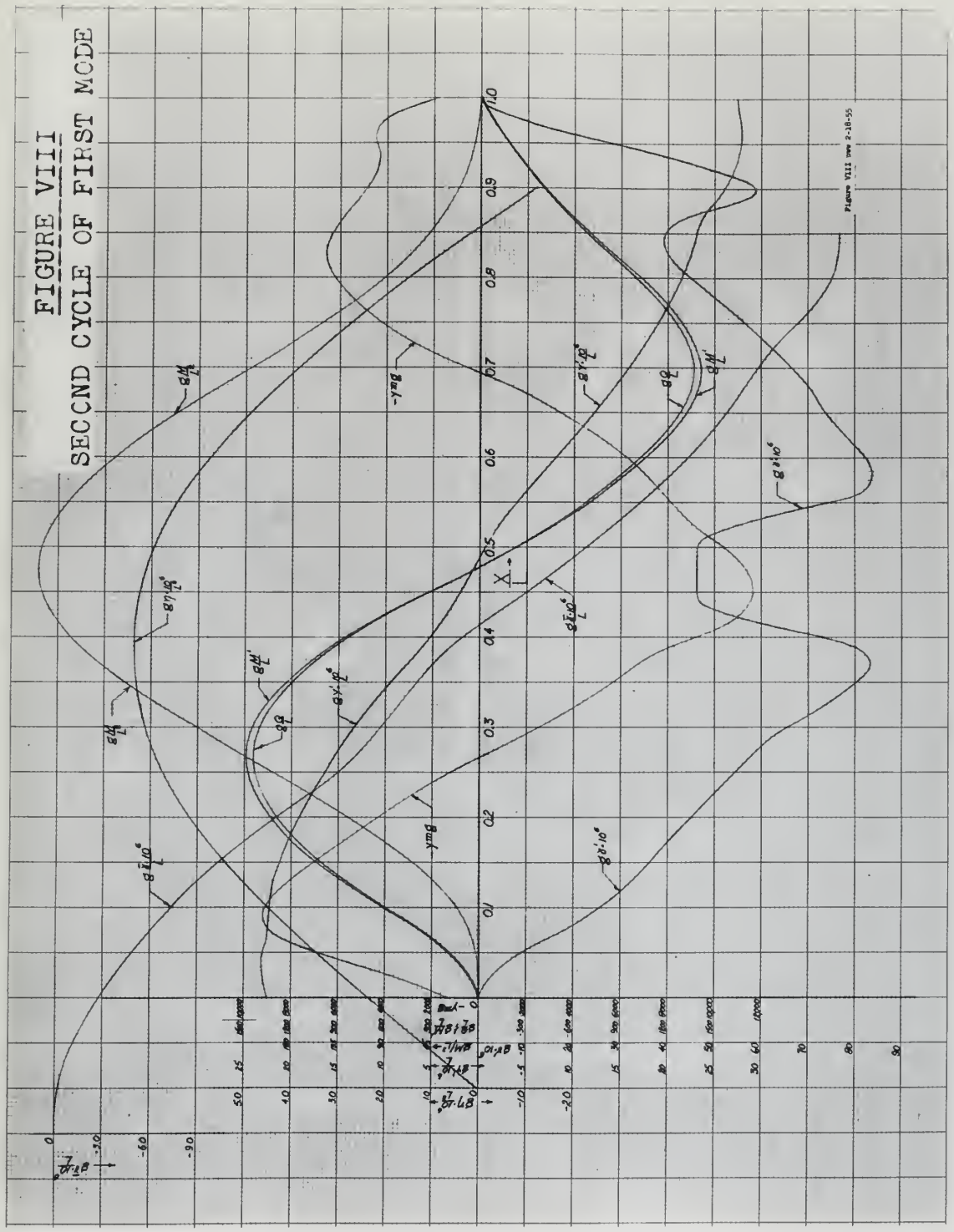
FIGURE VIII
SECCND CYCLE OF FIRST MODE

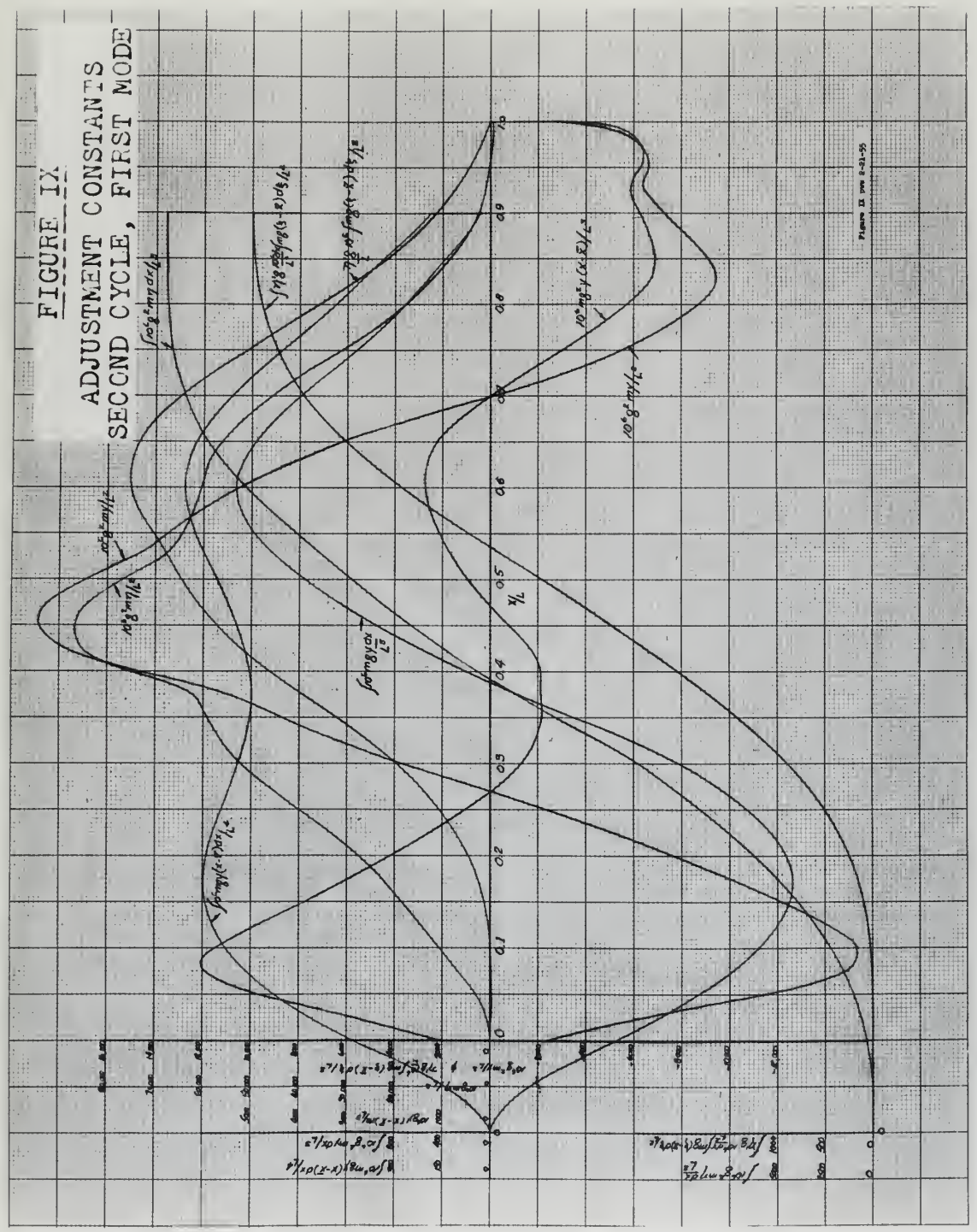
FIGURE IX
ADJUSTMENT CONSTANTS
SECOND CYCLE, FIRST MODE

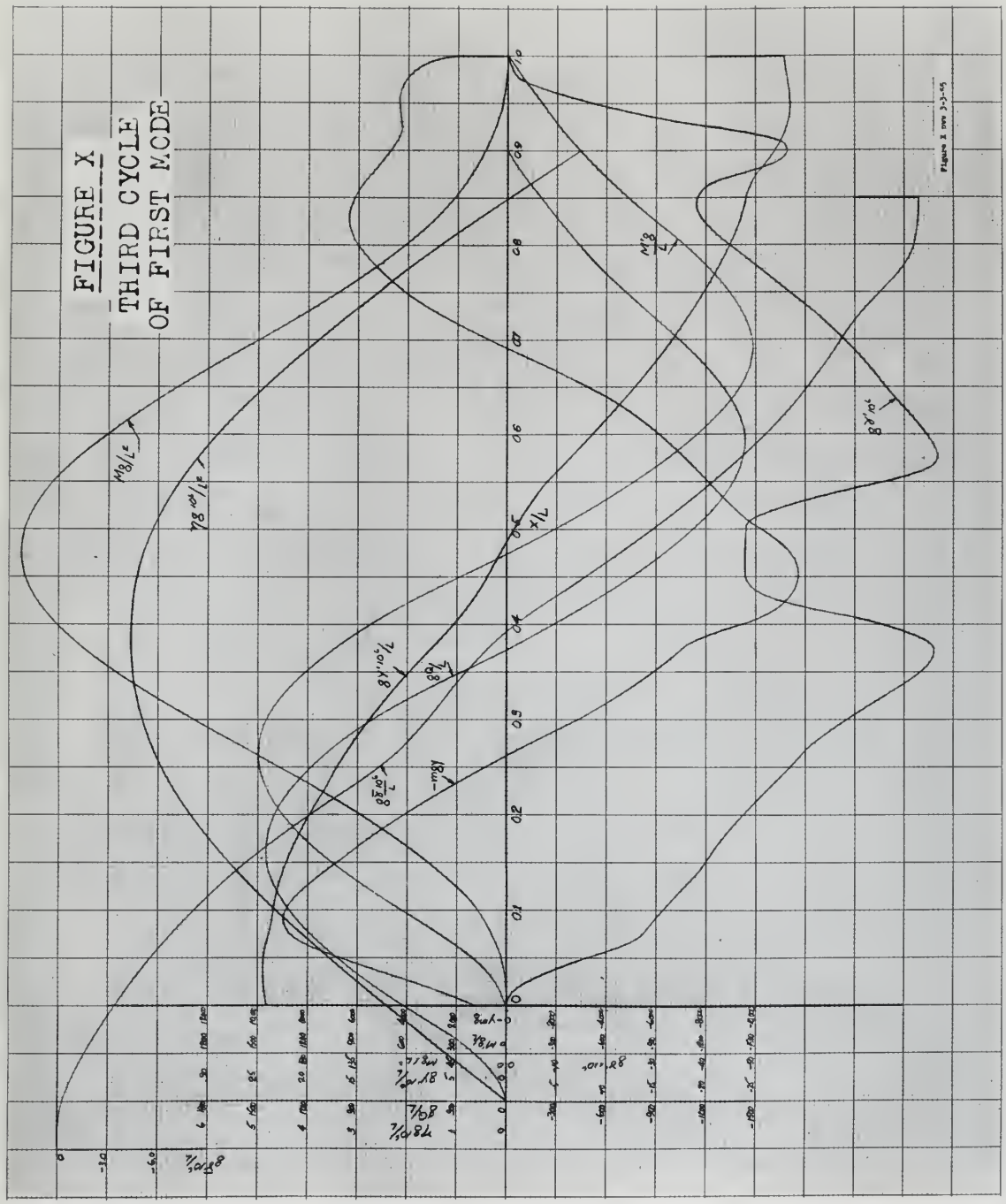

FIGURE X
THIRD CYCLE
OF FIRST MODE

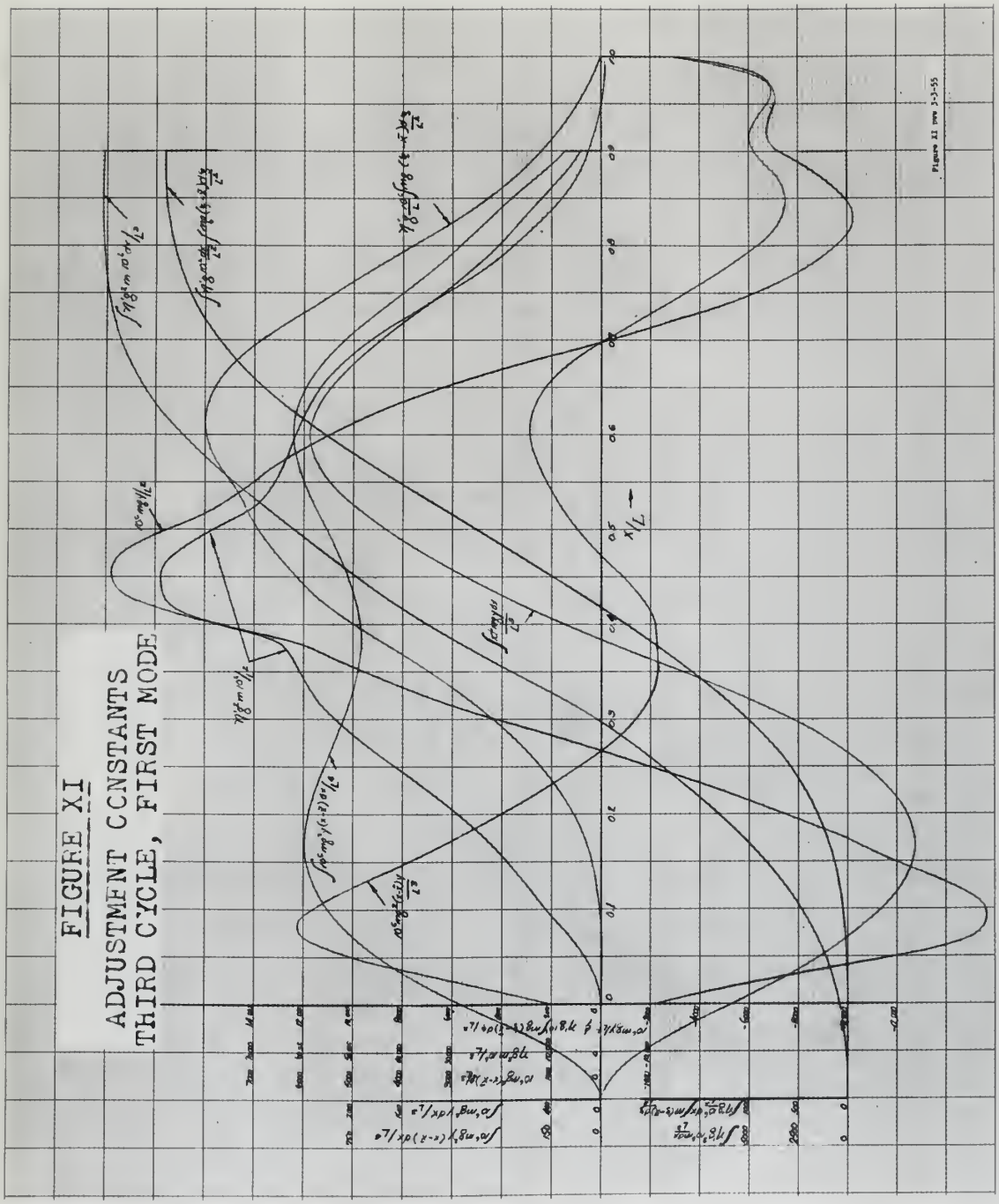

FIGURE XI
ADJUSTMENT CONSTANTS
THIRD CYCLE, FIRST MODE

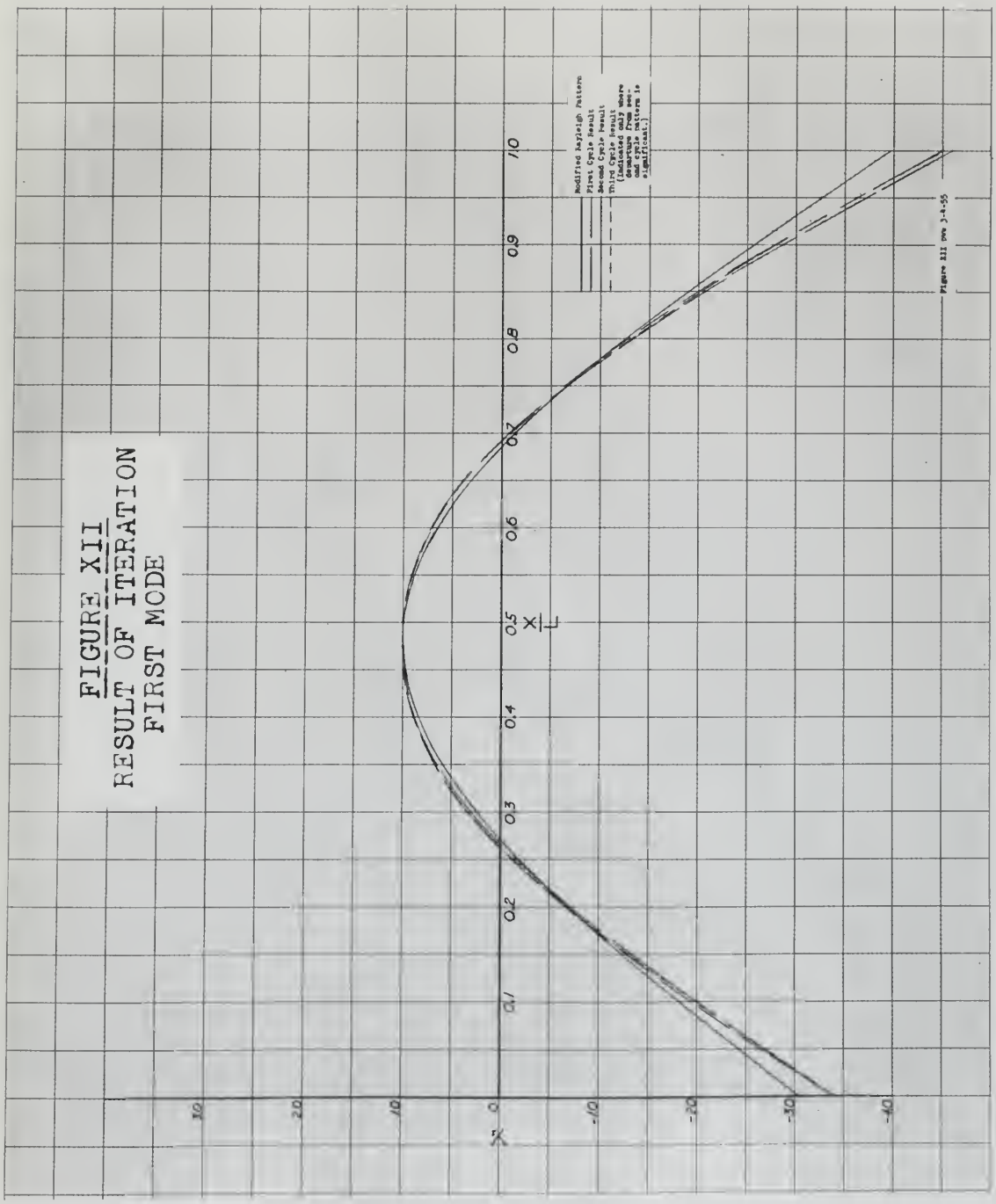
FIGURE XII
RESULT OF ITERATION
FIRST MODE
Modified Rayleigh Pattern
First Cycle Result
Second Cycle Result
Third Cycle Result
(Indicates that where
curves coincide, no
departure from pre-
scribed pattern is
specified.)
X
X/L
0.1
0.2
0.3
0.4
0.5
0.6
0.7
0.8
0.9
1.0
10
20
10
0
-10
-20
-30
-40
Figure XII pwa 3-4-55

FIGURE XIII
CONSTANTS FOR CORRECTIONS
SECOND MODE RAYLEIGH PATTERN

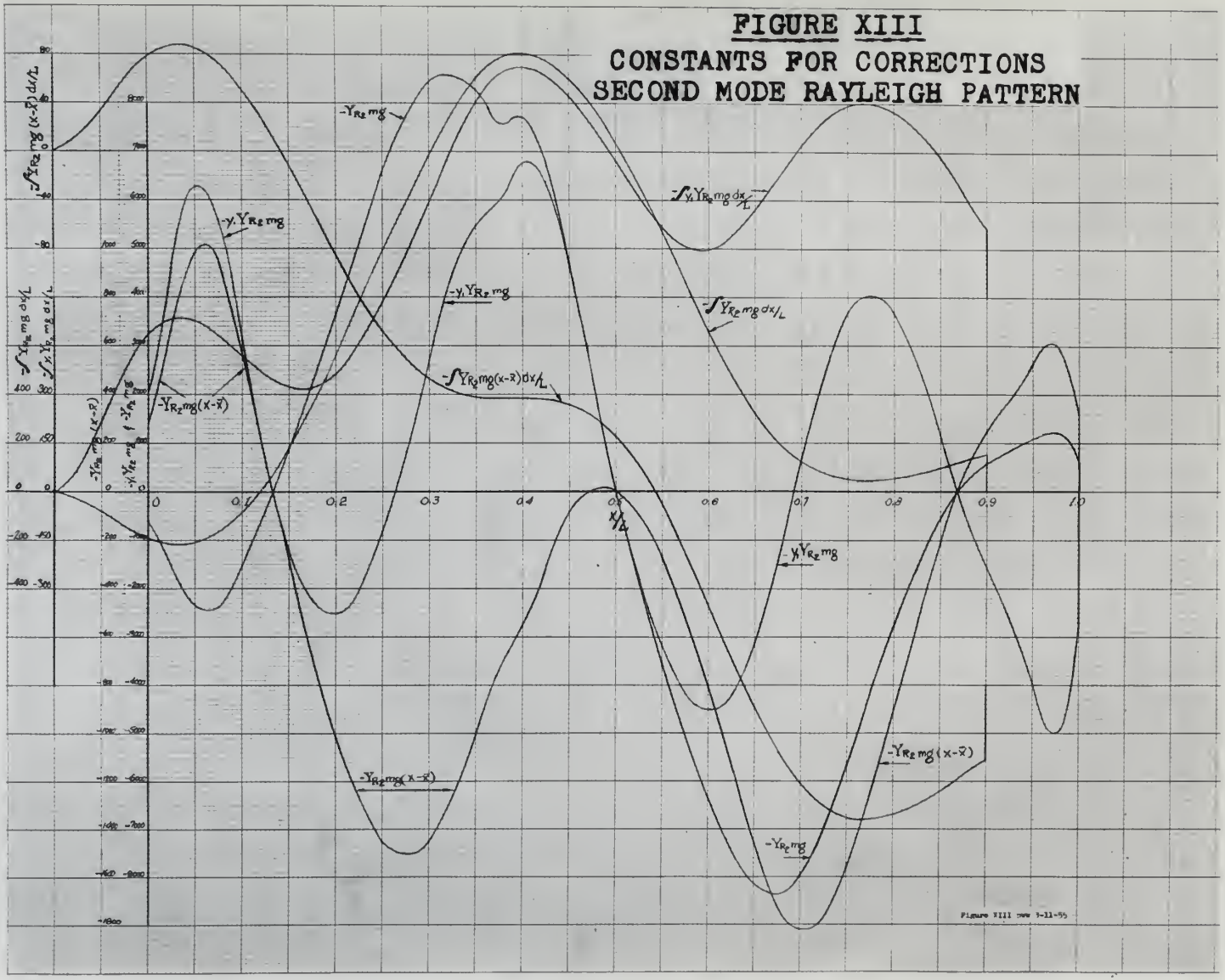

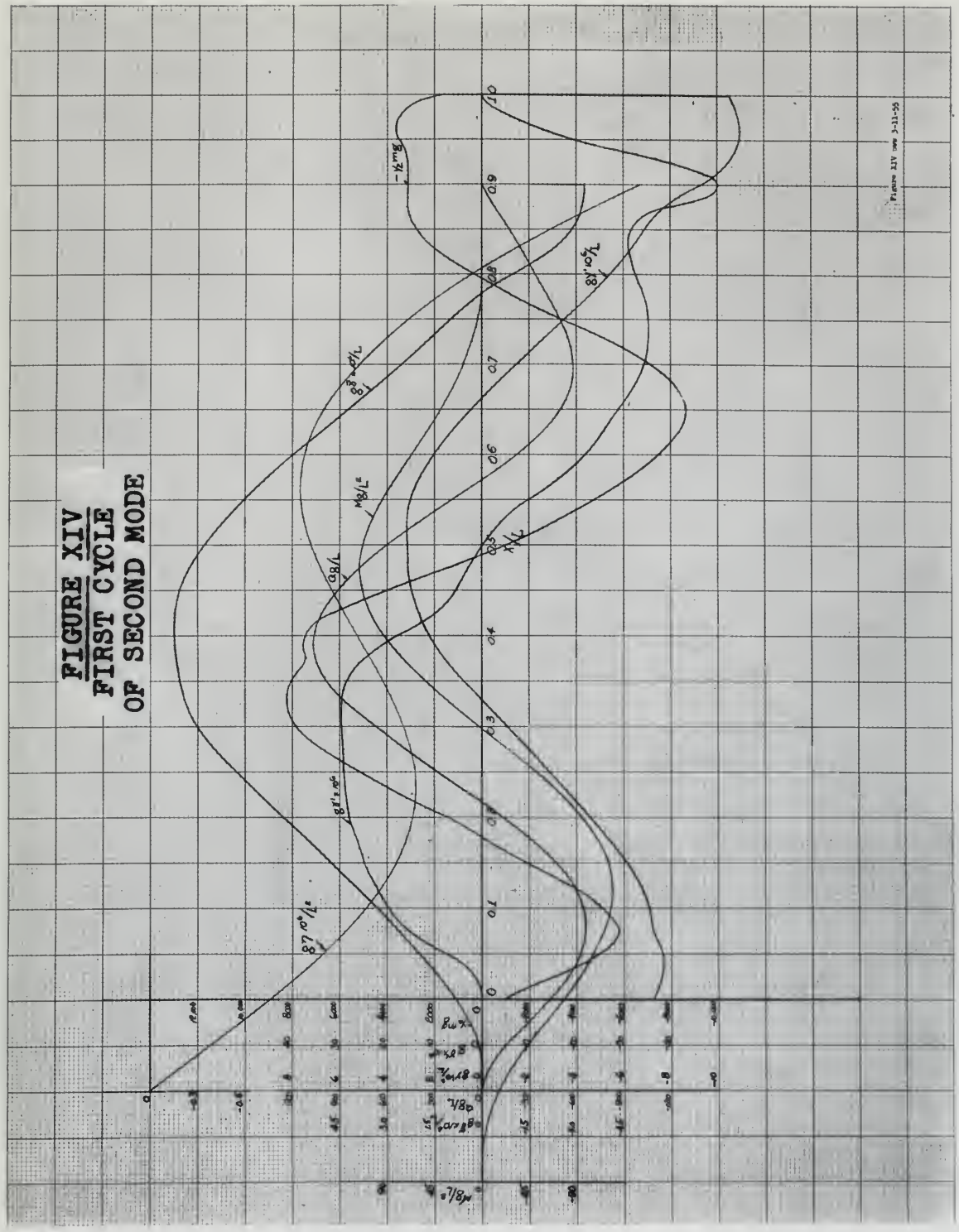

FIGURE XIV
FIRST CYCLE
OF SECOND MODE

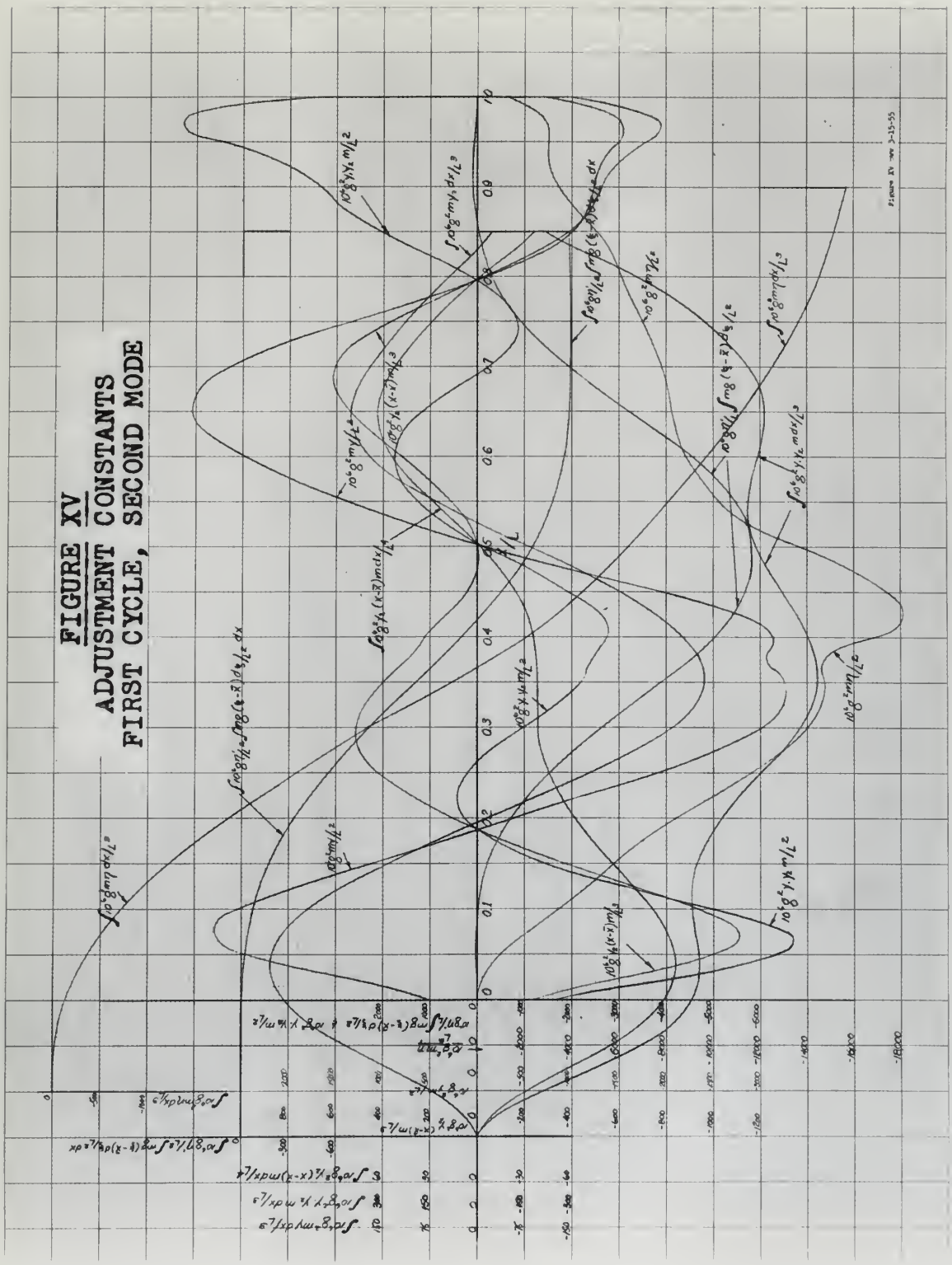

FIGURE XV
ADJUSTMENT CONSTANTS
FIRST CYCLE, SECOND MODE

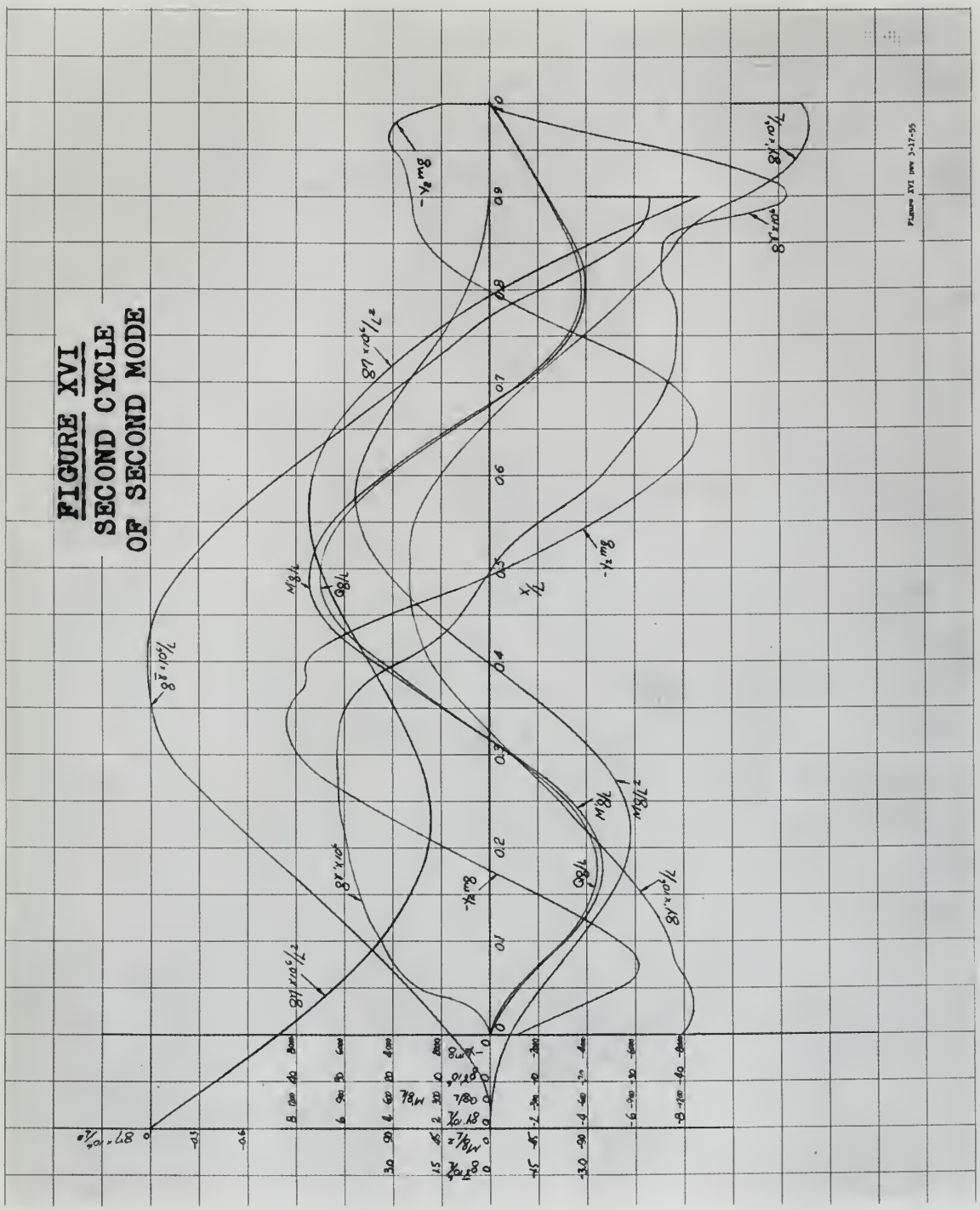
FIGURE XVI
SECOND CYCLE
OF SECOND MODE

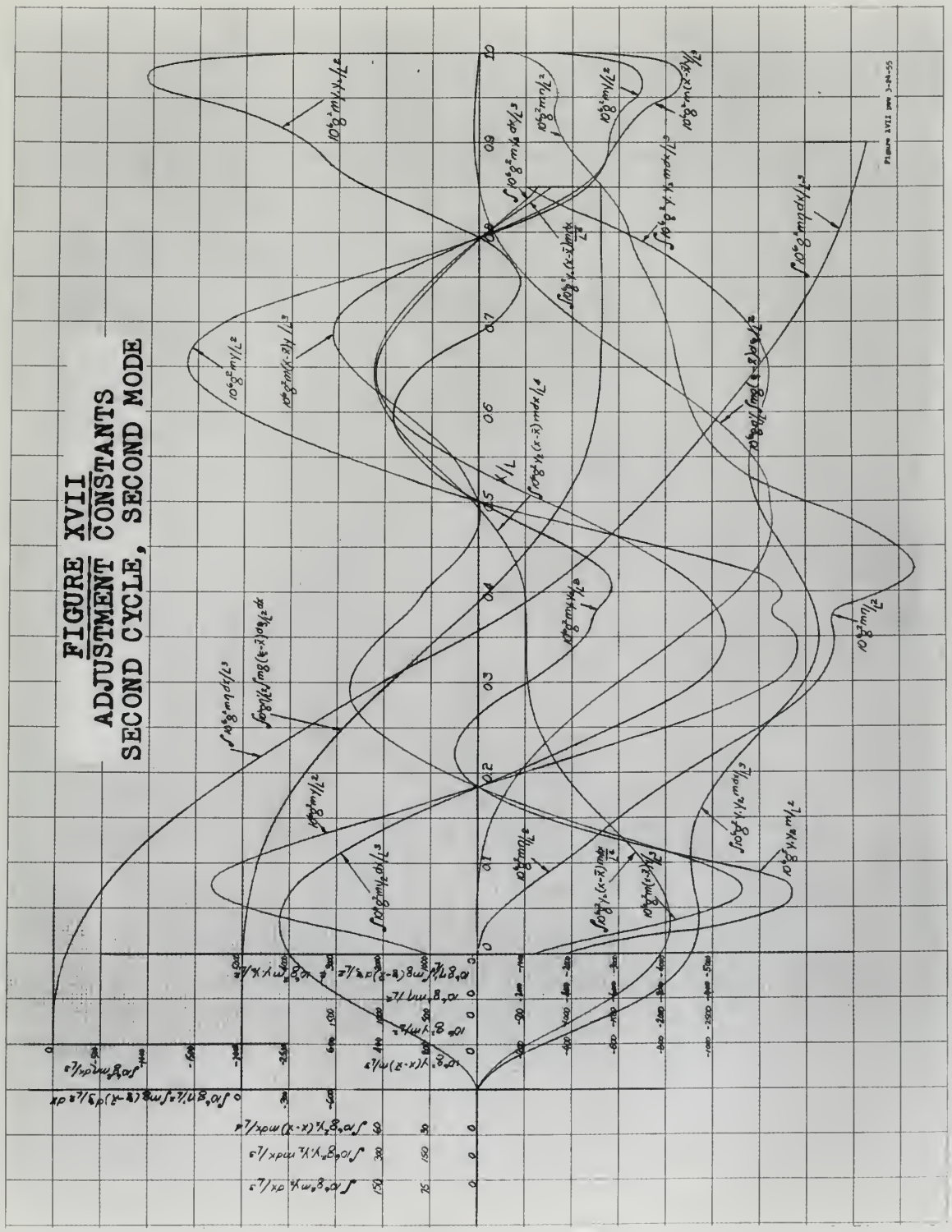

FIGURE XVII
ADJUSTMENT CONSTANTS
SECOND CYCLE, SECOND MODE

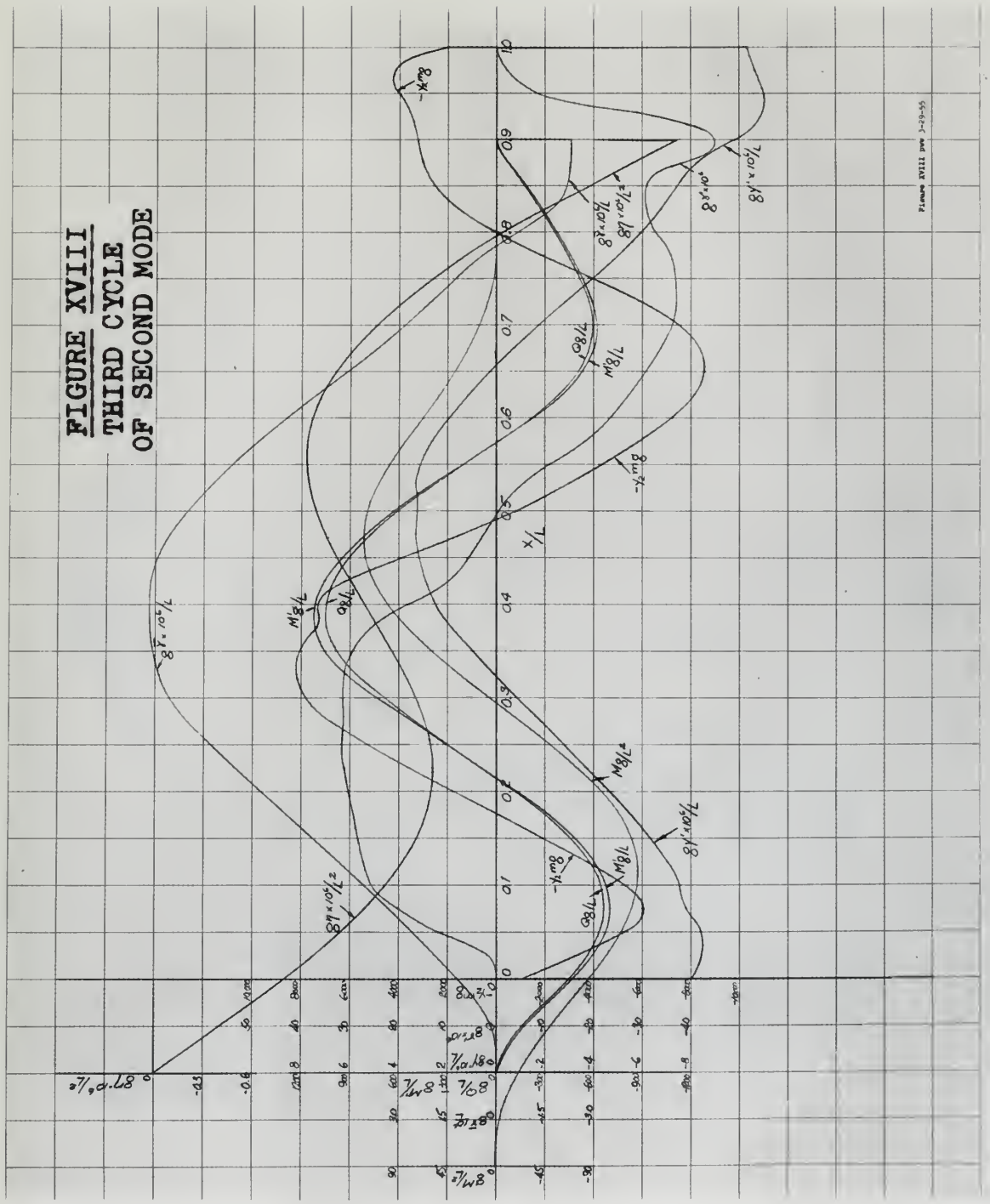
FIGURE XVIII
THIRD CYCLE
OF SECOND MODE
X/L
0
0.1
0.2
0.3
0.4
0.5
0.6
0.7
0.8
0.9
1.0
8w/L
8M/L
8Q/L
8T/L
8N/L
8u/L
8v/L
7/8M
7/8Q
7/8T
7/8N
7/8u
7/8v
8v x 10⁴/L²
8u x 10⁴/L²
8N x 10⁴/L²
8T x 10⁴/L²
8Q x 10⁴/L²
8M x 10⁴/L²
8w x 10⁴/L²
7/8v x 8
7/8u x 8
7/8N x 8
7/8T x 8
7/8Q x 8
7/8M x 8
7/8w x 8
Figure XVIII 3-29-55

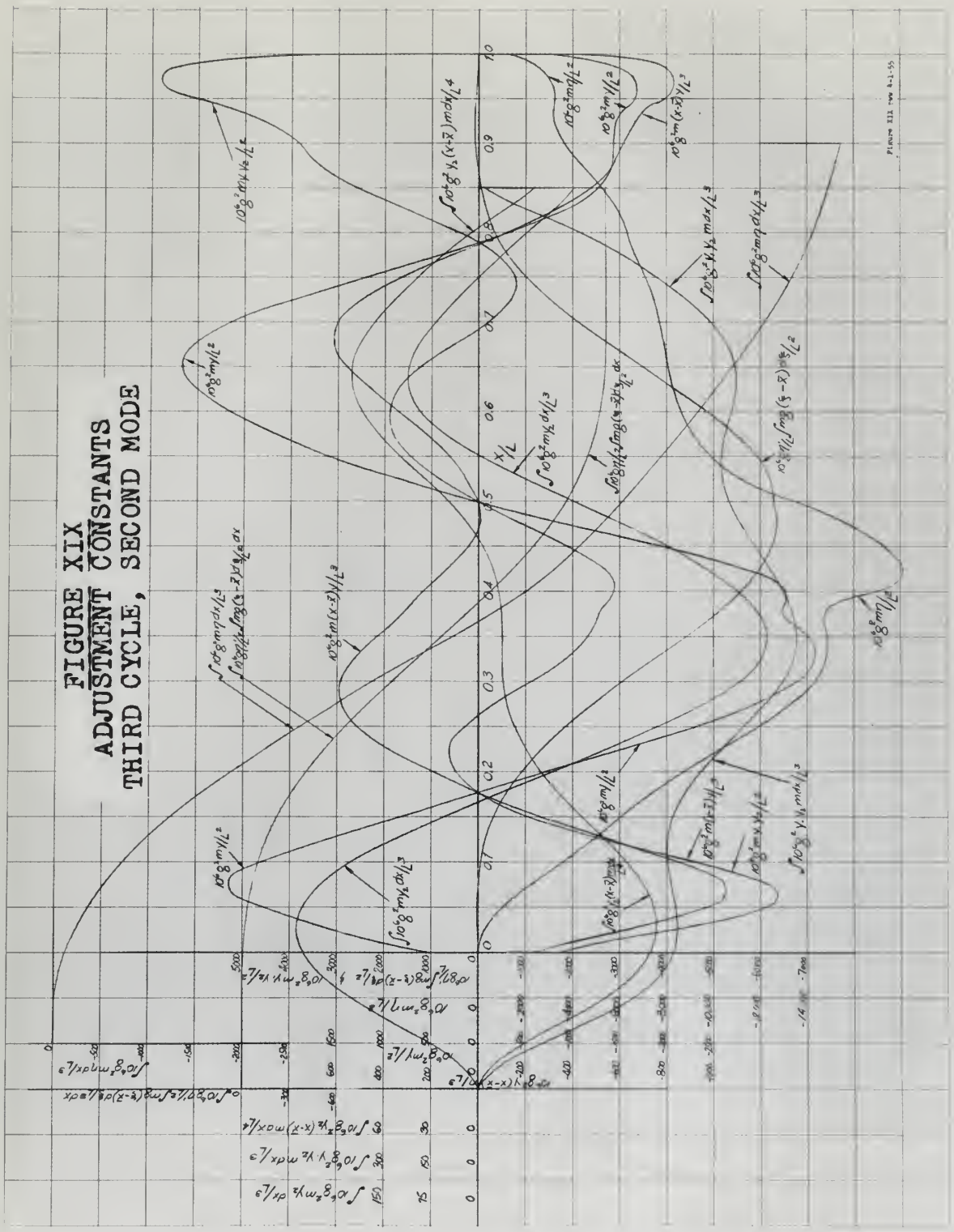
FIGURE XIX
ADJUSTMENT CONSTANTS
THIRD CYCLE, SECOND MODE

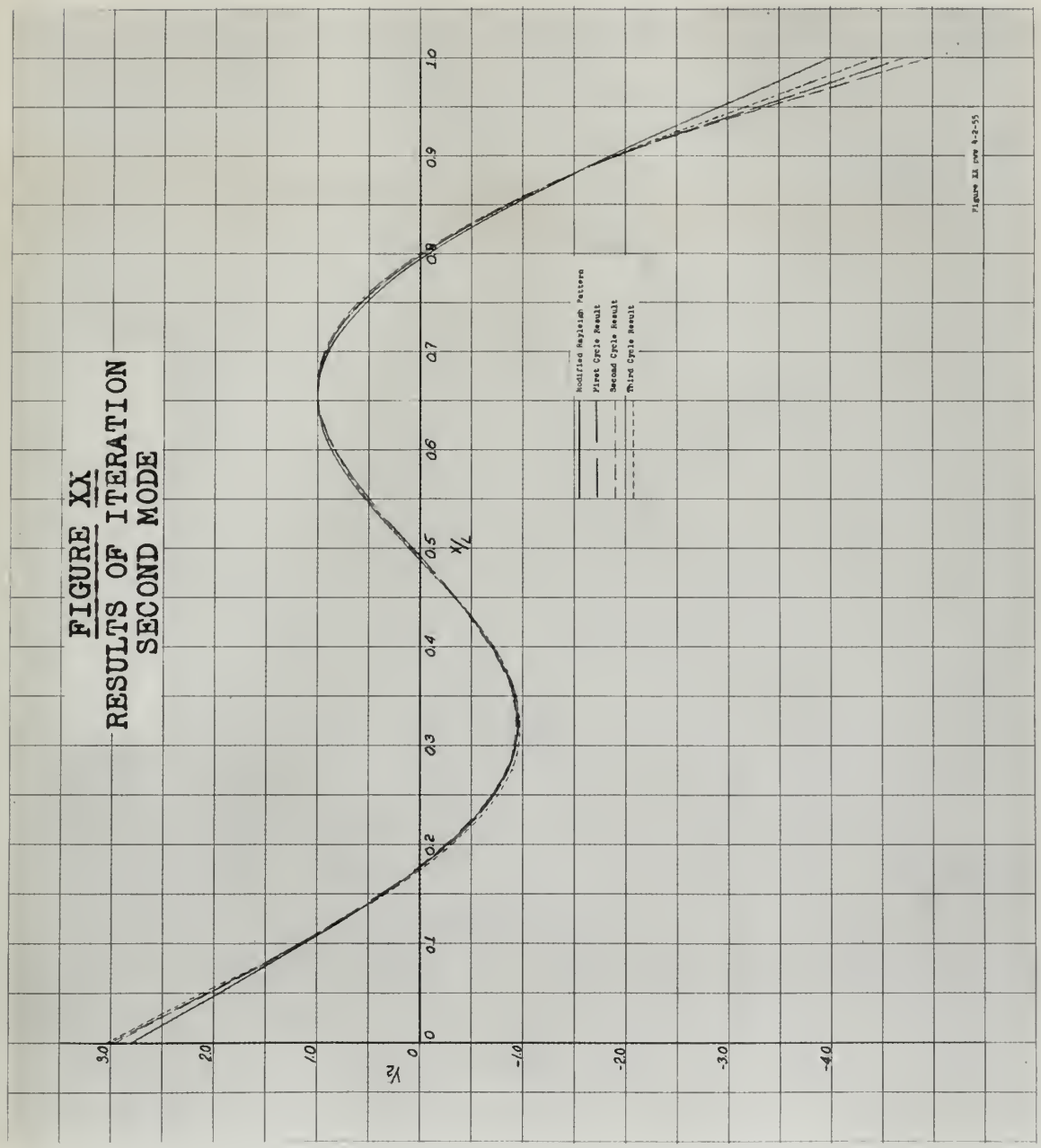
FIGURE XX
RESULTS OF ITERATION
SECOND MODE
Modified Rayleigh Pattern
First Cycle Result
Second Cycle Result
Third Cycle Result
Figure XX rev 4-2-55

FIGURE XXI
CONSTANTS FOR MODE CORRECTIONS

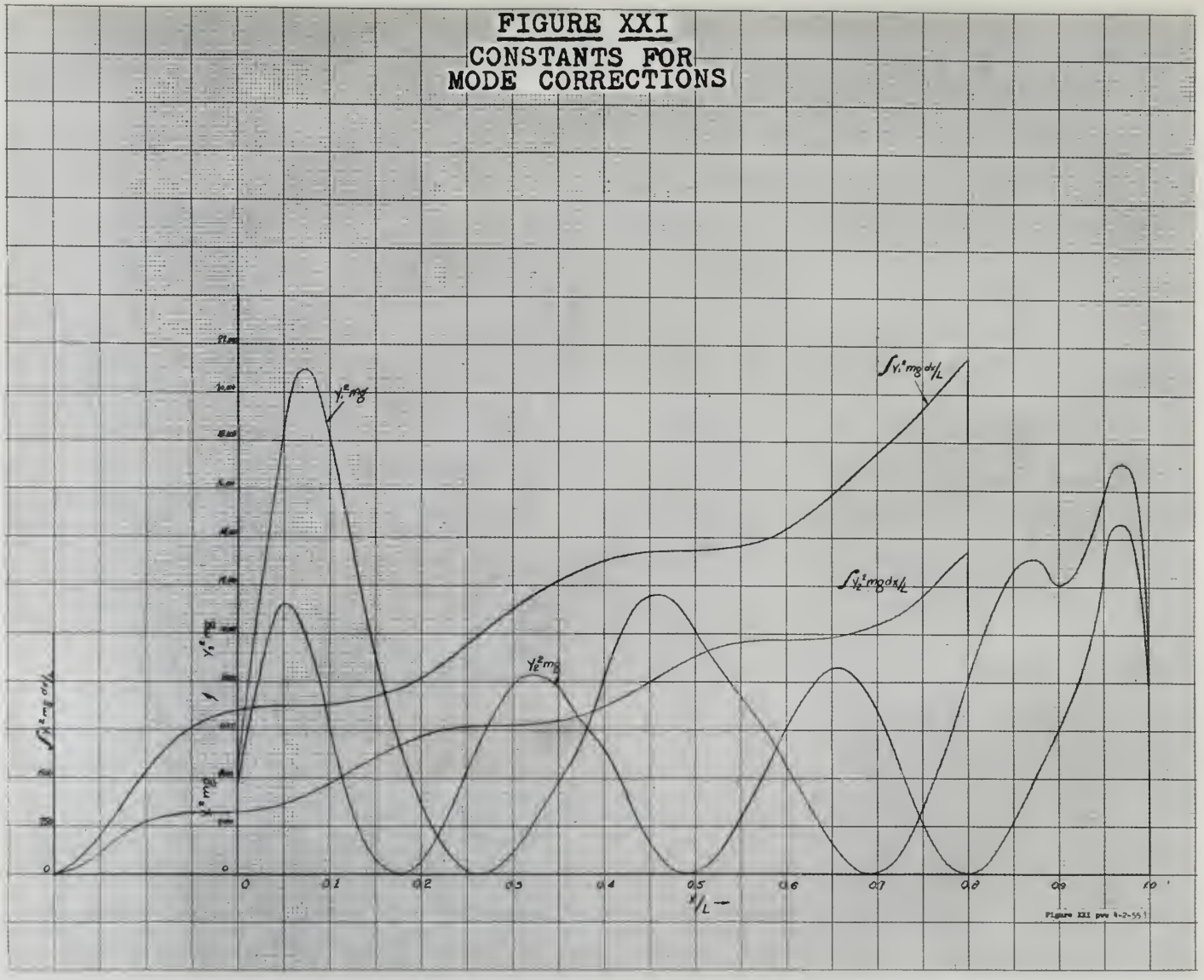

FIGURE XXII
CONSTANTS FOR CORRECTIONS
THIRD MODE RAYLEIGH PATTERN

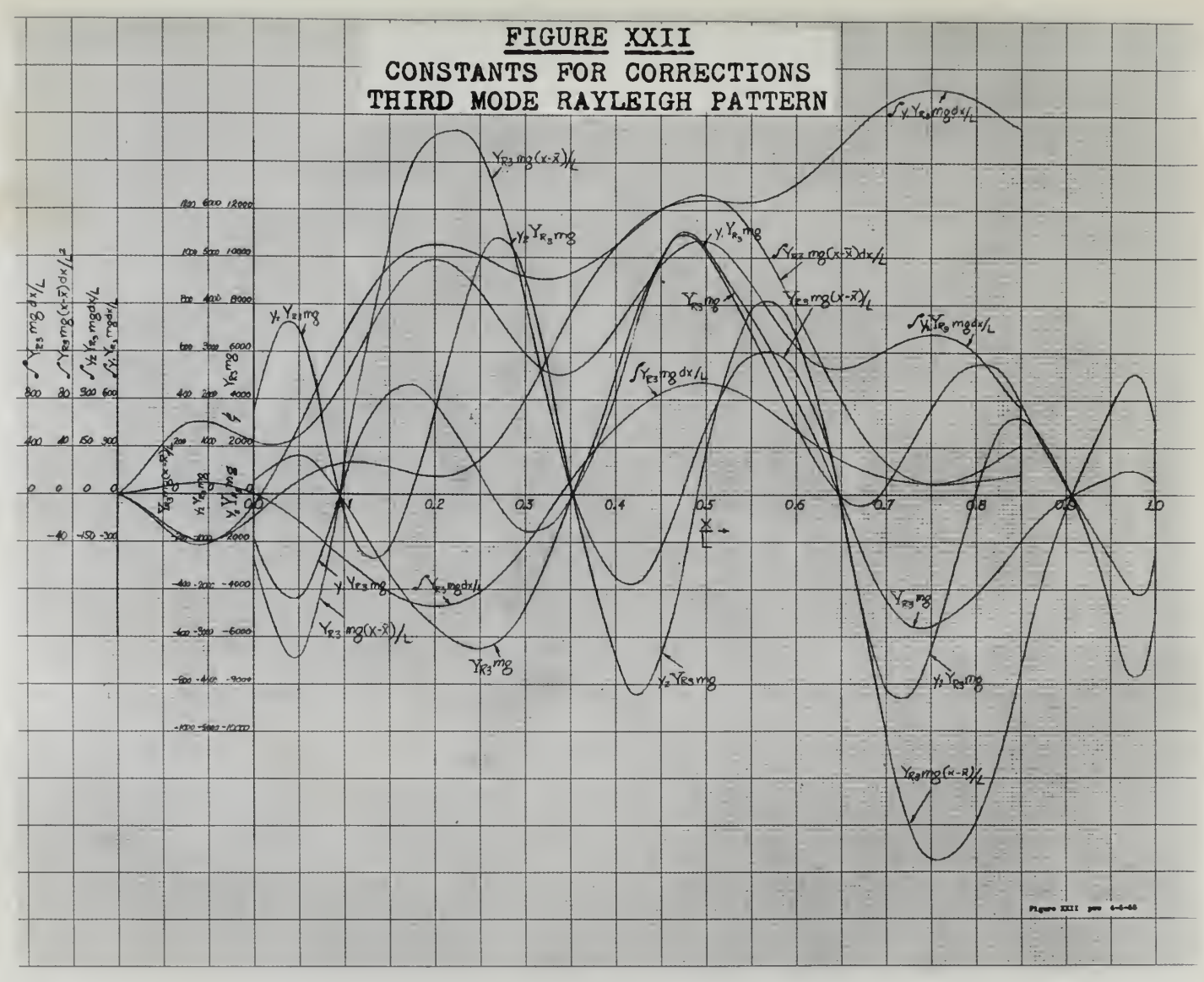

FIGURE XXIII
FIRST CYCLE OF THIRD MODE

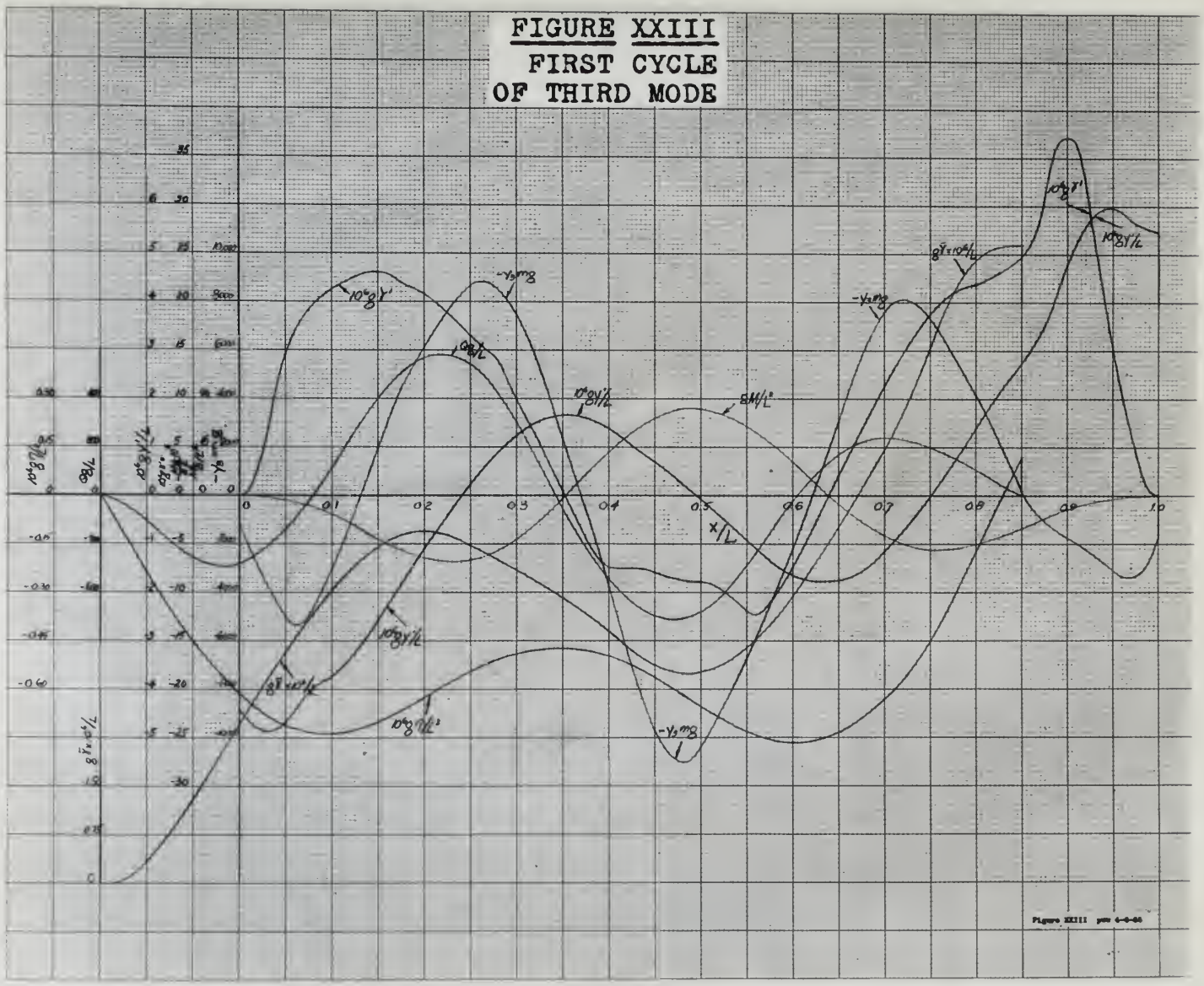

Figure XXIII pm 6-8-66

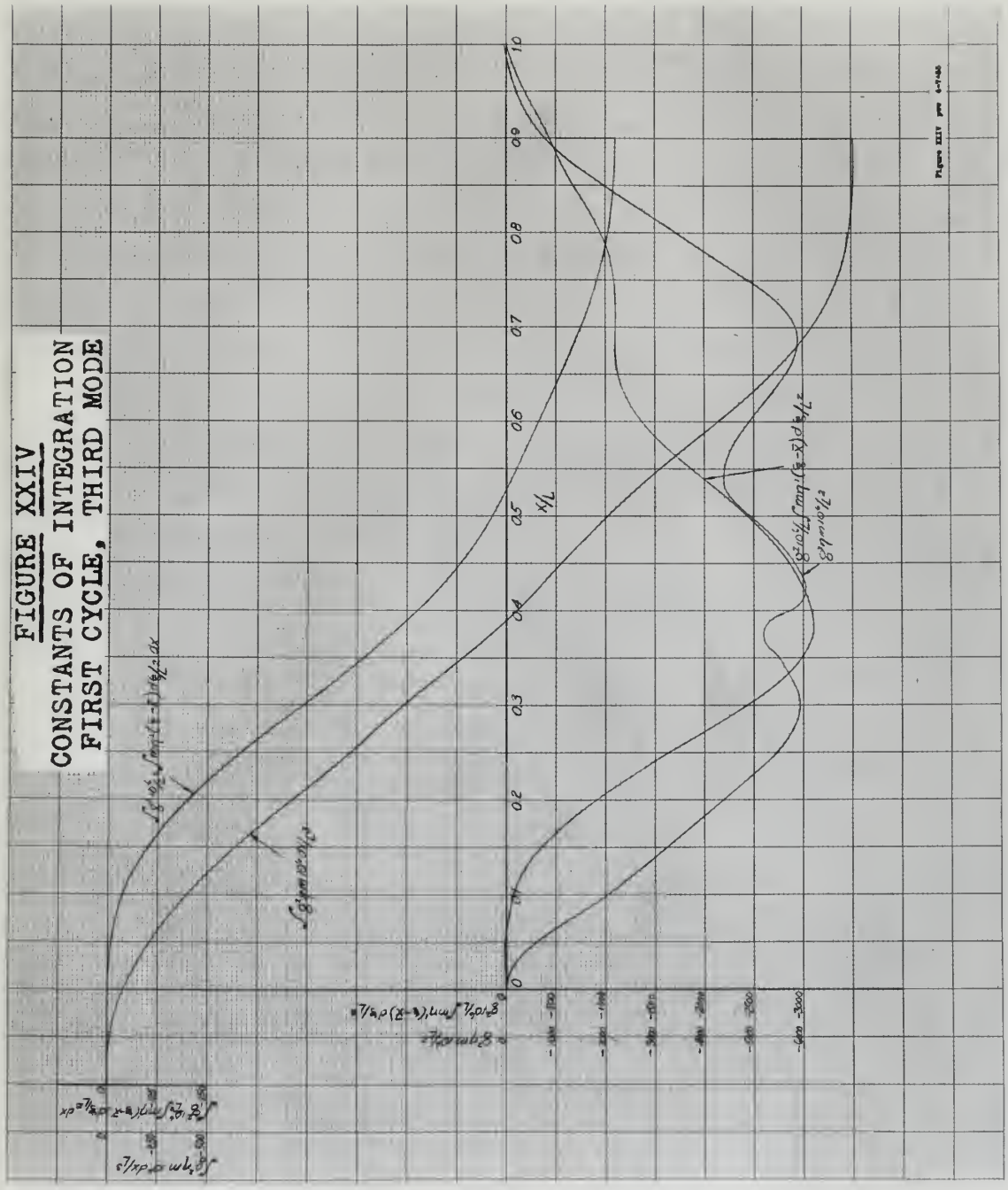

FIGURE XXIV
CONSTANTS OF INTEGRATION
FIRST CYCLE, THIRD MODE

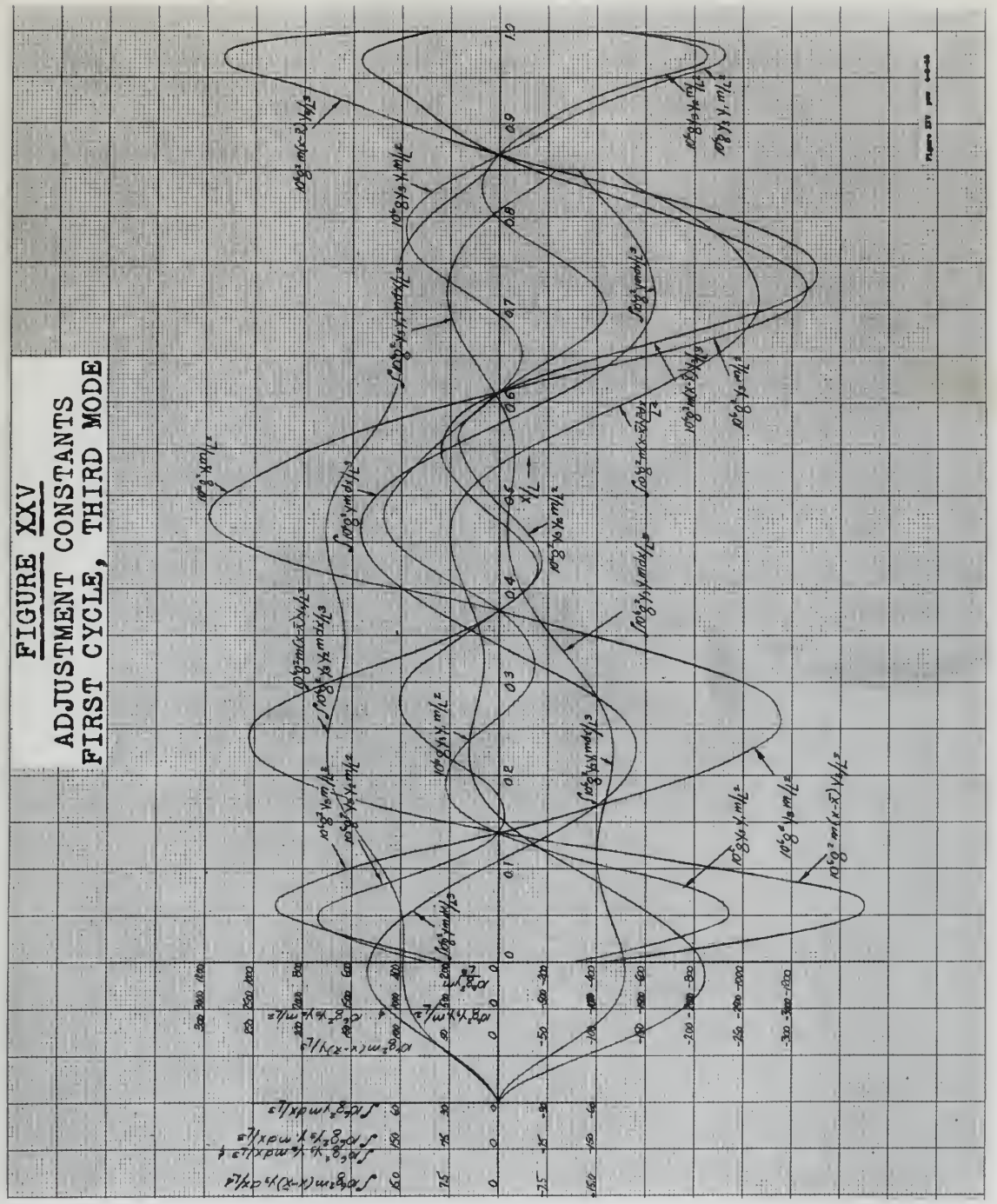

FIGURE XXV
ADJUSTMENT CONSTANTS
FIRST CYCLE, THIRD MODE

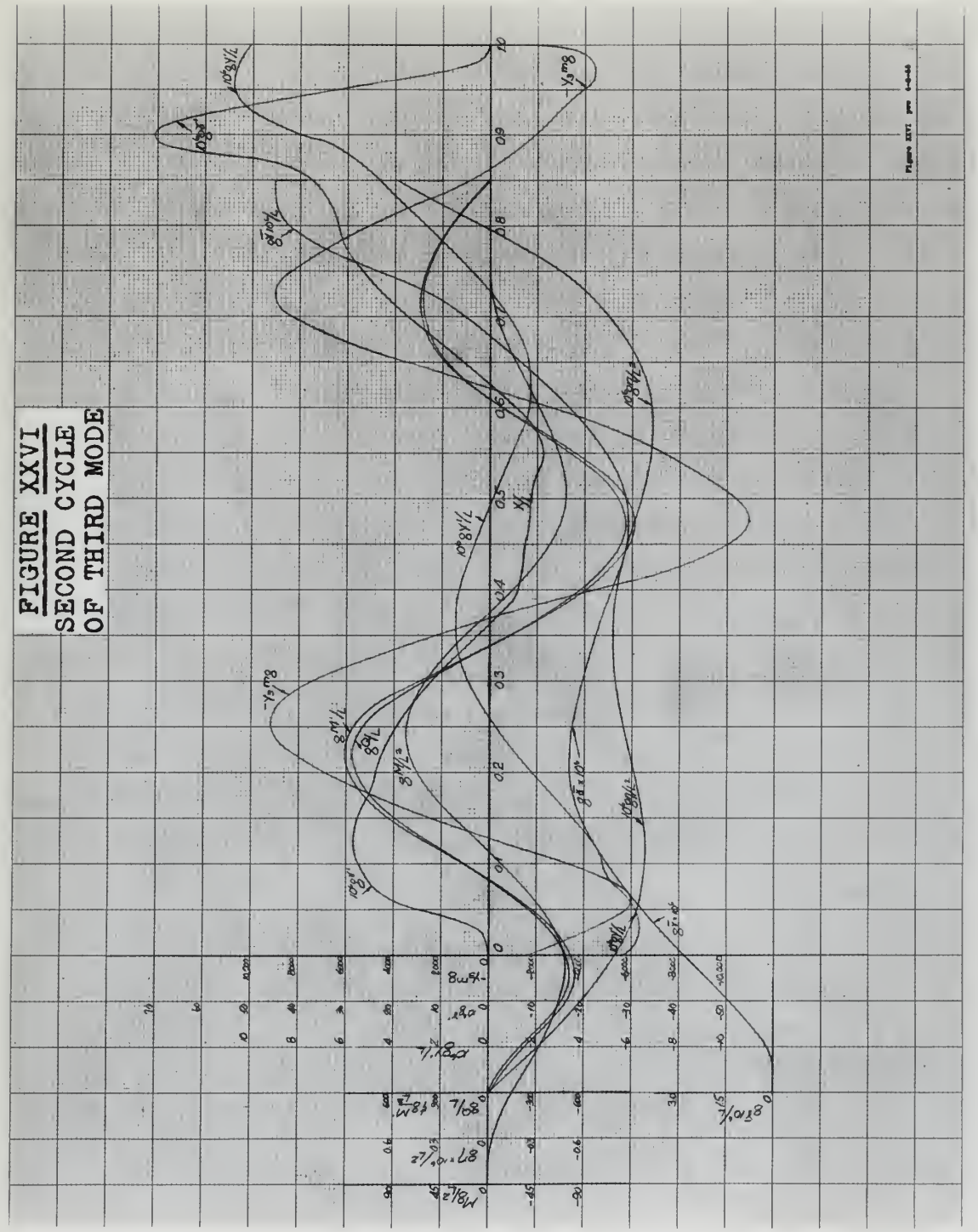

FIGURE XXVI
SECOND CYCLE
OF THIRD MODE

FIGURE XXVII
CONSTANTS OF INTEGRATION
SECOND CYCLE, THIRD MODE

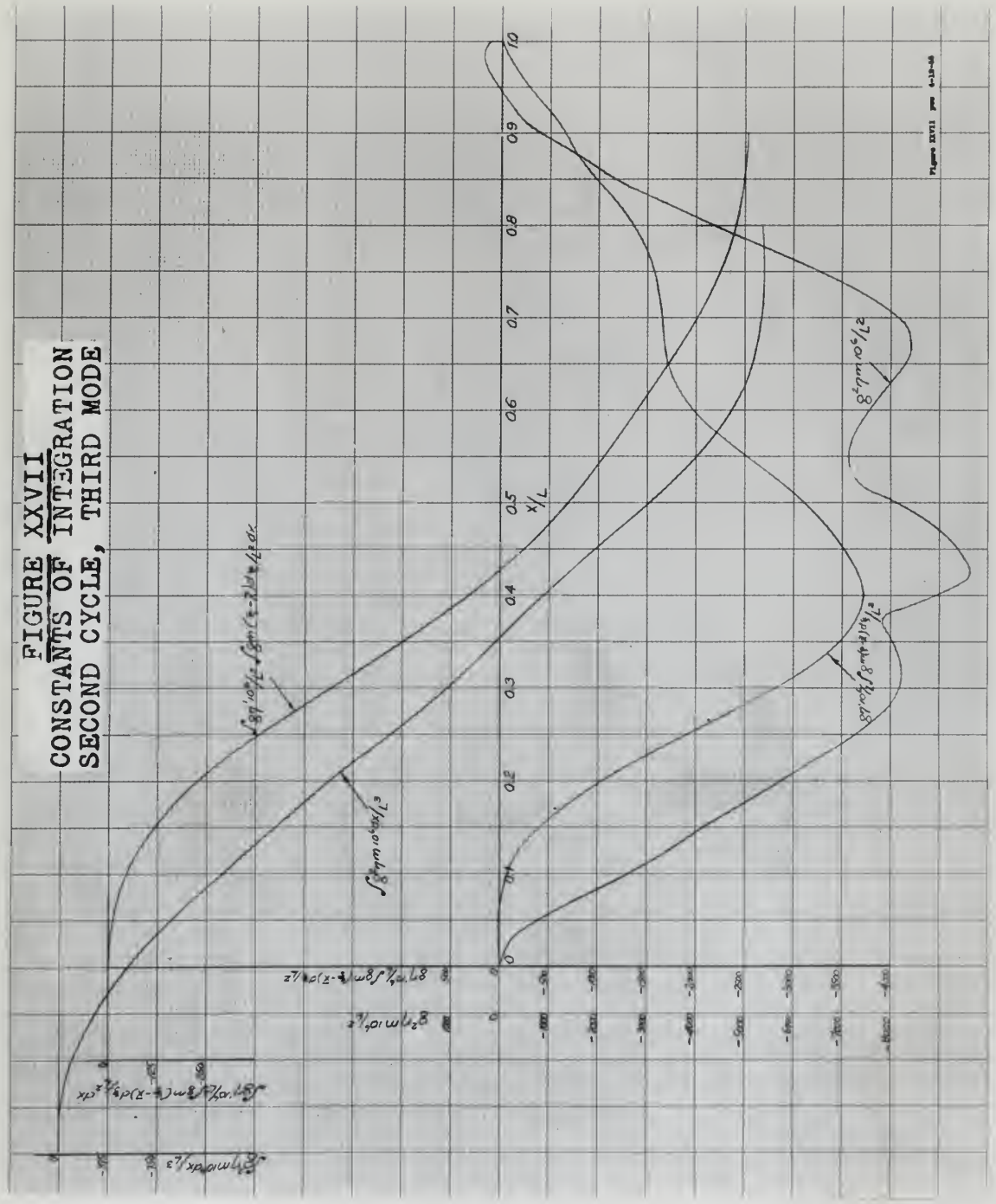

FIGURE XXVIII
ADJUSTMENT CONSTANTS
SECOND CYCLE. THIRD MODE

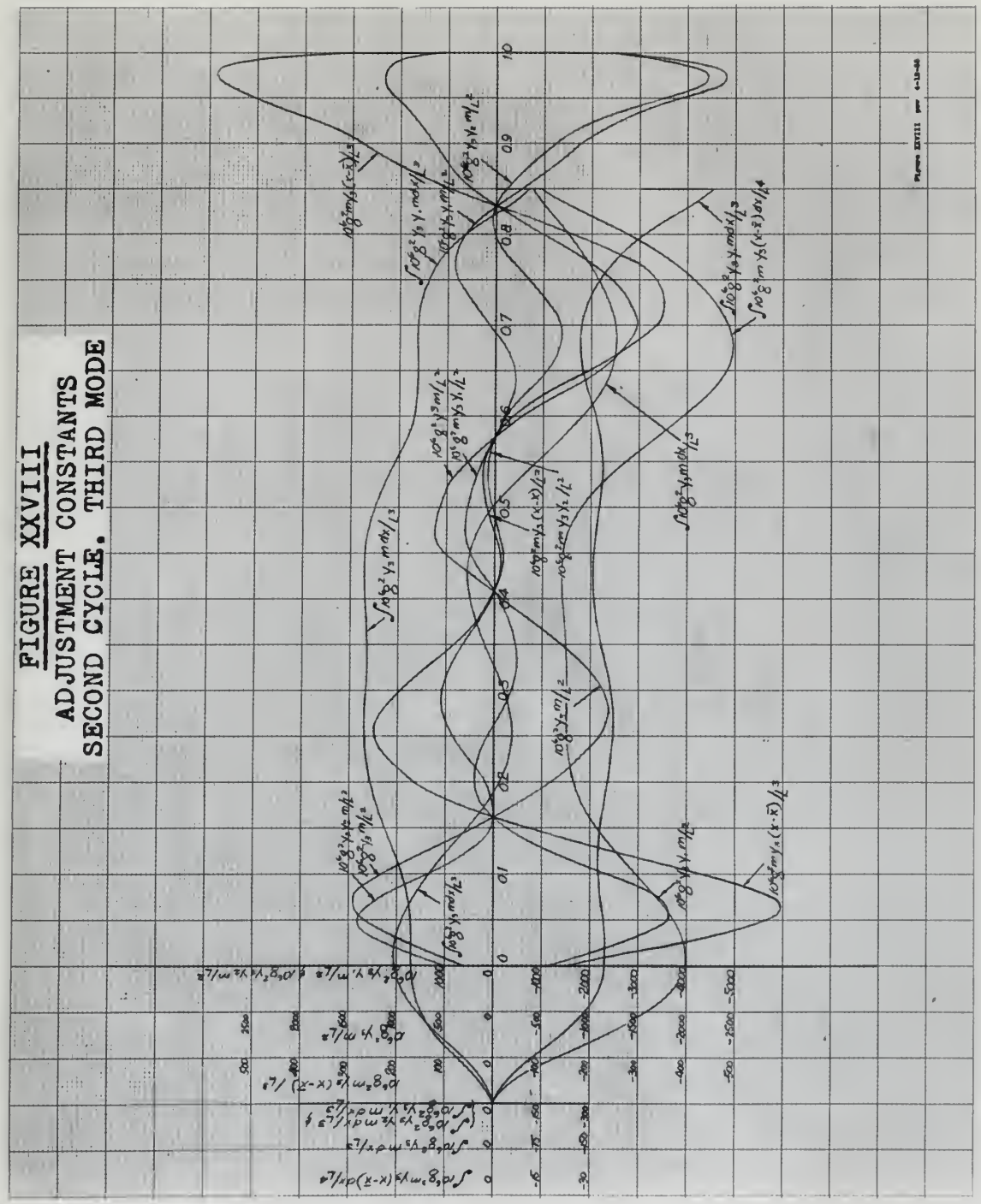

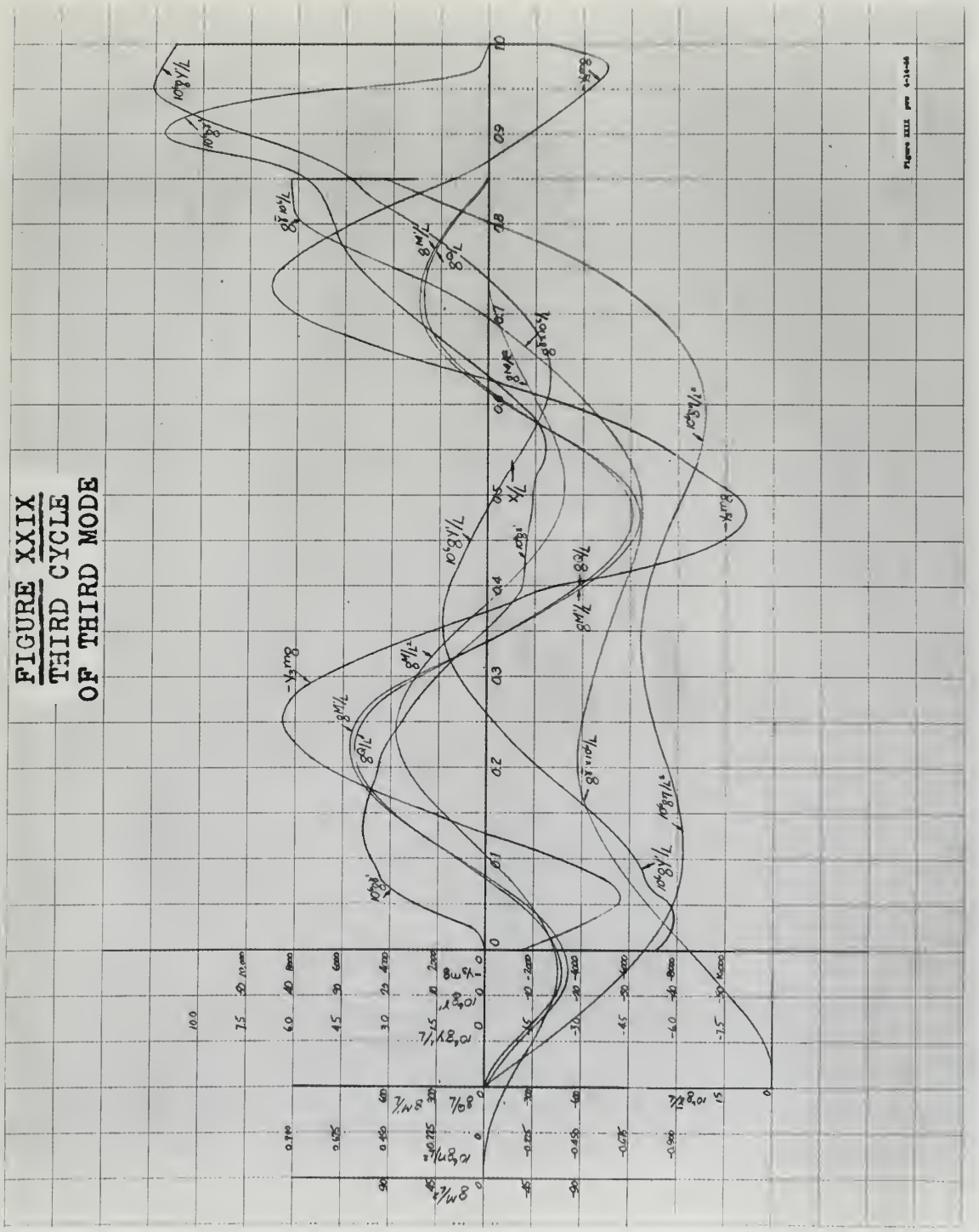

FIGURE XXIX
THIRD CYCLE
OF THIRD MODE

FIGURE XXX
CONSTANTS OF INTEGRATION
THIRD CYCLE, THIRD MODE

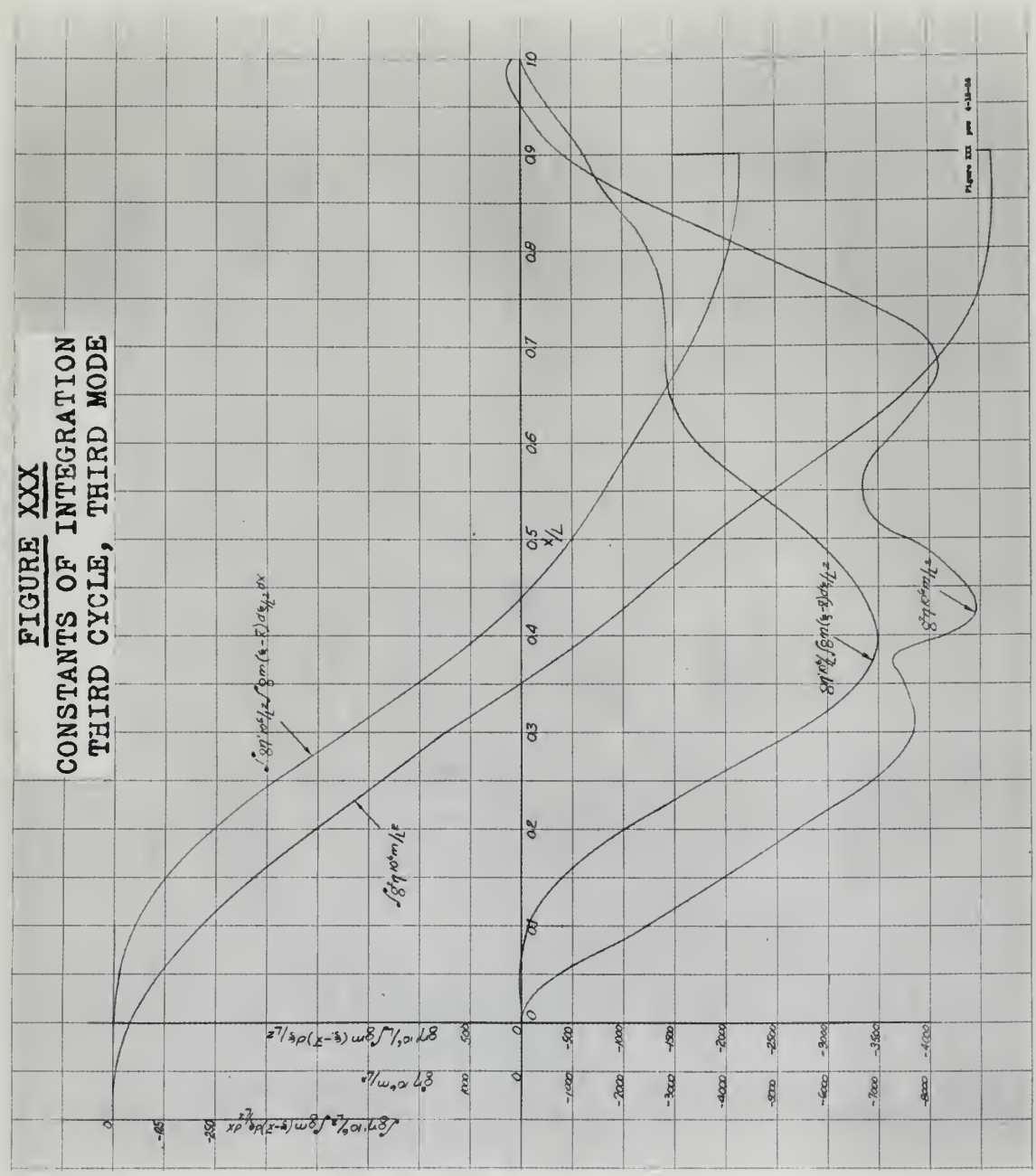

FIGURE XXXI
ADJUSTMENT CONSTANTS
THIRD CYCLE, THIRD MODE

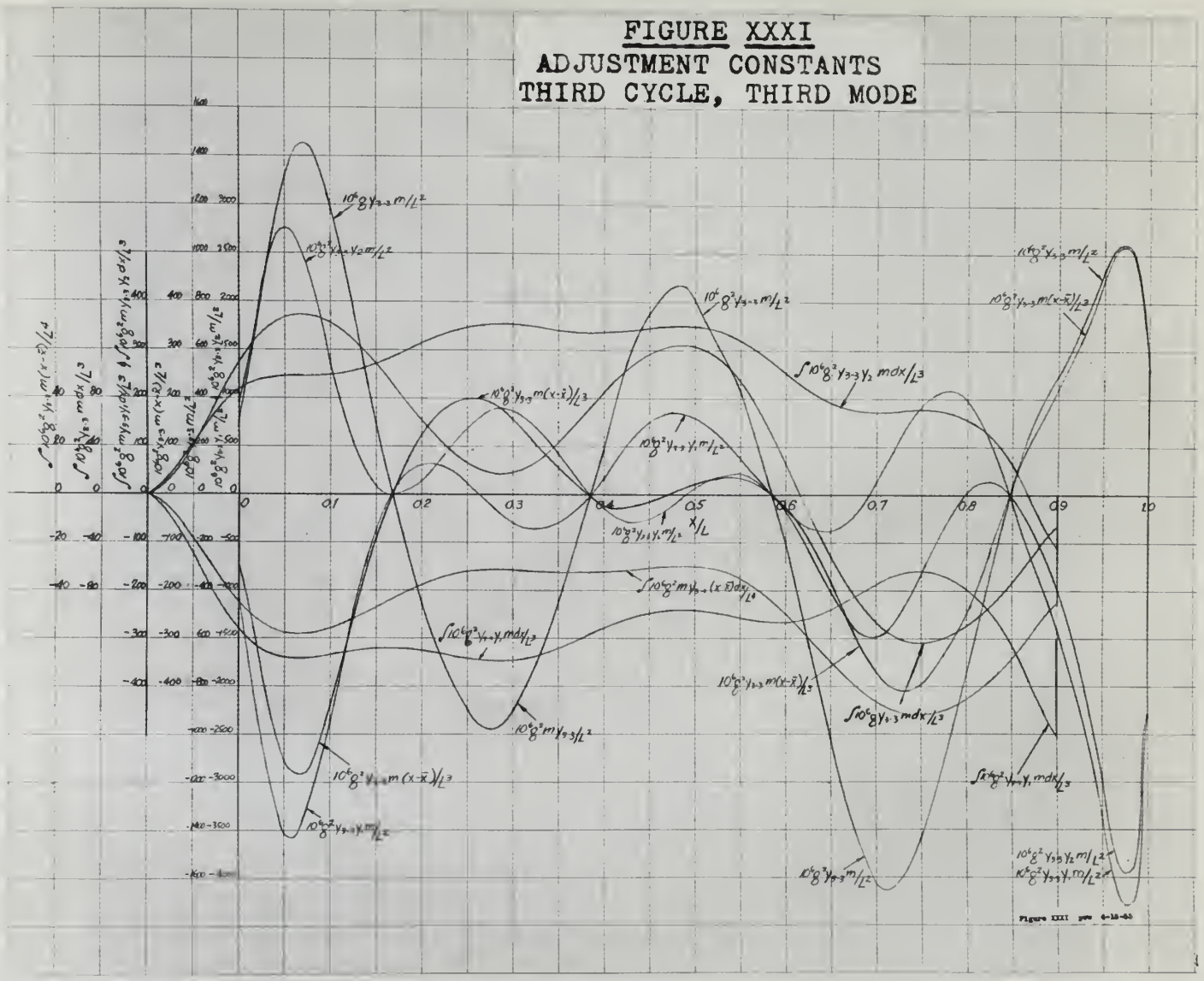

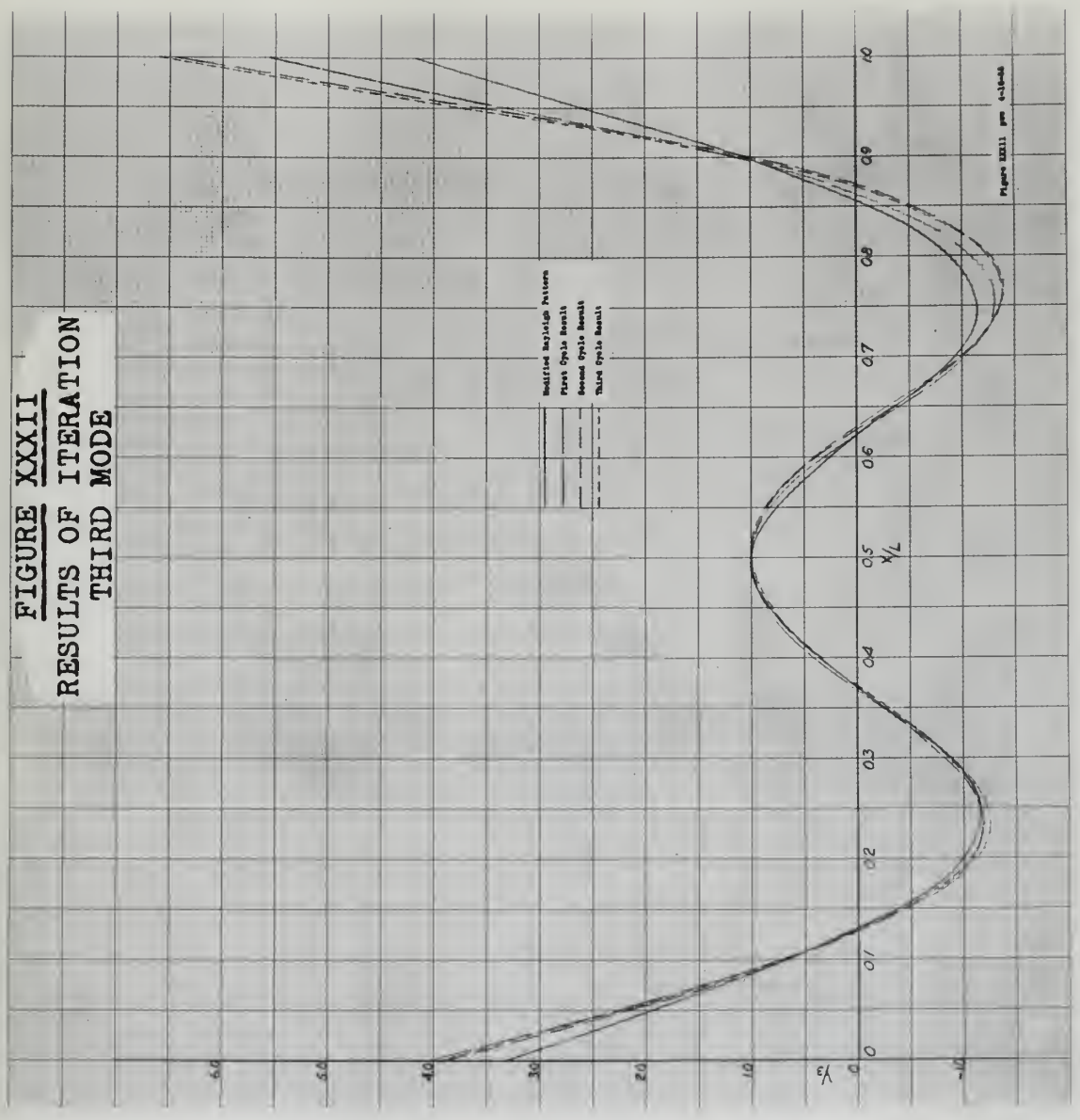

FIGURE XXXII
RESULTS OF ITERATION
THIRD MODE

FIGURE XXXIII
FINAL DEFLECTION PATTERNS AND FREQUENCIES

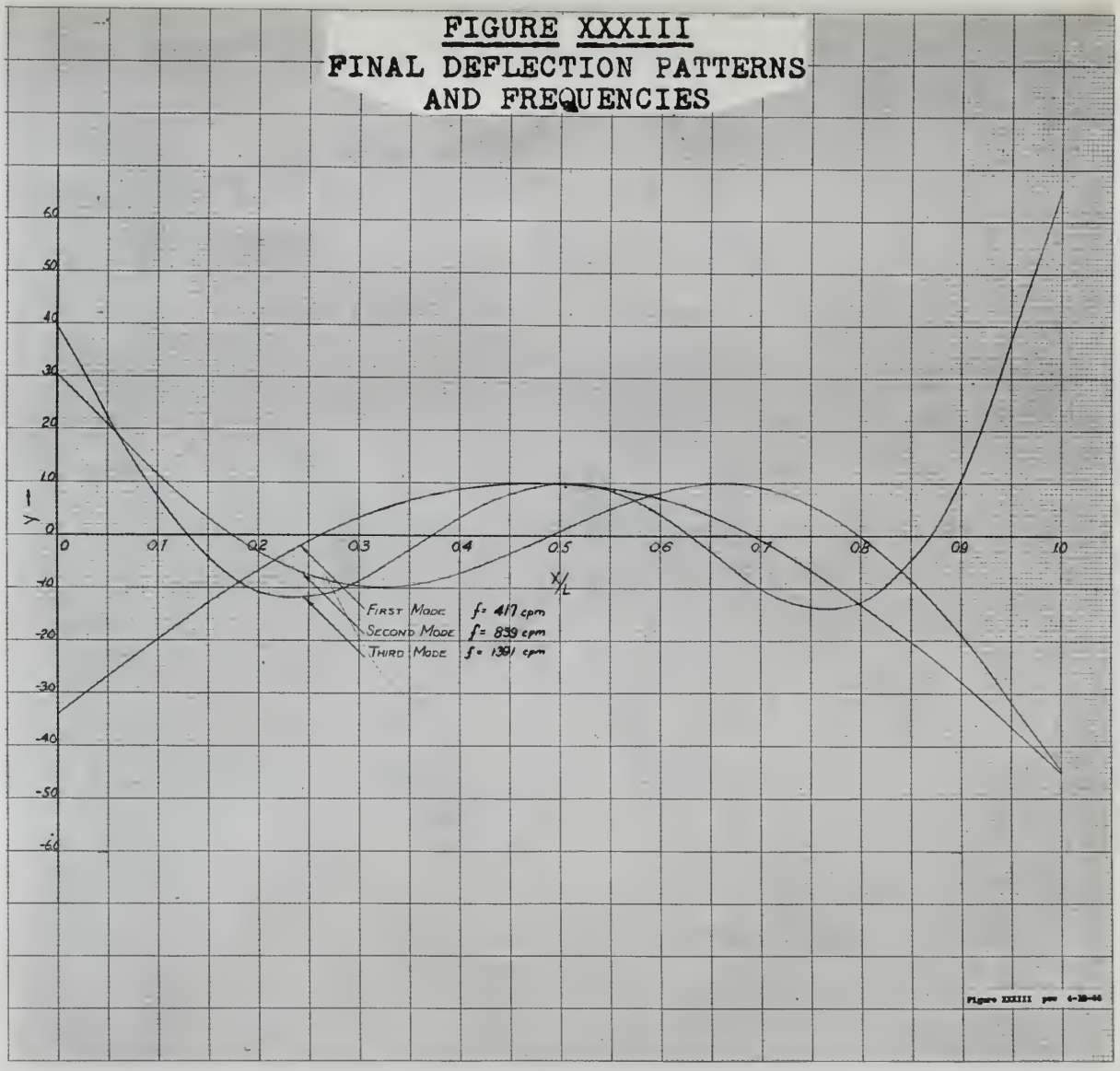

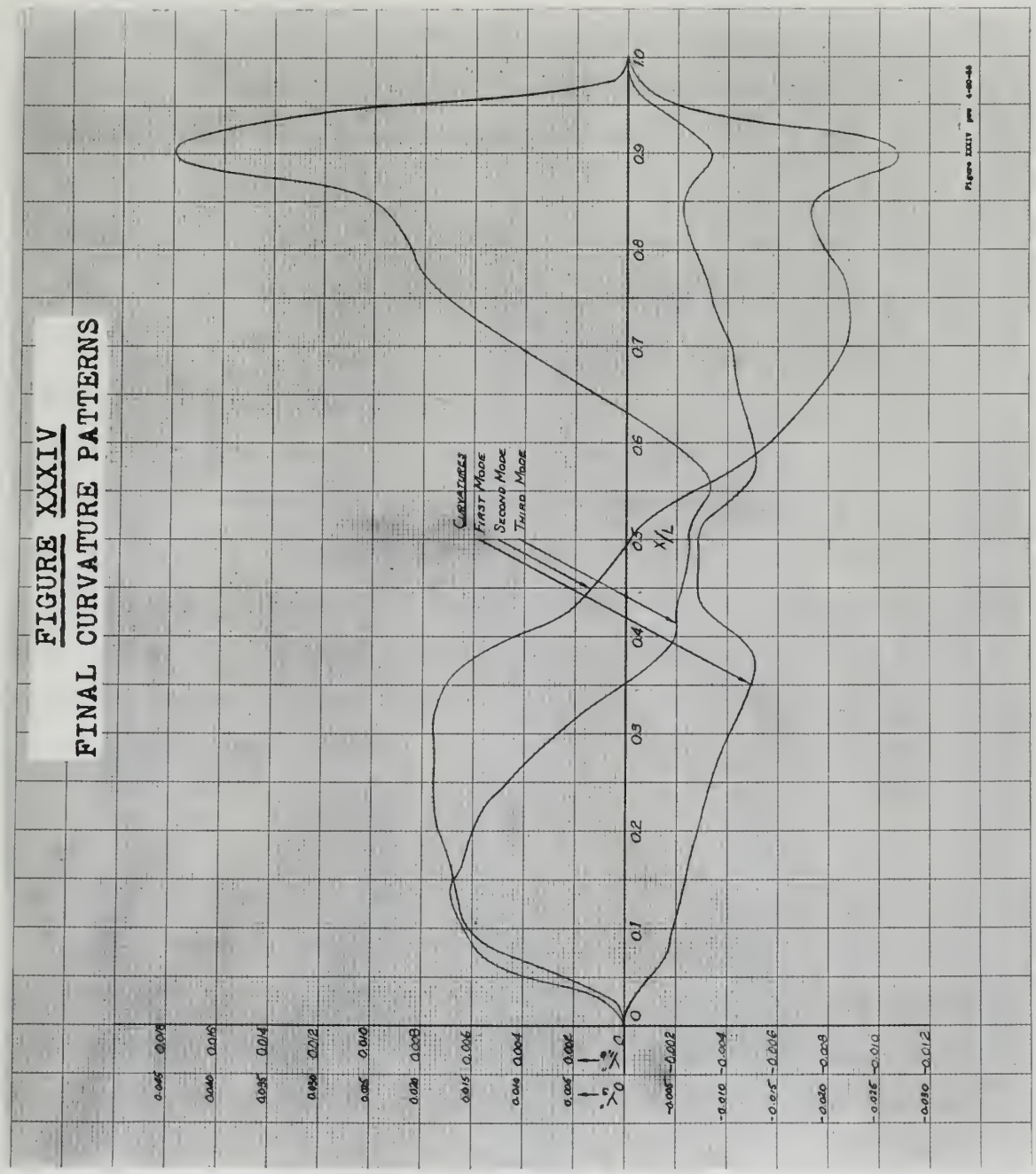
FIGURE XXXIV
FINAL CURVATURE PATTERNS
Curvatures
First Mode
Second Mode
Third Mode
X/L
0
0.1
0.2
0.3
0.4
0.5
0.6
0.7
0.8
0.9
1.0
0.018
0.016
0.014
0.012
0.010
0.008
0.006
0.004
0.002
-0.002
-0.004
-0.006
-0.008
-0.010
-0.012

APPENDIX C

Sample Calculation

This appendix contains a tabulation of the working functions for iteration, a table of constants used in the iteration, and a sample calculation in tabular form. All symbols are in accordance with those appearing in the Nomenclature.

The working functions (Table IV) pertain to all of the modal calculations. These functions were calculated as a matter of convenience as well as necessity. Their form is governed both by theory and by the conventions adopted and explained in Appendix A.

Table V contains a list of constants which, in general, apply to all three modal calculations. Orthogonality adjustment constants W_1 and W_2 apply to all modal calculations beyond the first mode and the second mode respectively. The derivation and explanation of the constants arising from integration may be found in Part I of Appendix A. The usual value of Young's Modulus was adopted, and the shear modulus was then computed from the well known relation:

$$G = \frac{E}{2(1 - \mu)} ,$$

where μ is Poisson's Ratio, taken equal to 0.3.

The sample calculation embraces the third cycle of the third mode. This mode was chosen as being the most general of the three with respect to the orthogonality conditions. The third cycle of this mode was chosen for the calculations because it includes the rotatory inertia correction. (The second cycle does also, but the results thereof are less conclusive than those of the third cycle). The calculation is presented in tabular form in Table VI. The source of each function appears beneath its symbol at the head of the column. Amplifying remarks pertinent to the sample calculation appear at the end of Table VI.

APPENDIX C

Sample Calculation

This appendix contains a tabulation of the working equations for iteration, a table of constants used in the iterations, and a sample calculation in tabular form. All symbols are in accordance with those appearing in the nomenclature.

The working equations (Table IV) pertain to all of the modal calculations. These equations were calculated as a matter of convenience as well as necessity. Their form is governed both by theory and by the conventions adopted and explained in Appendix A.

Table V contains a list of constants which, in general, apply to all three modal calculations. Orthogonality adjustment constants M_1' and M_2' apply to all modal calculations beyond the first mode and the second mode respectively. The derivation and explanation of the constants arising from integration may be found in Part 3 of Appendix A. The usual value of Young's modulus was adopted, and the shear modulus was then computed from the well known relation:

$$G = \frac{E}{2(1+\mu)} ,$$

where μ is Poisson's ratio, taken equal to 0.3.

The sample calculation summarizes the third cycle of the third mode. This mode was chosen as being the most general of the modes with respect to the orthogonality conditions. The third cycle of this mode was chosen for the calculations because it includes the relatively lengthy correction. (The second cycle does also, but the results thereof are less conclusive than those of the third cycle). The calculation is presented in machine form in Table VI. The source of each location appears beneath its symbol at the head of the column. Applying remarks pertinent to the sample calculation appear at the end of Table VI.

TABLE IV

WORKING FUNCTIONS FOR ITERATION

x/L	mg	gmI_{zz}/L^2A	$KAG/10^6$	$10^6L^2/EI_{zz}$	$(x-\bar{x})/L$
Units	lb/ft	lb/ft	lb	lb^{-1}	-
0.000	400	0.4125	80.62	3.232	-0.472
.025	1270	.8506	126.10	3.232	.447
.050	2550	.9194	274.96	3.232	.422
.075	3800	.7839	798.56	2.020	.397
.100	4550	1.1824	644.78	1.212	.372
.125	5000	1.8079	649.66	0.795	.347
.150	5290	2.5176	725.87	0.570	.322
.175	5680	3.0802	801.80	0.432	.297
.200	6150	3.5065	951.07	0.359	.272
.225	6750	4.1259	1125.11	0.308	.247
.250	7450	4.8824	1207.72	0.276	.222
.275	8000	5.7269	1246.91	0.252	.197
.300	8450	6.2268	1266.08	0.242	.172
.325	8680	6.3097	1307.14	0.239	.147
.350	8800	6.2896	1331.19	0.236	.122
.375	8910	6.5440	1348.67	0.225	.097
.400	10200	9.1276	1399.02	0.186	.072
.425	11800	11.3521	1590.31	0.129	.047
.450	11850	11.4385	1567.78	0.110	-0.022
.475	11400	10.9989	1560.96	0.109	+0.003
.500	10400	10.0333	1727.01	0.110	.028
.525	9300	9.8506	1439.06	0.133	.053
.550	8880	8.2764	1349.89	0.186	.078
.575	8730	6.8408	1315.94	0.223	.103
.600	8700	6.5169	1302.26	0.235	.128
.625	8700	6.4157	1275.82	0.242	.153
.650	8650	6.1477	1249.20	0.255	.178
.675	8450	5.6035	1219.86	0.278	.203
.700	8000	4.9544	1186.64	0.303	.228
.725	7300	4.2214	1134.05	0.334	.253
.750	6400	3.4543	1100.75	0.373	.278
.775	5450	2.7277	918.46	0.425	.303
.800	4660	2.2035	832.70	0.485	.328
.825	3900	1.6861	718.31	0.592	.353
.850	3060	1.1393	805.30	0.808	.378
.875	2300	0.6257	681.92	1.469	.403
.900	1700	0.3511	318.94	2.851	.428
.925	1330	0.2564	240.69	4.041	.453
.950	1200	9.2427	213.88	4.848	.478
.975	1000	0.2438	226.03	4.848	.503
1.000	400	0.1100	184.00	4.848	+0.528

TABLE IV

[illegible]

TABLE IV (cont'd)

WORKING FUNCTIONS FOR ITERATION

x/L	$mg(x-\bar{x})/L$	$g\int_{o}^{x} m(\xi-\bar{x})d\xi/L^2$	y_1	$y_1 mg$	y_2	$y_2 mg$
Units	lb/ft	lb/ft	ft	lb	ft	lb
0.000	- 188.8	0	-3.408	-1363.2	+3.041	+1216.4
0.025	567.69	- 9.6	3.054	3878.58	2.578	3274.06
0.050	1076.1	30.6	2.695	6872.25	2.101	5357.55
0.075	1508.6	64.8	2.347	8918.6	1.609	6114.2
0.100	1692.6	103.2	1.994	9072.70	1.161	5282.55
0.125	1735.0	144.6	1.641	8205.0	0.726	3630.0
0.150	1703.38	185.4	1.299	6871.71	+ .336	+1777.44
0.175	1686.96	232.8	0.988	5611.84	- .018	- 107.24
0.200	1672.8	269.4	.682	4194.3	.307	1888.05
0.225	1667.25	311.4	.395	2666.25	.567	3827.25
0.250	1653.9	352.2	- .125	- 931.25	.762	5676.9
0.275	1576.0	391.2	+ .109	+ 872.0	.891	7128.0
0.300	1453.4	427.8	.325	2746.25	.963	8137.35
0.325	1275.96	460.8	.511	4435.48	.977	8480.36
0.350	1073.6	488.4	.661	5816.8	.940	8272.0
0.375	864.27	513.6	.788	7021.08	.845	7528.95
0.400	76[illegible].2	532.8	.878	9306.8	.706	7483.6
0.425	554.6	548.4	.944	11139.2	.532	6277.6
0.450	- 260.7	55[illegible].0	.987	11695.95	.336	3981.6
0.475	+ 34.2	561.6	1.000	11400.0	- .133	-1516.2
0.500	291.2	558.0	.989	10285.6	+ .085	+ 884.0
0.525	492.9	549.0	.965	8974.5	.302	2808.6
0.550	692.64	534.0	.912	8098.56	.519	4608.72
0.575	899.19	514.2	.835	7289.55	.693	6049.89
0.600	1113.6	489.0	.711	6185.7	.838	7290.6
0.625	1331.1	457.8	.568	4941.6	.938	8160.6
0.650	1539.7	423.0	.383	3312.95	.995	8606.75
0.675	1715.35	382.2	+ .169	+1428.05	.987	8340.15
0.700	1824.0	337.2	- .087	- 696.0	.920	7360.0
0.725	1846.9	289.8	.350	2555.0	.780	5694.0
0.750	1779.2	245.4	.654	4185.6	.582	3724.8
0.775	1651.35	203.4	.976	5319.2	+ .304	+1656.8
0.800	1528.48	163.2	1.310	6104.6	- .024	- 111.84
0.825	1376.7	126.6	1.662	6481.8	.411	1602.9
0.850	1156.68	94.8	2.032	6217.92	.849	2597.94
0.875	926.9	68.4	2.389	5494.7	1.337	3075.1
0.900	727.6	48.0	2.783	4731.1	1.883	3201.1
0.925	602.5	30.6	3.207	4265.3	2.503	3328.99
0.950	573.6	17.4	3.624	4348.8	3.174	3808.8
0.975	503.0	- 7.2	4.066	4126.0	3.808	3808.0
1.000	+ 211.2	0	-4.502	-1800.8	-4.450	-1780.0

TABLE V

CONSTANTS REQUIRED FOR ITERATION

CONSTANT	SYMBOL	VALUE
$\int_0^L mg \frac{dx}{L}$	Δ/L	6450 lb/ft
$\int_0^L \int_0^x \frac{(\xi - \bar{x})}{L} mg \frac{d\xi}{L} \frac{dx}{L}$	P	-287.64 lb/ft
$\int_0^L \frac{(x-\bar{x})^2}{L^2} mg \frac{dx}{L}$	N	300 lb/ft
$\int_0^L y_1^2 mg \frac{dx}{L}$	W_1	8062.5 ft-lb
$\int_0^L y_2^2 mg \frac{dx}{L}$	W_2	5040.9 ft-lb
Length of model	L	100.5 ft
Longitudinal centroid (from bow)	$\bar{x}$	(0.472) L ft.
Shear Modulus	G	11.5×10^6 lb/in.^{2}
Young's Modulus	E	30.0×10^6 lb/in.^{2}

TABLE V

COMPARAISON DES ITERATIONS

TABLE VI

- SAMPLE CALCULATION -

THIRD CYCLE OF THIRD MODE

(1)	(2)	(3)	(4)	(5)	(6)
x/L	Y_{3-2}	g_4'	g_4/L	$\gamma_{3-2}\frac{EI}{LA}$	g_4'/L
Source	Second Cycle 3rd mode	$-(2)mg\omega^2$	$\int_x (3)\,dx/L$	See Remarks	(4) + (5)
0.000	+3.8865	-1554.60	0	-15	- 15
0.025	3.0105	3823.34	- 66	31	97
0.050	2.1546	5494.23	189	33	222
0.075	1.3490	5126.20	330	25	355
0.100	.6706	3051.23	444	33	477
0.125	+ .0522	- 261.	480	42	522
0.150	- .4299	+2274.17	450	47	497
0.175	.8467	4809.26	360	43	403
0.200	1.0802	6643.23	213	35	248
0.225	1.1644	7859.7	- 24	25	- 49
0.250	1.1507	8572.72	+183	-13	+170
0.275	1.0320	8256.	393	+ 2	395
0.300	.8174	6907.03	573	18	591
0.325	.5519	4790.49	720	28	748
0.350	- .2616	+2302.08	804	32	834
0.375	+ .0626	- 557.77	825	33	858
0.400	.3536	3748.16	777	43	820
0.425	.6171	7281.78	651	41	692
0.450	.8304	9840.24	417	28	445
0.475	.9498	10827.72	+147	+13	+160
0.500	1.0000	10400.	-129	- 3	-132
0.525	.9641	8966.13	366	17	383
0.550	.8545	7587.96	579	30	609
0.575	.6660	5814.18	753	37	790
0.600	.3894	3387.78	867	43	910
0.625	+ .0385	- 334.95	915	44	959
0.650	- .3607	+3120.06	879	40	919
0.675	.6882	5815.29	765	27	792
0.700	1.0052	8041.6	591	-11	602
0.725	1.2355	9019.15	351	+ 5	346
0.750	1.3653	8737.92	-132	15	-117
0.775	1.3738	7487.21	+ 63	27	+ 90
0.800	1.2433	5793.78	222	34	256
0.825	.9713	3788.07	339	35	374
0.850	- .5199	+1590.89	396	30	426
0.875	+ .0874	- 201.02	405	21	426
0.900	.9876	1678.92	381	16	397
0.925	2.1970	2922.01	321	14	335
0.950	3.5343	4241.16	228	15	243
0.975	5.0216	5021.60	+108	16	124
1.000	+6.4208	-2568.32	0	+ 7	+ 7

TABLE XI

- BESSEL EIGENFUNCTIONS -

Nu	Second Order Bessel Function	$-(1)\sin\nu\pi$	$\int_0^x (3)\,dx/x$	Sum (1) + (3)
0.000	+ 3.0464	-1334.60	0	- 42
0.025	3.2267	3923.34	- 62	27
0.050	3.1804	2469.23	128	3872
0.075	3.2899	2126.00	190	3872
0.100	.2702	2021.23	244	3872
0.125	+ .0234	1900	293	3872
0.150	- .0279	+ 2274.12	340	3872
0.175	.0807	2600.36	384	3872
0.200	3.0802	2647.29	429	3872
0.225	3.1206	2750.7	- 84	3872
0.250	3.1407	2772.72	+1287	-1370
0.275	3.0784	2826.	1323	3872
0.300	.0179	2907.03	1373	3872
0.325	.9719	2990.80	1430	3872
0.350	.9264	+3009.08	1504	3872
0.375	+ .0806	- 357.77	1555	3872
0.400	.2944	3048.19	1611	3872
0.425	.8273	3071.79	1664	3872
0.450	.7884	3090.34	1717	3872
0.475	.8879	3107.72	+1767	+1767
0.500	3.0000	3126.00	- 1818	-1732
0.525	.9541	3144.13	1870	3872
0.550	.8803	3157.96	1922	3872
0.575	.6000	3171.48	1977	3872
0.600	.2884	3179.70	2031	3872
0.625	+ .0744	- 3184.89	2085	3872
0.650	- .0607	+ 3180.50	2139	3872
0.675	.1883	3172.29	2193	3872
0.700	3.0013	3161.6	2247	3872
0.725	3.2239	3013.13	2302	-12
0.750	3.3697	2972.78	-1372	+ 2
0.775	3.3238	2948.7	+ 85	+ 2
0.800	3.2473	2929.76	2582	2582
0.825	.9923	2908.07	2636	2636
0.850	- .2299	+2890.89	2686	2686
0.875	+ .0974	- 2831.02	2735	2735
0.900	.0974	2829.72	2784	2784
0.925	3.1770	2872.01	2833	2833
0.950	3.3917	2881.16	2882	2882
0.975	3.2274	2931.60	+1931	2931
1.000	+3.0000	-2980.72	0	+ 2

TABLE VI (cont'd)

(1)	(7)	(8)	(9)	(10)	(11)
X/L	$\Sigma M/L^2$	$\Sigma\gamma'_{3-3}\ 10^6$	$\Sigma\bar{\gamma}_{3-3}\ \frac{10^6}{L}$	$\Sigma\beta\ \frac{10^6}{L}$	$\Sigma\eta'\ \frac{10^6}{L}$
Source	$\int_x (6)\,dx/L$	$(7).\ \frac{10^6 L}{EI}$	$\int_x (8)\,dx/L$	$(4).\ \frac{10^6}{KAG}$	(9)+(10)
0.000	0	0	0	0	0
0.025	- 0.90	+ 2.909	+ 0.015	-0.5234	- 0.5084
0.050	4.50	14.544	.255	0.6874	- 0.4324
0.075	10.80	21.816	.735	0.4132	+ 0.3218
0.100	19.80	23.998	1.335	0.6886	0.6464
0.125	32.40	25.758	1.980	0.7388	1.2412
0.150	44.55	25.394	2.655	0.6199	2.0351
0.175	55.35	23.911	3.300	0.4490	2.8510
0.200	63.45	22.779	3.915	0.2240	3.6910
0.225	68.40	21.067	4.500	-0.0213	4.4787
0.250	63.45	17.512	5.010	+0.1515	5.1615
0.275	56.25	14.175	5.445	0.3152	5.7602
0.300	42.75	10.346	5.790	0.4526	6.2426
0.325	24.75	5.915	6.030	0.5508	6.5808
0.350	- 3.15	+ 0.743	6.120	0.6040	6.7240
0.375	+18.90	- 4.252	6.120	0.6117	6.7317
0.400	39.60	7.366	6.000	0.5554	6.5554
0.425	60.75	7.837	5.820	0.4094	6.2294
0.450	75.15	8.266	5.640	0.2660	5.9060
0.475	83.25	9.074	5.445	+0.0942	5.5392
0.500	84.60	9.306	5.220	-0.0747	5.1453
0.525	78.30	10.414	4.980	0.2543	4.7257
0.550	66.60	12.388	4.710	0.4289	4.2811
0.575	49.50	11.038	4.425	0.5722	3.8528
0.600	28.80	6.768	4.200	0.6658	3.5342
0.625	+ 5.40	- 1.307	4.125	0.7172	3.4078
0.650	-18.00	+ 4.590	4.155	0.7036	3.4514
0.675	37.80	10.508	4.350	0.6271	3.7229
0.700	54.45	16.498	4.725	0.4980	4.2270
0.725	66.60	22.244	5.235	0.3095	4.9255
0.750	72.00	26.856	5.850	-0.1199	5.7301
0.775	72.00	30.600	6.585	+0.0686	6.6536
0.800	66.60	32.301	7.410	0.2666	7.6766
0.825	58.50	34.632	8.415	0.4719	8.8869
0.850	47.25	38.178	9.195	0.4917	9.6867
0.875	36.00	52.884	10.335	0.5939	10.9289
0.900	23.85	67.996	11.880	1.1946	13.0746
0.925	14.85	60.009	13.560	1.3337	14.8937
0.950	6.75	32.724	14.835	1.0660	15.9010
0.975	- 0.45	+ 2.182	15.180	+0.4778	15.6578
1.000	0	0	+15.225	0	+15.225

TABLE VI (cont'd)

(1)	(12)	(13)	(14)	(15)	(16)
x/L	$\beta^2\eta' \cdot \frac{10^6}{L}\int_0^x m \frac{(\xi-\bar{x})}{L}\frac{d\xi}{L}$	$\beta y'_{3-3} \cdot \frac{10^6}{L}$	$\beta\gamma \cdot \frac{10^6}{L^2}$	$10^6\beta^2\eta\frac{m}{L^2}$	$\beta\bar{y}_{3-3} \cdot \frac{10^6}{L^2}$
Source	(11)$\int_0^x \beta m \frac{(\xi-\bar{x})}{L}\frac{d\xi}{L}$	(11) + $C_3\beta\frac{10^6}{L}$	$\int_x$(13)$\frac{dx}{L}$	(14) mβ	(14)+$\frac{C_4\beta 10^6}{L^2}$
0.000	0	- 5.3539	0	0	+0.8023
0.025	+ 4.881	5.8623	-0.1372	- 174.2	0.6651
0.050	+ 13.231	5.7863	0.2858	728.8	0.5165
0.075	- 20.853	5.0321	0.4208	1599.0	0.3815
0.100	66.708	4.7075	0.5422	2467.0	0.2601
0.125	179.478	4.1127	0.6525	3262.5	0.1498
0.150	377.308	3.3188	0.7470	3951.6	+0.0553
0.175	663.713	2.5029	0.8212	4664.4	-0.0189
0.200	994.355	1.6629	0.8775	5396.6	0.0752
0.225	1394.667	0.8752	0.9090	6135.8	0.1067
0.250	1817.880	- 0.1924	0.9225	6872.6	0.1202
0.275	2253.390	+ 0.4063	0.9248	7398.4	0.1225
0.300	2670.584	0.8887	0.9090	7681.1	0.1067
0.325	3032.433	1.2269	0.8842	7674.9	0.0819
0.350	3284.002	1.3701	0.8528	7504.6	0.0505
0.375	3448.156	1.3778	0.8168	7277.7	-0.0145
0.400	3492.717	1.2015	0.7852	8323.1	+0.0171
0.425	3416.203	0.8755	0.7560	8920.8	0.0463
0.450	3295.548	0.5521	0.7380	8745.3	0.0643
0.475	3110.815	+ 0.1853	0.7268	8285.5	0.0755
0.500	2871.077	- 0.2086	0.7245	7534.8	0.0778
0.525	2594.409	0.6282	0.7346	6831.8	0.0677*
0.550	2286.107	1.0728	0.7549	6703.5	0.0474*
0.575	1981.110	1.5011	0.7875	6874.9	+0.0148
0.600	1728.224	1.8197	0.8258	7184.5	-0.0235
0.625	1560.091	1.9461	0.8730	7595.1	0.0707
0.650	1459.942	1.9025	0.9202	7959.7	0.1179
0.675	1422.892	1.6310	0.9675	8175.4	0.1652
0.700	1425.344	1.1269	1.0058	8046.4	0.2035
0.725	1427.41	- 0.4284	1.0239	7473.7	0.2215
0.750	1406.167	+ 0.3762	1.0260	6566.4	0.2237
0.775	1353.342	1.2997	1.0058	5481.6	0.2035
0.800	1252.821	2.3227	0.9652	4497.8	0.1629
0.825	1125.082	3.5330	0.8888	3466.3	-0.0865
0.850	918.299	4.3328	0.7898	2416.8	+0.0125
0.875	747.537	5.5750	0.6638	1526.7	0.1385
0.900	627.581	7.7207	0.4972	845.1	0.3051
0.925	455.747	9.5398	0.2722	362.0	0.5301
0.950	276.677	10.5471	-0.0225	- 27.	0.7798
0.975	- 112.736	10.3039	+0.2362	+ 236.2	1.0385
1.000	0	+ 9.8711	+0.4860	+ 194.4	+1.2883

TABLE IV (continued)

(1)	(30)	(29)	(28)	(27)	(26)
$\frac{\partial \psi}{\partial x}$	$\beta_0 \lambda_0 \cdot \frac{\Gamma}{10^2} \int_0^{\infty} \frac{\Gamma}{\Gamma} \frac{(2-x)}{2} \frac{\partial \psi}{\partial x}$	$\beta \lambda^{2-3} \cdot \frac{\Gamma}{10^2}$	$\beta \Gamma \cdot \frac{\Gamma}{10^2}$	$10^2 \beta_0 \lambda_0 \frac{\Gamma}{10^2}$	$\beta \lambda^{2-3} \cdot \frac{\Gamma}{10^2}$

Equation (11)	$\int_0^{\infty} \frac{\Gamma}{\Gamma} \beta_0 (2-x) \frac{\partial \psi}{\partial x}$	$(11) + c_3 \beta \frac{\Gamma}{10^2}$	$\int_x (13) \frac{\Gamma}{\partial x}$	(28) and	$(14) + c_4 \frac{\Gamma}{10^2}$

TABLE VI (cont'd)

(1)	(17)	(18)	(19)	(20)	(21)
x/L	$10^6 g^2 \bar{y}_{3\cdot3}\, m/L^2$	$\frac{10^6 g^2}{L^2} \bar{y}_{3\cdot3}\, m\frac{(x-\bar{x})}{L}$	$\frac{10^6 g^2}{L^2} \bar{y}_{3\cdot3}\, y_1 m$	$\frac{10^6 g^2}{L^2} \bar{y}_{3\cdot3}\, y_2 m$	$C_i\, y_1$
Source	(16)·mg	$(16)\cdot mg\frac{(x-\bar{x})}{L}$	$(16)\cdot y_1 m g$	$(16)\cdot y_2 mg$	See Remarks
0.000	+ 320.9	-151.5	-1093.7	+ 975.9	-0.2133
0.025	844.7	377.6	2579.64	2177.6	.1912
0.050	1317.1	555.8	3549.5	2767.2	.1687
0.075	1449.7	575.5	3402.4	2332.6	.1469
0.100	1183.5	440.2	2359.8	1374.0	.1248
0.125	749.	259.9	1229.1	543.8	.1027
0.150	+ 292.5	- 94.2	- 380.0	+ 98.3	.0813
0.175	- 107.4	+ 31.9	+ 106.1	+ 1.9	.0618
0.200	462.5	125.8	315.4	142.0	.0427
0.225	720.2	177.9	284.5	408.4	.0247
0.250	895.5	198.8	+ 111.9	682.4	- .0078
0.275	980.0	193.1	- 106.8	873.2	+ .0068
0.300	901.6	155.1	293.0	868.3	.0203
0.325	710.9	104.5	363.3	694.5	.0320
0.350	444.4	54.2	293.7	417.7	.0414
0.375	- 129.2	+ 12.5	- 101.8	+ 109.2	.0493
0.400	+ 181.3	- 13.1	+ 159.1	- 128.0	.0550
0.425	546.3	- 25.7	515.7	- 290.7	.0591
0.450	762.0	- 16.8	752.0	- 256.0	.0618
0.475	860.7	+ 2.6	860.7	- 114.5	.0626
0.500	809.1	22.7	800.2	+ 68.8	.0619
0.525	629.6	33.4	607.6	+ 190.1	.0604
0.550	420.9	32.8	383.9	+ 218.5	.0571
0.575	+ 129.2	+ 13.3	+ 107.9	+ 89.5	.0523
0.600	- 204.5	- 26.2	- 145.4	- 171.3	.0445
0.625	615.1	94.1	349.4	577.0	.0356
0.650	1019.8	181.5	390.6	1014.7	.0240
0.675	1395.9	283.4	- 235.9	1377.8	+ .0106
0.700	1628.0	371.2	+ 141.6	1497.7	- .0054
0.725	1617.0	409.1	565.6	1261.2	.0219
0.750	1431.7	398.0	936.3	833.2	.0409
0.775	1109.1	336.0	1082.5	- 337.2	.0611
0.800	759.1	249.0	994.4	+ 18.2	.0820
0.825	- 337.4	-119.1	+ 560.7	+ 138.70	.1040
0.850	+ 38.3	+ 14.5	- 77.7	- 32.5	.1272
0.875	318.6	128.4	761.0	425.9	.1496
0.900	518.7	222.0	1443.5	976.7	.1742
0.925	705.0	319.4	2261.0	1764.7	.2008
0.950	935.8	447.3	3391.2	2970.1	.2269
0.975	1038.5	522.4	4284.9	3954.6	.2583
1.000	+ 515.3	+272.1	-2320.0	-2293.2	- .2818

TABLE VI (continued)

(1)	(17)	(18)	(19)	(20)	(21)
x/L	$10^6 \beta^2 \bar{\lambda}^3 m_1/L^2$	$\frac{10^6 \beta^2 \bar{\lambda}^3 m(x-\bar{x})}{L}$	$\frac{10^6 \beta^2 \bar{\lambda}^3 \lambda_m}{L^2}$	$\frac{10^6 \beta^2 \bar{\lambda}^3 \lambda_m}{L^2}$	$C_1 \lambda_1$
Source (16)·mg	(15)·mg $\frac{(x-\bar{x})}{L}$	(15)·$\lambda_1 m_0^2$		(15)·$\lambda_2 m_0^2$	Sum Ordinates
0.000	+ 320.9	-1321.3	-1093.7	+ 975.9	-0.2133
0.050	800.7	3277.6	2529.6	2177.6	.1913
0.090	1342.7	5523.8	3549.2	3167.5	.1687
0.075	1809.7	7515.2	3402.8	3232.6	.1409
0.100	2145.5	8840.2	2329.8	1374.0	.1348
0.125	2481.	10239.2	1439.2	943.3	.1077
0.150	+ 2812.3	- 9.8	- 980.0	+ 98.3	.0813
0.175	- 3107.1	+ 31.9	+ 106.1	+ 1.9	.0618
0.200	3451.5	1394.8	312.4	1443.0	.0457
0.225	3730.3	1711.9	284.4	1008.4	.0357
0.250	3952.1	1900.0	+ 121.8	682.4	- .0078
0.275	4060.0	1923.3	- 106.8	679.2	+ .0066
0.300	4021.4	1859.2	203.0	886.3	.0393
0.325	3726.9	1614.5	363.3	694.4	.0780
0.350	3444.0	1414.2	393.7	817.7	.0414
0.375	- 3178.9	+ 12.3	- 101.8	+ 109.5	.0493
0.400	+ 2891.3	+ 17.1	+ 159.1	- 138.0	.0459
0.425	2466.3	- 24.7	215.7	- 230.7	.0374
0.450	2066.0	- 16.8	232.0	- 256.0	.0214
0.475	1800.0	+ 5.6	200.7	- 114.5	.0424
0.500	1000.2	82.1	200.2	+ 58.8	.0619
0.525	639.6	223.2	607.6	+ 190.1	.0804
0.550	430.9	313.8	383.8	+ 256.5	.0571
0.575	+ 1299.2	+ 17.3	+ 107.9	+ 89.1	.0529
0.600	- 3044.7	- 26.2	- 149.4	- 171.3	.0446
0.625	4261.1	94.1	340.4	577.0	.0758
0.650	1029.8	181.5	790.6	1034.7	.0840
0.675	1324.9	284.4	- 279.7	1377.8	+ .0106
0.700	1286.0	272.3	+ 141.4	1499.7	- .0058
0.725	1417.0	409.1	555.6	1251.3	.0218
0.750	1428.7	398.0	974.3	819.3	.0409
0.775	1119.1	336.0	1083.3	- 337.3	.0511
0.800	793.1	249.0	994.0	+ 18.3	.0830
0.825	- 377.0	-119.1	+ 560.7	+ 178.70	.1040
0.850	+ 36.3	+ 14.3	- 77.7	- 78.5	.1273
0.875	318.6	120.4	761.0	615.9	.1895
0.900	618.7	232.0	1449.3	979.7	.2742
0.925	705.0	314.0	2051.0	1760.7	.2008
0.950	447.3	2393.1	2970.1	2909.1	.1249
0.975	1098.3	522.2	4004.6	3944.6	.2593
1.000	+ 325.3	+3726.1	-3230.0	-2283.3	- .2818

TABLE VI (cont'd)

(1)	(22)	(23)	(24)	(25)	(26)
x/L	$C_{11}\gamma_2$	$\bar{B}(x-\bar{x})$	$10^6\beta\, y_{3\text{-}3}/L^2$	$y_{3\text{-}3_n}$	$L\gamma_{3\text{-}3_n}$
Source	See Remarks	See Remarks	(16)+$\bar{A}$+(21)+(22)+(23)	$\frac{(24)}{y^*_{3\text{-}3}\ \frac{10^6\beta}{L^2}}$	(13) - $\frac{(10)}{y^*_{3\text{-}3}\ \frac{10^6\beta}{L^2}}$
0.000	+0.0675	-0.0705	+.5899	+3.9248	-35.622
0.025	.0572	.0667	.4683	3.1158	35.522
0.050	.0466	.0630	.3353	2.2309	33.925
0.075	.0357	.0593	.2149	1.4298	30.731
0.100	.0258	.0555	.1095	0.7285	26.739
0.125	.0161	.0518	+.0153	+0.1018	22.448
0.150	+.0075	.0481	-.0627	-0.4172	17.957
0.175	-.0004	.0443	.1215	0.8084	13.665
0.200	.0068	.0406	.1614	1.0739	9.574
0.225	.0126	.0369	.1770	1.1777	5.681
0.250	.0169	.0331	.1741	1.1584	- 2.288
0.275	.0198	.0294	.1610	1.0712	+ 0.606
0.300	.0214	.0257	.1296	0.8623	2.902
0.325	.0217	.0219	.0896	0.5961	4.498
0.350	.0209	.0182	-.0443	-0.2947	5.097
0.375	.0188	.0145	+.0054	+0.0359	5.097
0.400	.0157	.0107	.0496	0.3300	4.299
0.425	.0118	.0070	.0905	0.6021	3.101
0.450	.0075	- .0033	.1192	0.7931	1.904
0.475	- .0030	+ .0004	.1394	0.9275	+ 0.606
0.500	+ .0019	.0042	.1497	0.9960	- 0.891
0.525	.0067	.0079	.1466	0.9754	2.488
0.550	.0015	.0116	.1315	0.8749	4.284
0.575	.0154	.0154	.1018	0.6773	6.180
0.600	.0186	.0191	.0626	0.4165	7.677
0.625	.0208	.0228	+.0124	+0.0825	8.176
0.650	.0221	.0266	-.0413	-0.2748	7.977
0.675	.0219	.0303	.0985	0.6554	6.679
0.700	.0204	.0340	.1506	1.0020	4.184
0.725	.0173	.0378	.1844	1.2269	- 0.791
0.750	.0129	.0415	.2063	1.3726	+ 3.301
0.775	+ .0067	.0452	.2088	1.3892	8.191
0.800	- .0005	.0490	.1925	1.2808	13.680
0.825	.0091	.0527	.1430	0.9514	20.367
0.850	.0188	.0564	-.0732	-0.4870	25.556
0.875	.0297	.0602	+.0233	+0.1550	33.141
0.900	.0418	.0639	.1569	1.0439	43.421
0.925	.0556	.0676	.3452	2.2967	54.598
0.950	.0705	.0714	.5577	3.7106	63.082
0.975	.0845	.0751	.7747	5.1544	65.377
1.000	- .0988	+ .0788	+.9904	+ 6.5895	+65.676

TABLE 12. (cont'd)

(1)	(22)	(23)	(24)	(25)	(26)
x/σ	G_{44}/σ	$\bar{\beta}(x-\bar{x})$	$10^8 \lambda_{3-3}/t_s$	λ_{3-3}	L_{3-3}

Position	Non-dim.	Sum	(16)+(21)+(22)+(23)	$\frac{\lambda_{3-3}}{10^8}$ (24)	(13) − $\frac{\lambda_{3-3}}{10^8}$ (10)
0.000	+0.0075	-0.0075	+0.5979	+3.0848	-38.5848
0.021					
0.050					
0.075					
0.100					
0.125					
0.150	+0.0075		+0.0119	+0.6134	
0.175	-0.0000		-0.0619	-0.3193	
0.200					
0.225					
0.250					
0.275					
0.300					
0.325					
0.350					
0.375					
0.400					
0.425					
0.450					
0.475					
0.500					
0.525					
0.550					
0.575					
0.600					
0.625					
0.650					
0.675					
0.700					
0.725					
0.750					
0.775					
0.800					
0.825					
0.850					
0.875					
0.900					
0.925					
0.950					
0.975					
1.000	-0.0000	+0.0000	+0.0000	+0.0000	+65.3782

TABLE VI (Continued)

AMPLIFYING REMARKS RELATIVE TO SAMPLE CALCULATION

COLUMN	REMARKS
3	Inertia loading with ω^2 taken equal to 1.
5	γ_{3-2} is the normalized component of slope due to bending, taken from the previous cycle.
5, 6	$\gamma_{3-2}\, g\frac{mI}{LA}$ is the derivative with respect to x of the moment of the inertia forces, at any section, about the vertical centroidal axis. When $\gamma_{3-2}\, g\frac{mI}{LA}$ is added to the shear force, one obtains dM/dx, which reflects the effect of lateral inertia forces plus shear due to rotatory inertia within the approximation imposed by using γ from the previous cycle.
9	Component of slope due to bending moment before determination of its true axis.
10	Component of slope due to shear flexibility.
11	Column 9 plus column 10. Slope before true axis determination.
12	$\int_0^L g\eta' \frac{10^6}{L}\int_0^x g m \frac{(\xi-\bar{x})}{L}\frac{d\xi}{L}\frac{dx}{L} = -1540$

$$C_3\left(g\frac{10^6}{L}\right) = -\frac{\int_0^L g\eta'\frac{10^6}{L}\int_0^x g m\frac{(\xi-\bar{x})}{L}\frac{d\xi}{L}\frac{dx}{L}}{P}$$

$$= -\frac{-1540}{-287.64} = -5.3539$$

TABLE VI (Continued)

AMPLIFYING NUMBERS RELATIVE TO SHEARS CALCULATION

COLUMN	REMARKS
8	---------- Inertia loading with ω^2 taken equal to 1.
9	---------- χ_{3-2} is the corrected component of slope due to loading, taken from the previous cycle.
8, 9	---------- $\chi_{3-2}\frac{g_m I}{L^2}$ is the derivative with respect to x of the moment of the inertia normal, at any section about the vertical centroidal axis. When $\chi_{3-2}\frac{g_m I}{L^2}$ is added to the shear force, one obtains $\frac{dM}{dx}$, which relates the effect of lateral inertia forces upon shear due to rotatory inertia within the system.
9	---------- Component of slope due to bending moment before correction of its zero axis.
10	---------- Component of slope due to shear flexibility.
11	---------- Column 9 plus column 10. Slope ratio to true axis of deflection.
12	---------- $\int_0^L \beta_m \frac{10^6}{E}\left(\int_0^x \beta_m (\bar{x}-\bar{x}) \frac{g}{E} d\bar{x}\right) dx$

$$= -\frac{-207.64}{-7.1840} = -2.3239$$

$$\int_0^L \beta_m \frac{10^6}{E}\left(\int_0^x \beta_m (\bar{x}-\bar{x}) \frac{g}{E} d\bar{x}\right)$$

TABLE VI Continued

COLUMN	REMARKS
15	$\int_0^L 10^6 \frac{\eta g^2 m}{L^2} \frac{dx}{L} = -5175$ $C_4\left(\frac{g \cdot 10^6}{L^2}\right) = -\frac{\int_0^L \frac{10^6 \eta g^2 m}{L^2} \frac{dx}{L}}{\Delta / L}$ $= -\frac{-5175}{6450} = +0.8023$
17, 18, 19, 20	Calculations necessary for determination of adjustment constants to be applied to $\frac{10^6 g \bar{y}_{3\text{-}3}}{L^2}$ in order that the resultant deflection pattern is orthogonal with respect to: 1. Rigid body translation 2. Rigid body rotation 3. First mode deflection pattern 4. Second mode deflection pattern
17	1. Orthogonality with respect to rigid body translation: Condition: $\int_0^L y_3 m \, dx = 0$ Result: $\int_0^L \frac{10^6 g \bar{y}_{3\text{-}3} m}{L^2} \frac{dx}{L} = -25.2$ $\bar{A} = -\frac{\int_0^L \frac{10^6}{L^2} g^2 \bar{y}_{3\text{-}3} \frac{m dx}{L}}{\Delta / L}$ $= -\frac{-25.2}{6450} = +0.0039$

TABLE VI Continued

COLUMN	REMARKS
15	
17, 18, 19, 20	Calculations necessary for determination of adjustment constants to be applied to $\frac{10^6 \beta_z \bar{y}^{3-3}}{L^3}$ in order that the resultant deflection pattern is orthogonal with respect to:
	1. Rigid body translation
	2. Rigid body rotation
	3. First mode deflection pattern
	4. Second mode deflection pattern
17	5. Orthogonality with respect to rigid body translation:

Condition: $\int_0^L \bar{y}_3 m \, dx = 0$

Result:

$$\frac{\int_0^L \frac{10^6 \beta_z \bar{y}^{3-3} m}{L^3} dx}{\Delta} = -13.3$$

$$\bar{x} = \frac{\int_0^L \frac{10^6}{L^3} \beta_z \bar{y}^{3-3} m dx}{\Delta} = \frac{-28.3}{6450} = +0.0139$$

$$\left(\frac{\beta \cdot 10^6}{L^3}\right) = \frac{\int_0^L \frac{10^6 \beta_z m}{L^3} dx}{\Delta} = \int_0^L \frac{10^6 \beta_z m}{L^3} dx = -3173$$

$$= -\frac{-3173}{6450} = +0.4923$$

TABLE VI Continued

COLUMN	REMARKS
18	2. Orthogonality with respect to rigid body rotation

Condition: $\int_0^L y_3 mg\,(x - \overline{x})\,dx = 0$

Result:

$$\int_0^L \frac{10^6 g^2 \bar{y}_{3\text{-}3}\, m}{L^3}\,(x - \bar{x})\,\frac{dx}{L} = -44.8$$

$$\overline{B}(L) = -\frac{\int_0^L 10^6 g^2 \bar{y}_{3\text{-}3}\, m\,\frac{(x-\bar{x})}{L^3}\,\frac{dx}{L}}{N}$$

$$= -\frac{-44.8}{300} = +0.1493$$

19	3. Orthogonality with respect to 1st mode:

Condition: $\int_0^L y_1 y_3\, m\, dx = 0$

Result: $\int_0^L \frac{10^6 g^2}{L^2}\, y_1\, \bar{y}_{3\text{-}3}\, m\, \frac{dx}{L} = -505$

$$\frac{10^6 g}{L^2}\,(C_1) = -\frac{\int_0^L \frac{10^6 g^2}{L} y_1\, \bar{y}_{3\text{-}3}\, m\, \frac{dx}{L}}{W_1}$$

$$= -\frac{-505}{8062.5} = +0.0626$$

20	4. Orthogonality with respect to 2nd mode

Condition: $\int_0^L y_2\, y_3\, m\, dx = 0$

TABLE VI (Continued)

COLUMN

15 3. Orthogonality with respect to mass moment

Condition: $\int_0^L \lambda_3 m (x - \bar{x}) \, dx = 0$

Result:

$$\frac{D(r)}{M} = \frac{\int_0^{10^6 \beta_2 \lambda_{3\cdot 3} m \frac{(x-\bar{x})}{r_3} \frac{r}{dx}}}{\int_0^L m \, dx} = \frac{-56.8}{300} = -0.1893$$

15 3. Orthogonality with respect to 1st moment

Condition: $\int_0^L \lambda_1 \lambda_3 m \, dx = 0$

Result: $\frac{10^6}{r^2} (C_1^r) = -\frac{\int_0^{10^6 \beta_2 \lambda_1 \lambda_{3\cdot 3} m \frac{dx}{r}}}{M^1}$

$$= -\frac{-305}{8002.3} = +0.0256$$

20 4. Orthogonality with respect to 2nd moment

Condition: $\int_0^L \lambda_2 \lambda_3 m \, dx = 0$

Result: $\frac{10^6}{r^2} (C_2^r) = -\frac{\int_0^{10^6 \beta_2 \lambda_2 \lambda_{3\cdot 3} m \frac{dx}{r}}}{M^2}$

$$= -\frac{-305}{8002.3} = +0.0256$$

TABLE VI Continued

COLUMN	REMARKS
20	Result: $\int_0^L \frac{10^6 g^2}{L^2} \bar{y}_{3-3}\, y_2\, m\, \frac{dx}{L} = -112$ $C_{ii} = - \frac{\int_0^L \frac{10^6 g^2}{L^2} \bar{y}_{3-3}\, y_2\, m\, \frac{dx}{L}}{W_2}$ $= - \frac{-112}{5040} = + 0.0222$
21	Adjustment to be applied to $\frac{10^6 g}{L^2} \bar{y}_{3-3}$ for orthogonality with first mode deflection pattern.
22	Adjustment to be applied to $\frac{10^6 g}{L^2} \bar{y}_{3-3}$ for orthogonality with second mode deflection pattern
23	Adjustment to be applied to $\frac{10^6 g}{L^2} \overline{y}_{3-3}$ for orthogonality with rigid body rotation.
24	$\frac{10^6 g}{L^2} y_{3-3} = \frac{10^6 g}{L^2} \bar{y}_{3-3} + \bar{A} + \bar{B}(x-\bar{x}) + C_i y_i + C_{ii} y_2$ The value of $\frac{10^6 g}{L^2} y_{3-3}$ at the positive anti-node  (near X/L = 0.5) is the normalizing value and also a function of the eigenvalue. Its value is 0.1503 for this cycle, i.e., $\frac{10^6 g}{L^2} y^*_{3-3} = 0.1503$

TABLE VI Continued

COLUMN	REMARKS
20	Recall: $\int_0^{\Gamma_s} \frac{10^{\beta}\,\bar{\gamma}^{3-3}\,\gamma^{3}\,m\,d\alpha}{\Gamma_s} = -112$
	$C_{12} = -\frac{\int_0^{\Gamma_s} \frac{10^{\beta}\,\bar{\gamma}^{3-3}\,\gamma^{3}\,m\,d\alpha}{\Gamma_s}}{\bar{\gamma}^{3}}$
	$= -\frac{-112}{3140} = 0.0252$
21	Adjustment is to be applied to $\frac{10^{\beta}}{\Gamma_s}\,\bar{\gamma}^{3-3}$ for
	antisymmetry with first mode deflection pattern.
22	Adjustment is to be applied to $\frac{10^{\beta}}{\Gamma_s}\,\bar{\gamma}^{3-3}$ for
	antisymmetry with second mode deflection pattern
23	Adjustment is to be applied to $\frac{10^{\beta}}{\Gamma_s}\,\bar{\gamma}^{3-3}$ for
	antisymmetry with third body rotation.
24	$\frac{10^{\beta}}{\Gamma_s}\gamma^{3-3} = \frac{10^{\beta}}{\Gamma_s}\bar{\gamma}^{3-3} + \bar{\gamma} + \beta(\alpha-\bar{\alpha}) + C^{1}\gamma^{1} + C^{11}\gamma^{2}$
	The value of $\frac{10^{\beta}}{\Gamma_s}\,\bar{\gamma}^{3-3}$ at the previous anti-node
	is the normalizing value and also a function of the
	eigenvalue. Its value is 0.1823 for this cycle, i.e.,
	$\frac{10^{\beta}}{\Gamma_s}\,\bar{\gamma}^{3-3} = 0.1823$

TABLE VI Continued

COLUMN	REMARKS
25	Normalized resultant deflection pattern, $y_{3\text{-}3\,n}$ $$y_{3\text{-}3\,n} = \frac{10^6\, g\, \bar{y}_{3\text{-}3}}{L^2\,(0.1503)}$$
26	Normalization of $\gamma_{3\text{-}3}$ for use in next cycle.

CALCULATION OF FREQUENCY

$$\omega^2_{3\text{-}3} = \frac{1}{y^*_{3\text{-}3}} = \frac{10^6\, g/L^2}{\frac{10^6\, g y^*_{3\text{-}3}}{L^2}} = \frac{10^6 .\ 32.2}{(0.1503)(100.5)^2}$$

$$\omega^2_{3\text{-}3} = \frac{3168.025}{.1503} = 21,211$$

$$\omega_{3\text{-}3} = 145.64 \text{ rad/sec}$$

$$T_{3\text{-}3} = \frac{2\pi}{\omega_{3\text{-}3}} = \frac{6.28318}{145.64} \times 1000 = 43.14 \text{ Milli-seconds}$$

$$f_{3\text{-}3} = \omega_{3\text{-}3}\,\frac{60}{2\pi} = \frac{145.64 \cdot 60}{6.28318} = 1391 \text{ c.p.m.}$$

TABLE VI Continued

COLUMN	EQUATIONS
35	Normalized eventual deflection factor, λ_{3-3}^{n}
36	Normalization of λ_{3-3} for use in next cycle.

CALCULATION OF RESONANCE

APPENDIX D - SUPPLEMENTARY DISCUSSION

1. Secondary Effects Not Treated:

Shear Lag: The classical beam vibrations as applied to ships do not take special notice of the fact that resistance to deflection is concentrated generally at the extremes of the cross section and that, in horizontal bending, stress transmitted from the deck to the side will not maintain a constant level down the side as indicated by the constant distance from the neutral axis. This is because of the effect known as shear lag. While important in lightly framed ships where decks and longitudinal bulkheads play little part structurally, it was not thought to be significant in the ring-framed model of this investigation. Shear lag is treated in detail by R. A. Anderson and J. C. Houbolt ("The Effect of Shear Lag in the Bending Vibrations of Box Beams", NACA TN No. 1583, May 1948) and others.

Second Frequency Spectrum: The simple Harmonic assumption applied to Timoshenko's complete mechanism leads to an equation which is fourth order in circular frequency , indicating the possibility of a second real value of frequency for a given mode . Traill-Nash and Collar [63] were able to determine this second spectrum of frequencies for certain special cases of uniform beams. Its physical importance was not determined, but it was thought to arise from a resonant interaction between rotatory inertia forces and shear stiffness.

The iterative method of this paper, while considering both effects, and permitting them to interact in the sequence, is based on a single assumed frequency, and does not facilitate simultaneous interaction. Hence the second frequency spectrum is not explicitly noted.

Torsional Coupling: It should be noted that coupling can occur between torsional and horizontal flexural vibration, with resultant effects on the patterns and frequencies of each. Such coupling has not been treated in this investigation.

APPENDIX D - SUPPLEMENTARY DISCUSSION

1. Secondary Effects Not Treated:

Shear Lag: The classical beam relations as applied to ships do not take account of the fore-and-aft resistance to deflection in concentrated generally at the ends of the cross section and that, in horizontal bending, stress transmitted from the deck to the side will run parallel a constant level down the side as indicated by the constant distance from the neutral axis. This is because of the effect known as shear lag. While important in highly framed ships where decks and longitudinal bulkheads play little part structurally, it was not thought to be significant in the ring-framed model of this investigation. Shear lag is treated in detail by H. A. Pohlhausen and I. C. Howell ("The Effect of Shear Lag in the Bending Vibrations of Box Beams", NACA TN No. 1393, May 1947) and others.

Second Frequency Spectrum: The simple Rayleigh-Ritz principle applied to Timoshenko's complete equations leads to an equation which is fourth-order in circular frequency, indicating the possibility of a second real value of frequency for a given mode. Trail-Nash and Collar [17] were able to determine this second spectrum of frequencies for certain special cases of vertical beams. Its physical importance was not determined, but it was thought to arise from a resonant interaction between rotatory inertia terms and shear stiffness.

The iterative method of this paper, while considering both effects, and permitting them to interact in the sequence, is based on a single assumed frequency, and does not facilitate simultaneous iteration. Hence the second frequency spectrum is not explicitly sought.

Torsional Coupling: It should be noted that coupling can exist between torsional and horizontal flexural vibration, with resultant effects on the natures and frequencies of each. Such coupling has not been treated in this investigation.

2. More Exact Orthogonality Formulation:

A review of the theoretical development of this method revealed that the formulation of the orthogonality relationships used were inexact when applied to orthogonalizing with non-trivial modes when rotatory inertia is considered. The effect of the discrepancy is discussed in the next subsection. The development of the more exact formulation* will now be given.

The normalized deflection and bending slope, and the circular frequency of each of two different modes are given by

$$Y_i,\ \gamma_i,\ \omega_i,\quad Y_j,\ \gamma_j,\ \omega_j .$$

Multiplying equations (25) and (27) of Appendix A-1 by γ_j and Y_j respectively, and integrating, we have for mode i,

$$\int_0^L \gamma_j (EI\ \gamma_i')'dx + \int_0^L \frac{Im}{A}\omega_i^2 \gamma_i \gamma_j\, dx + \int_0^L KAG(Y_i'\gamma_j - \gamma_i \gamma_j)dx = 0 \quad (69a)$$

$$\int_0^L m\, Y_i Y_j \omega_i^2\, dx + \int_0^L \left[KAG\,(Y_i' - \gamma_i)\right]' Y_j\, dx = 0 \quad (69b)$$

and using the multipliers from mode i, we have for mode j,

$$\int_0^L \gamma_i (EI\ \gamma_j')'dx + \int_0^L \frac{Im}{A}\omega_j^2 \gamma_i \gamma_j\, dx + \int_0^L KAG(Y_j'\gamma_i - \gamma_j \gamma_i)dx = 0 \quad (70a)$$

$$\int_0^L m\, Y_i Y_j \omega_j^2\, dx + \int_0^L \left[KAG(Y_j' - \gamma_j)\right]' Y_i\, dx = 0 \quad (70b)$$

Integrating the first term of (69a) by parts, we have

$$EI\ \gamma_j \gamma_i' \Big]_0^L - \int_0^L EI\ \gamma_i' \gamma_j'\, dx + \int_0^L \frac{Im}{A}\omega_i^2 \gamma_i \gamma_j dx + \int_0^L KAG(Y_i'\gamma_j - \gamma_i \gamma_j)\, dx = 0 \quad (71)$$

*Due to Prof. S. H. Crandall, Massachusetts Institute of Technology and to C. L. Dolph, Willow Run Research Center, University of Michigan

1. Wave Impact Overpressure Parameters:

A review of the theoretical development of this method revealed that the determination of the orthogonality relationships used were inexact when applied to orthogonalizing with non-trivial modes when rotatory inertia is considered. The effect of the discrepancy is discussed in the next subsection. The development of the more exact formulation will now be given.

The natural modes of vibration and bending slope, and the circular frequency of each of two different modes are given by

$$Y_i,\ \theta_i,\ \omega_i,\ \lambda_i,\ \chi_i,\ \Omega_i.$$

Multiplying equations (13) and (17) of Appendix A-1 by χ_i and λ_i respectively, and integrating, we have for mode i,

$$\int_0^L \chi_i^2 \left(\Sigma I\ \chi_i'\right)' dx + \int_0^L \frac{I_m}{g}\omega_i^2 \chi_i \chi_i\, dx + \int_0^L EAG\left(\lambda_i' \chi_i' - \lambda_i \chi_i\right) dx = 0 \qquad (39a)$$

$$\int_0^L \lambda_i \lambda_i \omega_i^2\, dx + \int_0^L \left[EAG\left(\lambda_i' - \chi_i\right)\right]' \lambda_i\, dx = 0 \qquad (39b)$$

and using the multipliers from mode i, we have for mode j,

$$\int_0^L \chi_j\left(\Sigma I\ \chi_i'\right)' dx + \int_0^L \frac{I_m}{g}\omega_i^2 \chi_i \chi_j\, dx + \int_0^L EAG\left(\lambda_i' \lambda_j - \chi_i \chi_j\right) dx = 0 \qquad (40a)$$

$$\int_0^L \lambda_j \lambda_i \omega_i^2\, dx + \int_0^L \left[EAG\left(\lambda_i' - \chi_i\right)\right]' \lambda_j\, dx = 0 \qquad (40b)$$

Integrating the first term of (39a) by parts, we have

$$\left[\Sigma I\ \chi_i' \chi_j\right]_0^L - \int_0^L \Sigma I\ \chi_i' \chi_j'\, dx + \int_0^L \frac{I_m}{g}\omega_i^2 \chi_i \chi_j\, dx + \int_0^L EAG\left(\lambda_i' \lambda_j - \chi_i \chi_j\right) dx = 0 \qquad (41)$$

*Due to Prof. R. M. Orandoff, Rensselaer Institute of Technology and to C. L. Dolph, Willow Run Research Center, University of Michigan

where the first term vanishes since curvature in a free-free beam vanishes at both ends. The corresponding operation is carried out on (70a), and the result subtracted from (71), giving

$$(\omega_i^2 - \omega_j^2) \int_0^L \frac{Im}{A} \gamma_i \gamma_j \, dx + \int_0^L KAG \left[\gamma_i' \gamma_j - \gamma_j' \gamma_i \right] dx = 0 \quad (72)$$

Now (69b) is rewritten, integrating the second term by parts, giving

$$\int_0^L m \gamma_i \gamma_j \omega_i^2 \, dx + KAG (\gamma_i' - \gamma_i) \gamma_j \Big]_0^L - \int_0^L KAG(\gamma_i' \gamma_j' - \gamma_i \gamma_j') dx = 0 \quad (73)$$

where the second term vanishes, since $KAG (\gamma_i' - \gamma_i)$ is identical to shear, which must vanish at both ends of a free-free beam. The corresponding operation is carried out for (70b), and the resulting equation is subtracted from (73), giving

$$(\omega_i^2 - \omega_j^2) \int_0^L m y_i y_j \, dx + \int_0^L KAG \left[\gamma_i y_j' - \gamma_j y_i' \right] dx = 0 \quad (74)$$

Adding (72) and (74) gives the orthogonality relationship

$$(\omega_i^2 - \omega_j^2) \int_0^L \left(\frac{Im}{A} \gamma_i \gamma_j + m y_i y_j \right) dx = 0 \quad (75)$$

which, for $\omega_i \neq \omega_j$, leaves the useful relationship

$$\int_0^L \left(\frac{Im}{A} \gamma_i \gamma_j + m y_i y_j \right) dx = 0 \quad (76)$$

This should be compared with the relationship used in the investigation

$$\int_0^L (m y_i y_j) dx = 0 \quad (77)$$

which is seen to be in error by the integral of the first term in (76).

The importance of this term varies from mode to mode, and must be evaluated for higher modes to determine the necessity of applying the exact condition. It does not lend itself readily to application in the iterative procedure of this thesis, since it provides corrections

to bending slope and deflection, quantities which become available at different stages of the process, and which cannot be corrected separately. An acceptable, though somewhat unwieldy approach would be to apply the complete check at the deflection level, examining the slope correction to see if its magnitude warrants its use. If it is significant, the bending slope is corrected, and the new total slope integrated. The new deflection curve is given the exact orthogonality check, this time assuming that the slope needs no correction.

In the case of this thesis, an auxiliary investigation showed that the complete check changed the natural frequency for the third modes (previously corrected by the approximate relationship) by 0.36%, and that the effect was even smaller on the second mode frequency. It appears that for the modes ofinterest, the added inconvenience of the full correction may have but little justification. Where applied, the correction is stated by the following equations:

$$(y_j)_c = y_j + C_i y_i + C_{ii} y_{ii} \tag{78}$$

$$(\gamma_j)_c = \gamma_j + C_i \gamma_i + C_{ii} \gamma_{ii} \tag{79}$$

where the constant for each prior mode is defined by:

$$C_i = - \frac{\int_0^L \frac{m I}{A} \gamma_i \gamma_j \, dx + \int_0^L m y_i y_j \, dx}{\int_0^L \frac{m I}{A} \gamma_i^2 \, dx + \int_0^L m y_i^2 \, dx} \tag{80}$$

3. Third Mode Frequency:

As noted in the Discussion of Results, the natural frequency obtained for the third mode (1391 cpm) by the iterative process and orthogonality filtering is considered to be slightly high. This section

presents estimates of the correct value obtained from several independent approaches.

a. The cycle-by-cycle behavior of frequencies in the third mode calculation manifests alternation casting some doubt on the value from the third cycle. Consideration of this behavior seems to indicate ultimate convergence to a value somewhere between the second and third cycle results, whereas earlier modes showed continually falling trends. The change in behavior in the third mode appears to stem from a starting assumption which was in error, even after orthogonalization, to a greater degree than were those of the other modes. This may be due in part to the use of the inexact orthogonality check, as well as to any of the sources of error listed in the Discussion of Results. We conclude from this approach that the third mode natural frequency should be in the neighborhood of 1385 to 1390 cps.

b. The more exact orthogonality check formulated in equation (80) was applied to the result of the last iteration of the third mode, disregarding the effect on slope. The constants became

$$C_i = - \frac{-505 - 17}{8062.5 + 57.8} = + 0.06428$$

instead of

$$C_i = - \frac{- 505}{8062.5} = + 0.0626$$

and

$$C_{ii} = - \frac{-112 + 1.2}{5040 + 76.3} = + 0.02166$$

instead of

$$C_{ii} = - \frac{-112}{5040} = + 0.0222$$

The net effect was to lower the natural frequency from 1391 to 1386 cps. The change in mode shape was insignificant.

c. The empirical ratio of natural frequencies observed for a number of ships, 1: 2: 3, although approximate, and not verified for submarines, is applied for interest. It results in no significant change in the second mode, but depresses the third mode frequency to 1251 cpm. This is clearly much lower than there is reason to expect, but tends to verify the suspicion that 1391 is perhaps high.

d. Table VII lists frequencies for the model under consideration, obtained theoretically. Tabulated with the values obtained formally in this investigation (MIT) are those obtained by David Taylor Model Basin (DTMB) by analog computer and those obtained by the authors at Underwater Explosion Research Division (UERD), both sets including shear flexibility but not rotatory inertia.

TABLE VII

CALCULATED MODEL FREQUENCIES (cpm)

Mode	MIT	DTMB	UERD
1	417	444	428
2	838	888	857
3	1391	1392	-

Since the added refinement of rotatory inertia should tend to lower the frequencies of this thesis as compared to the other sets, it again appears that 1391 cpm is too high for the third mode, and that perhaps a reasonable value to expect would be 1320 cpm. This is based on both the ratio series for the DTMB data and the suspected trend of equal or greater reduction with mode number due to rotatory inertia.

It should be pointed out that neither set of comparison frequencies is corroborated, and experimental frequencies have not yet been obtained for the model under consideration.

e. Considering all of the above factors, it can best be concluded that the third mode frequency is 1355 $\pm$ 2.6%.

c. The empirical ratio of natural frequencies observed for a simulated delta, 1: 2: 3, although approximate, and not verified for antisymmetry, is applied for interest. It reveals in no significant change in the second mode, but depresses the third mode frequency to 1591 cps. This is clearly much lower than there is reason to expect, but tends to verify the suspicion that 1791 is perhaps high.

d. Table VII lists frequencies for the 1-bodal modes considered, obtained theoretically. Terminology with the symbols customary in this investigation (MIT) and those employed by David Taylor Model Basin (DTMB) by analog computer and those obtained by the authors at Underwater Explosions Research Division (UERD), note main including above flexibility but not rotatory inertia.

TABLE VII

CALCULATED MODAL FREQUENCIES (cps)

Mode	MIT	DTMB	UERD
1	417	444	446
2	836	888	857
3	1591	1812	-

Since the added entrainment of rotatory inertia should tend to lower the frequencies of this finite as contrasted to the other note, it again appears that 1591 cps is too high for the third mode, and that perhaps a reasonable value to expect would be 1320 cps. This is noted on both the ratio series for the DTMB data and the suggested trend of equal or greater reduction with mode number due to rotatory inertia.

It should be pointed out that neither set of computations frequencies is corroborated, and experimental frequencies have not yet been obtained for the model under consideration.

4. Considering all of the above factors, it can best be concluded that the third mode frequency is 1320 ± 3.4%.

APPENDIX E - STRUCTURAL DATA

Table VIII contains a tabulation of structural data necessary for the modal calculations. The source of these data is the Underwater Explosions Research Division of the Norfolk Naval Shipyard, under whose auspices the model submarine referred to in this work was constructed.

The mass appearing in Table VIII includes the structural mass of the submarine, the mass of her ballast water, the mass of her solid contents, and the virtual water mass.

The virtual water mass was calculated from the following formula:

$$m_v = \rho \pi b^2 \tag{81}$$

where b is half the depth of the submarine structure at any section, including the protuberance of the rudder and conning tower where applicable, and ρ = density of water in lb/ft^3.

Equation (81) is based on the assumption that the cross section is elliptical with the major axis congruent with the vertical center line of the submarine. The wash of the water through the superstructure is neglected. The resulting curve of virtual water mass was further modified by an empirical correction explained in David Taylor Model Basin Report # 632. This correction consisted of multiplying the m_v curve by 0.83 over most of its length, with a more severe correction at the ends. Only one-third of the additional virtual water mass contributed by the rudder and the conning tower was used.

These corrections, are somewhat arbitrary, as all estimates of virtual water mass tend to be. The total empirical correction causes only a very slight change in the ship vibration behavior. No experimental data that verifies the virtual water mass distribution is available for this submarine.

The ends of the total mass curve used by the authors were altered

APPENDIX B — STRUCTURAL DATA

Table VIII contains a tabulation of structural data necessary for the modal calculations. The source of these data is the Underwater Explosions Research Division of the Norfolk Naval Shipyard, under whose auspices the model submarine referred to in this work was constructed.

The mass appearing in Table VIII includes the structural mass of the submarine, the mass of her ballast water, the mass of her solid contents, and the virtual water mass.

The virtual water mass was calculated from the following formula:

$$m_v = \rho \pi b^2 \qquad (81)$$

where b is half the depth of the submarine structure at any section, including the protuberance of the rudder and coaming tower where applicable, and ρ = density of water in lb/ft^3.

Equation (81) is based on the assumption that the cross section is elliptical with the major axis congruent with the vertical center line of the submarine. The weak of the water through the superstructure is neglected. The resulting curve of virtual water mass was further modified by an empirical correction explained in David Taylor Model Basin Report # 632. This correction consisted of multiplying the m_v curve by 0.83 over most of its length, with a more severe correction at the ends. Only one-third of the additional virtual water mass contributed by the rudder and the coaming tower was used.

These corrections, no somewhat arbitrary, do all estimates of virtual water mass tend to be. The total empirical correction causes only a very slight change in the mode vibration behavior. No experimental data that verifies the virtual water mass distribution is available for this submarine.

The ends of the total mass curve used by the authors were altered

slightly so that the ordinates did not approach zero rapidly, but remained at an arbitrary small amount, dropping abruptly to zero at $x = 0$ and $x = L$. This was done to conform with a similar adjustment to the moment of inertia curve. The need for the corrections arose when, in their absence, spurious values of curvature were obtained at the ends because, in general, the curve of inertia tended to converge on zero more rapidly than the curve of bending moment.

The K factor used to determine β from Q is defined as

$$K = \frac{\text{average shearing stress in cross section}}{\text{maximum shearing stress in cross section}}$$

or

$$K = \frac{IB}{A\int_0^{y_o} y\,dA} \tag{82}$$

where I and A have already been defined, and B is the total thickness of steel through which the vertical center line passes. (The center line vertical and flat keels were excluded from the calculation of K).

The integral of equation (82) was calculated separately for each component of the structure (i.e., the pressure hull, outer hull, deck, etc.), and all the integrals summed to give a value applicable to the entire section. Only members which make major contributions to the submarine's longitudinal strength were considered in the above calculation and in computing sectional moments of inertia. A discussion as to the validity of this practice appears in Appendix D.

TABLE VIII

STRUCTURAL CHARACTERISTICS OF 3/8 SCALE

MODEL SUBMARINE

x/l.	w, lb/ft	A, in^2	K	I_{xx}, in^4
0.000	400	10	0.701	15,000
.025	1270	15.4	.712	15,000
.050	2550	28.6	.836	15,000
.075	3800	80	.868	24,000
.100	4550	104.8	.535	40,000
.125	5000	116	.487	61,000
.150	5290	122.8	.514	85,000
.175	5680	142	.491	112,000
.200	6150	162.8	.508	135,000
.225	6750	176.6	.554	157,000
.250	7450	183.6	.572	175,000
.275	8000	184.4	.588	192,000
.300	8450	186.6	.590	200,000
.325	8680	192	.592	203,000
.350	8800	197.2	.587	205,000
.375	8910	202.2	.580	216,000
.400	10600	207.6	.586	260,000
.425	11800	268	.526	375,000
.450	11850	313.4	.435	440,000
.475	11400	316.4	.429	444,000
.500	10400	315	.445	442,000
.525	9300	237	.528	365,000
.550	8880	191.8	.612	260,000
.575	8730	190.4	.601	217,000
.600	8700	190	.596	207,000
.625	8700	187.4	.592	201,000
.650	8650	183.8	.591	190,000
.675	8450	180.4	.588	174,000
.700	8000	177.6	.581	160,000
.725	7300	172.4	.572	145,000
.750	6400	165.6	.578	130,000
.775	5450	156.6	.510	114,000
.800	4660	145.4	.498	100,000
.825	3900	130.4	.479	82,000
.850	3060	110.8	.632	60,000
.875	2300	83.4	.711	33,000
.900	1700	56.6	.490	17,000
.925	1330	42.8	.489	12,000
.950	1200	34.0	.547	10,000
.975	1000	28.2	.697	10,000
1.000	400	25	.640	10,000

x/L	ψ, lb/ft	A, in^2	ε	E_{sec}, lb/in^2
0.000	800	39	.700	12,000
.013	1370	32.4	.712	12,000
.050	1410	28.6	.874	12,000
.073	1500	30	.686	24,000
.100	1640	106.8	.574	60,000
.114	1800	116	.547	61,000
.148	1900	120.4	.521	65,000
.173	1950	122	.485	113,000
.200	2110	125.8	.450	117,000
.227	2250	129.4	.359	119,000
.250	2340	132.6	.334	119,000
.273	2500	136.4	.288	122,000
.300	2640	140.4	.260	122,000
.324	2800	144	.221	122,000
.350	2950	147.6	.195	122,000
.375	3110	151.4	.170	122,000
.400	3250	155	.151	122,000
.425	3400	158.8	.135	122,000
.450	3550	162.4	.121	122,000
.475	3700	166	.109	122,000
.500	3850	169.8	.098	122,000
.525	4000	173.4	.088	122,000
.550	4150	177	.080	122,000
.575	4300	180.8	.072	122,000
.600	4450	184.4	.065	122,000
.625	4600	188	.059	122,000
.650	4750	191.8	.054	122,000
.675	4900	195.4	.049	122,000
.700	5050	199	.045	122,000
.725	5200	202.8	.041	122,000
.750	5350	206.4	.038	122,000
.775	5500	210	.035	122,000
.800	5650	213.8	.032	122,000
.825	5800	217.4	.029	122,000
.850	5950	221	.027	122,000
.875	6100	224.8	.025	122,000
.900	6250	228.4	.023	122,000
.925	6400	232	.021	122,000
.950	6550	235.8	.019	122,000
.975	6700	239.4	.018	122,000
1.000	6850	243	.016	122,000

APPENDIX F: BIBLIOGRAPHY

Books

1. Bleich, Friederich, Buckling Strength of Metal Structures, McGraw-Hill Book Co., Inc., New York, 1952. pp. 81-82
2. Collatz, Lothar, Eigenwertprobleme und ihre Numerische Behandlung, Akademische Verlagsgesellshaft, Becker and Erler, Kom.-Ges., Leipzig, 1945. p 215.
3. Den Hartog, J.P., Mechanical Vibrations, McGraw-Hill Book Co., New York and London, 1940. pp. 164-196
4. Lamb, Sir Horace, The Dynamical Theory of Sound, Edward Arnold and Co., London, 1931.
5. Lewis, F. M. "Dynamic Effects", Chapter II, Vol. II of Seward, H. L., Marine Engineering, The Society of Naval Architects and Marine Engineering, New York, 1944. pp. 76-140.
6. Lord Rayleigh, Theory of Sound, 3rd. ed., MacMillan and Company, London, 1929. pp. 178, 257, 295.
7. Rossell and Chapman, Principles of Naval Architecture, The Society of Naval Architects and Marine Engineers, New York, 1949. pp. 23-27.
8. Stodola, A., Steam and Gas Turbines, (Translation by L.C. Lowenstein) McGraw-Hill Book Co., New York, 1927. Vol I, pp. 449-451, 460, 1092.
9. Timoshenko, S., Vibration Problems in Engineering, D. Van Nostrand and Co., New York, 1951. pp. 165, 221-226.

Articles and Papers

10. Akimoff, "On Vibration of Beams of Variable Cross-section", Society of Naval Architects and Marine Engineers, Transactions, Vol. 26, 1918.
11. Anderson, R. A., "Flexural Vibrations in Uniform Beams According to the Timoshenko Theory", Journal of Applied Mechanics, Vol. 20, No. 4, December, 1953.
12. Brown, T.W.F., "Vibration Problems from the Marine Engineering Point of View", North East Coast Institution of Engineers and Shipbuilders Transactions, 1934-35.
13. Burrill, L.C., "Ship Vibration: Simple Methods of Estimating Critical Frequencies", North East Coast Institution of Engineers and Shipbuilders Transactions, 1934-35.
14. Browne, A.D., Moullin, E.D., and Perkins, A.J., "The Added Mass of Prisms Floating in Water", Proceedings Cambridge Philosophical Society, Vol. 26, 1929-30.

APPENDIX I - BIBLIOGRAPHY

Books

1. Bleich, Friedrich, Buckling Strength of Metal Structures, McGraw-Hill Book Co., Inc., New York, 1952. pp. 81-82.
2. Collatz, Lothar, Eigenwertprobleme und ihre Numerische Behandlung, Akademische Verlagsgesellschaft, Becker und Erler, Kom.-Ges., Leipzig, 1945. p. 215.
3. Den Hartog, J. P., Mechanical Vibrations, McGraw-Hill Book Co., New York and London, 1940. pp. 184-194.
4. Lamb, Sir Horace, The Dynamical Theory of Sound, Edward Arnold and Co., London, 1931.
5. Lewis, F. M. "Dynamic Effects", Chapter II, Vol. II of Seward, H. L., Marine Engineering, The Society of Naval Architects and Marine Engineers, New York, 1944. pp. 76-140.
6. Lord Rayleigh, Theory of Sound, 2nd. ed., Macmillan and Company, London, 1929. pp. 171, 137, 293.
7. Rossell and Chapman, Principles of Naval Architecture, The Society of Naval Architects and Marine Engineers, New York, 1947. pp. 23-27.
8. Stodola, A., Steam and Gas Turbine, (Translation by L. C. Loewenstein) McGraw-Hill Book Co., New York, 1927. Vol I, pp. 449-451, 464, 1092.
9. Timoshenko, S., Vibration Problems in Engineering, D. Van Nostrand and Co., New York, 1928. pp. 165, 321-324.

Articles and Papers

10. Akimoff, "On Vibration of Beams of Variable Cross-section", Society of Naval Architects and Marine Engineers, Transactions, Vol. 24, 1916.
11. Anderson, R. A., "Flexural Vibrations in Uniform Beams According to the Timoshenko Theory", Journal of Applied Mechanics, Vol. 20, No. 4, December, 1953.
12. Lewis, F. M., "Vibration Problems from the Marine Engineering Point of View", North East Coast Institution of Engineers and Shipbuilders, Transactions, 1934-35.
13. Severud, L. C., "Only Vibration: Simple Methods of Estimating Critical Frequencies", North East Coast Institution of Engineers and Shipbuilders, Transactions 1934-35.
14. Urenne, A. D., Hamelin, E. D., and Perkins, A. J., "The Added Mass of Plates Vibrating in Water", Proceedings Canadian Philosophical Society, Vol. 25, 1929-30.

15. Calderwood, J., "Some General Observations on Vibration", North East Coast Institution of Engineers and Shipbuilders Transactions, 1940-41.
16. Chree, C., "The Whirling and Transverse Vibrations of Rotating Shafts", Philosophical Magazine, vol. 7, series 6, 1904.
17. Cole, A. P., "The Natural Periods of Vibration of Ships", Institute of Engineers and Shipbuilders, Scotland, Vol. LXXII, 1928-1929.
18. Constantini, M., "Vibration in Ships", Transactions of the Institution of Naval Architects, 1938.
19. Dalby, W. E., "Some Ship Vibration Problems", Transactions Institution of Mechanical Engineers, 1928.
20. Dalby, W. E.,"Vibrations in Ship Hulls", Engineering, 7 December 1928.
21. Darnley, E. R., "The Transverse Vibrations of Beams and the Whirling of Shafts Supported at Intermediate Points", Philosophical Magazine, Vol. XLI, series 6, 1921.
22. Garrett, C. A. B., "On the Lateral Vibration of Bars", Philosophical Magazine, Vol. 8, series 6, 1904.
23. Gatewood, W., "The Periods of Vibration of Steam Vessels", Society of Naval Architects and Marine Engineers Transactions, 1915.
24. Inglis, C. E., "Natural Frequencies and Modes of Vibration in Beams of Non-uniform Mass and Section", Transactions of the Institution of Naval Architects, 1929.
25. Inglis, C. E., "Suggested Method of Minimizing Vibration in Ships", Transactions of the Institution of Naval Architects, 1933.
26. Keating, F. S., "An Investigation of a More Exact Analytical Solution for the Case of a Simple Cantilever Beam with a Suddenly Applied Transverse Load at its End, B. S. Thesis, Massachusetts Institute of Technology, 1954.
27. Koch, J. J., Verhandl. 2. International Congress of Techn. Mechanics, Zurich, 1926, S 213-218.
28. Koch, J. J.,"Eine experimentelle Methode zur Bestimmung der reduzierten Masse des mitschwingen Wassers bei Schiffschwingungen", Ingenieur, Archiv. IV Band, 2 Heft, 1933.
29. Lewis, F. M., "The Inertia of Water Surrounding a Vibrating Ship", Society of Naval Architects and Marine Engineers Transactions, 1929.
30. Lewis, F. M., "Vibration and Engine Balance in Diesel Ships", Society of Naval Architects and Marine Engineers Transactions, 1929.

31. Mallock, A., "The Vibrations of Ships and Engines", Transactions of the Institution of Naval Architects, 1895.
32. Mellville, G. W., "The Vibration of Steam Ships with Particular Reference to those of the Second and Higher Periods", Society of Naval Architects and Marine Engineers Transactions, Vol. 10, 1902.
33. Miklowitz, Julius, "Flexural Wave Solutions of Coupled Equations Representing the More Exact Theory of Bending", Journal of Applied Mechanics, Vol. 20, No. 4, December 1953.
34. Mindlin, R. D., "The Influence of Rotatory Inertia and Shear on the Flexural Motion of Isotropic Elastic Plates", Journal of Applied Mechanics, March 1951.
35. Morrow, John, "On the Lateral Vibration of Bars of Uniform and Varying Sectional Area", Philosophical Magazine, Vol. 10, ser. 6, 1905.
36. Morrow, John, "On the Lateral Vibration of Loaded and Unloaded Bars", Philosophical Magazine, Vol. 11, ser. 6, 1906.
37. Moullin, L. B., "The Lateral Vibration of Non-uniform Bars with Application to Ships", Cambridge Philosophical Society Proceedings, Vol. XXIV, 1928.
38. Moullin, L. B., and Browne, A. D., "On the Periods of a Free-free Bar Immersed in Water", Cambridge Philosophical Society Proceedings, Vol. XXIV, May 1928.
39. Nicholls, H. W., "Vibration of Ships", Transactions of the Institution of Naval Architects, 1924.
40. Pavlenko, G. E., "A Method of Calculating Ship Vibration Frequencies", Engineering, 25 June 1926.
41. Pidduck, F. B., "The Vibration and Stability of a Rotating Cylinder", Proceedings of the London Mathematical Society, Vol. 18, ser. 2, 1918-19.
42. Prohaska, C. W., "The Vertical Vibration of Ships", The Ship Builder and Marine Engine Builder, October 1947.
43. Roop, W. P., "Natural Frequencies of Hull Vibration", Society of Naval Architects and Marine Engineers Transactions, 1930.
44. Schadlofsky, E., "Uber Rechnung und Messung der elastischen Eigenschwingungen von Schiffskorpern", Schiffbautechnische Gesellschaft, November 1932.
45. Schlick, O., "On the Vibration of Steam Vessels", Transactions of the Institution of Naval Architects, 1884.
46. Schlick, O., "Further Investigations of the Vibrations of Steamers", Transactions of the Institution of Naval Architects, 1894.
47. Schlick, O., "On the Vibration of Higher Order in Steamers, and On Torsional Vibration", Transactions of the Institution of Naval Architects, 1895.

48. Schlick, O., "Our Present Knowledge of the Vibration Phenomena of Steamers", Transactions of the Institution of Naval Architects, 1912.

49. Southwell, R. V., "On a Graphical Method for Determining the Frequencies of Lateral Vibration, or Whirling Speeds, for a Rod of Non-Uniform Cross Section", Philosophical Magazine, Vol. XLI, Series 6, 1921.

50. Taylor, J. Lockwood, "Dynamic Longitudinal Strength of Ships", Transactions of the Institution of Naval Architects, 1946.

51. Taylor, J. Lockwood, "Ship Vibration Periods", North East Coast Institution of Engineers and Shipbuilders Transactions, 1927-28.

52. Taylor, J. Lockwood, "Some Ship Strain Observations with a Simple Instrument", Transactions of the Institution of Naval Architects, 1926.

53. Taylor, J. Lockwood, "Some Hydrodynamic Inertia Coefficients", Philosophical Magazine, January 1930

54. Taylor, J. Lockwood, "Vibration of Ships", Transactions of the Institution of Naval Architects, 1930.

55. Timoshenko, S. P., "On the Correction for Shear of the Differential Equation for Transverse Vibration of Prismatic Bars", Philosophical Magazine, Vol. 41, Series 6, 1921.

56. Thompson, W. T., and Rogers, T. A., "Analog Solution for Beams Excited by an Arbitrary Force", Journal of Applied Mechanics, Vol. 20, No. 4, December 1953.

57. Tobin, T. C., "A Method of Determining the Natural Periods of Vibration of Ships", Transactions of the Institution of Naval Architects, 1922.

58. Todd, F. H., "Ship Vibration - A Comparison of Measured with Calculated Frequencies", North East Coast Institution of Engineers and Shipbuilders Transactions, 1933.

59. Todd, F. H., "The Fundamentals of Ship Vibration", The Shipbuilder and Marine Engine-Builder, May, June, and July 1947.

60. Todd, F. H., "Some Measurements of Ship Vibration", North East Coast Institution of Engineers and Shipbuilders Transactions, 1931.

61. Todd, F. H., "Vibration in Ships", Engineering, 16 and 23 September 1938.

62. Todd, F. H., and Morwood, W. J., "Ship Vibration", North East Coast Institution of Engineers and Shipbuilders Transactions, 1948.

63. Traill-Nash, R. W., and Collar, A. R., "The Effects of Shear Flexibility on the Bending Vibrations of Beams", Quarterly Journal of Mechanics and Applied Mathematics, Vol. VI, part 2, June 1953.

64. Blumberg, S. E., "The Bodily Response of U-1105", Underwater Explosions Research Division Report 1-50 on BuShips Project NS 724-003

65. Kruszewski, E.T., "Effect of Transverse Shear and Rotary Inertia on the Natural Frequency of a Uniform Beam", National Advisory Committee on Aeronautics Technical Note 1909, July 1949.

66. Leonard, R. W., and Budiansky, B., "On Traveling Waves in Beams," National Advisory Committee on Aeronautics Technical Note 2874, 1953.

67. Mathewson, A.W., "Preparation of Data for Computation of Vertical Flexural Modes of a Submarine by Digital Process", David Taylor Model Basin Report 632, 1949.

68. McGoldrick, R. T., "A Study of Ship Hull Vibration", David W. Taylor Model Basin Report No. 395, February 1935.

69. McGoldrick, R. T., Gleyzal, A.N., Hess, G. K., Jr., Hess, R.L. "Recent Developments in the Theory of Ship Vibration", David W. Taylor Model Basin Report No. 739, February 1951.

70. Murray, W.W., "On the Effect of Transverse Shear on Ship Vibrations", Underwater Explosions Research Division Report 2-53.

71. Murray, W.W., Otth, E.J., and Wood, P.W., "Frequencies and Mode Patterns of a Ship", Underwater Explosions Research Division Report F-46-54, Norfolk Naval Shipyard, Norfolk, Virginia, 1954.

Thesis
088 Otth
28779
On the natural transverse modes of a submarine.